Non-Enzymatic Paper-based Urea Sensor with Hierarchical NiO Catalysts

by

Doohee Lee

A dissertation submitted to the Graduate Faculty of
Auburn university
in partial fulfillment of the
requirements for the Degree of
Doctor of Philosophy
in Materials Engineering

Auburn, Alabama
December 10, 2022

Keywords: Electrochemical urea sensor, Electrophoretic Deposition, Hydrothermal Synthesis, Hierarchically structured catalyst, Nickel oxide-based catalyst, Paper-based sensor

Approved by

Dr. Dong-Joo (Daniel) Kim, Chair, Professor of Materials Engineering
Dr. ZhongYang Cheng, Professor of Materials Engineering
Dr. Pengyu Chen, Associate Professor of Materials Engineering
Dr. Tae-Sik Oh, Assistant Professor of Chemical Engineering
Dr. Minseo Park, Professor of Physics

Abstract

Urea has attracted attention because of its various potential applications, such as hydrogen production, fuel cells, fertilizers, and electrochemical sensors. Furthermore, as an end-product of human metabolism, urea is essential for analyzing various metabolic disorders, such as liver disease and renal function. In order to overcome the stability issue associated with enzyme-based sensors, a non-enzymatic nickel-based oxide catalyst was explored to fabricate a highly efficient urea sensor. The research aims to develop non-enzymatic catalysts (NiO) for use in urea electrochemical sensors and to increase sensitivity through synthesis (hierarchical structure), process (electrophoretic deposition), and flexible electrodes (cellulose paper).

First, a hierarchical NiO catalyst by a one-pot hydrothermal method was synthesized as a non-enzymatic catalyst. By introducing the SDBS soft template, the synthesis process became simpler by eliminating the removal process of a hard template. The hierarchical structure, in which 2D building block nanosheets comprise 3D hollow structures, could be achieved by the SDBS soft template during hydrothermal synthesis. The morphological modification of the NiO catalyst leads to a highly sensitive electrochemical urea sensor.

Second, the modification of morphology through the catalyst loading method was investigated by electrophoretic deposition (EPD). For EPDs, direct current (DC) electric fields are commonly used. When alternating current (AC) was introduced to the EPD process, however, the deposition behavior was modified; therefore, the current response toward urea was increased over DC-EPD electrodes. A more environmentally friendly catalyst loading process was also achieved by using water solvent with AC EPD as well as maintaining a modified packing behavior.

Third, as a substrate modification, the paper substrate was developed. The paper has the advantage of high surface area, cost, biocompatibility, and disposability, which makes it an ideal substrate material for use as point-of-care equipment. Having a complex cellulose network in the paper, it can be used to further enhance the electrochemical reaction. As the paper lacks electron conductivity, the mixed solution of CNT and NiO was used by means of the capillary property of the paper. The various design of paper electrodes were considered, and the optimization of electrode configuration was carried out to increase the current response toward urea.

In the dissertation, three approaches were investigated to develop a highly sensitive non-enzymatic urea sensor: hierarchical catalyst synthesis by hydrothermal method, modified loading method by AC-EPD, and cellulose networks on paper as a substrate.

Acknowledgements

Foremost, I would like to express my sincere gratitude to my advisor Prof. Dr.Dong-Joo Kim, for his guidance, support, knowledge, and patience during my Ph.D. program at Auburn University. It was a great honor to work and study under his guidance. I am deeply grateful for what he has offered me. This endeavor would not have been possible without my committee, Dr. ZhongYang Cheng, Dr. Pengyu Chen, Dr. Tae-Sik Oh, and Dr. Minseo Park, who generously provided knowledge and expertise.

I am also grateful to my group members: Dr. Jaesik Yoon, Dr. Yoonsung Chung, Dr. Eunji Lee, Christoper Lincoln, Mr. Guodong Wu, and Mr. Wonhyeong Kim.

Thanks should also go to all friends and colleagues at Wilmore Laboratory: Dr. Jiachen Liu, Dr. Jiacheng He, Dr. Lang Zhou, Dr.Yuzhu Liu, Ms. Cheryl Rhodes, and Mr. Steven Moore.

Last but not least, I would like to express my deepest appreciation to my family, Okju Lee, Yeonhee Park, and Nahee Lee.

Table of Contents

List of Figures

List of Tables

List of Abbreviations

AC	Alternating current
CA	Chronoamperometry
CV	Cyclic voltammetry
D.I.	Deionized
DC	Direct current
ED	Electrodeposition
EPD	Electrophoretic deposition
FE-SEM	Field emission scanning electron microscopy
MW	Molecular weight
MW-CNT	Multi walled carbon nanotube
$Ni(OH)_2$	Nickel hydroxide
NiO	Nickel oxide
PDADMAC	Poly(diallyldimethylammonium chloride)
PEI	Polyethyleneimine
PEMFC	Proton-exchange membrane fuel cells
SDBS	Sodium dodecyl benzene sulfonate
SS	Stainless steel
TGA	Thermogravimetric analysis
TiN	Titanium nitride
XRD	X-ray diffractometer

Chapter 1 Introduction and Literature Study

Urea has attracted attention because of its potential applications such as hydrogen production, fuel cells, fertilizers, and electrochemical sensors [1]. Urea has been extensively used in agriculture as a fertilizer, de-icing agent, and stabilizers in soap and detergents. Their long-term usage would increase urea concentration in land and water but also can lead to soil acidification and eutrophication, which disturb the ecosystem.[2] There have been reports of milk adulteration by adding urea into diluted milk to preserve the thickness and viscosity. (Naturally occurring urea concentrations in milk: 3.1 to 6.6 mM) Monitoring concentration of urea in food products is also crucial for food safety. [3]

The urea concentration ranges from 2.6 to 6.5 mM in human blood and 342 ± 67 mM in 490 to 2690 mL of human urine. Higher levels of urea in the blood can be related to kidney failure, urinary tract obstruction, dehydration, burns, gastrointestinal bleeding, and shock. In contrast, a lower level of urea can lead to hepatic failure, nephritic syndrome, and cachexia. [4] So, a susceptible and selective sensor could be a valuable tool for monitoring the urea concentration in food (milk), environment, and biological fluids (urine, blood, etc.).

The amperometric sensing technique is considered one of the most promising methods for urea sensing since it can provide a simple, fast, economic, and reliable detection [5]. The ammonium ions in the amperometric sensor can be oxidized by either enzyme or metal catalysts. However, enzyme-based sensors have issues with high fabrication cost, complex processes of enzyme immobilization, and lack of long-term stability due to enzyme denaturation, which can be caused by temperature (above 40 °C) and low or high humidity. [6]

Recently, non-enzymatic sensors with metal-based catalysts have been widely studied. Various noble metals have been utilized as catalysts for urea oxidation. Metal oxides such as ZnO, CuO, and NiO were also actively investigated because of their low cost. Nickel oxide-based catalysts, in particular, have shown excellent electrocatalytic properties in detecting urea by forming the redox couple of Ni(II) and Ni(III) [7]. To uniformly load such catalysts on electrodes, various techniques were utilized, such as electrodeposition [8], sputtering [9], brushing [10], spin coating [11], and EPD [12]. Among these methods, electrophoretic deposition (EPD) offers a versatile, simple, and cost-effective technique. It is also easy to adjust coating thickness while achieving a uniform coating even on complex-shaped substrates with an electric field. To improve the sensitivity of the non-enzymatic sensor, various approaches for increasing reaction surface area were researched vigorously by introducing a hierarchical structure and support matrix. Still, the construction of such a structure accompanies a series of complicated processes. [12] The application of paper as point-of-care testing devices is gaining attraction because they are affordable, chemically stable, and environmentally friendly. [13] Most importantly, since the paper has a porous fiber matrix, it naturally allows a liquid sample to infiltrate inside the paper matrix by capillary force. Furthermore, the capillary force-driven transport can be utilized in the catalyst loading process to distribute the catalyst and conductive network uniformly within the paper, which makes the fabrication process simpler and performance enhanced. Here, I investigated the EPD as a deposition process, hydrothermal process as preparation of effective catalyst syntheses, and application into a paper substrate for urea detection.

1.1 Synthesis of hierarchical structure and an amphiphilic organic compound

1.1.1 Hierarchical structure

Hierarchical structures are the higher dimensional structures that are comprised of low dimensional nano building blocks, such as nanoparticles (0D), nanorods (1D), and nanosheets (2D). For example, certain structure shows 3D sphere shape, but looking closely, it is assembled with nanorods. This structure can be said as 1-3 hierarchical structure from the nomenclature of hierarchical structure from Lee et al. (Figure 1) [14] The former number means the dimension of the nano-building block, and the latter number after the hyphen is the consequent hierarchical structure.

The biggest advantage of the hierarchical structure is that it doesn't sacrifice the high surface area of nanoparticles, because they are well aligned through the structure and maintain the porous structure without aggregate.

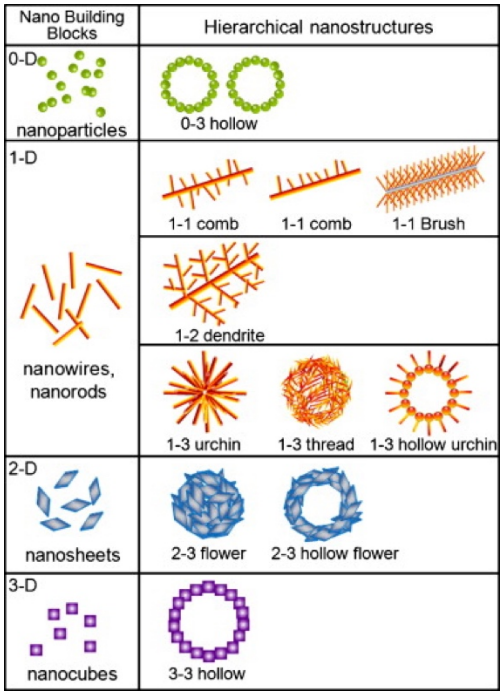

Figure 1-1 Nomenclature of hierarchical structures. [14]

The hierarchical structure is beneficial to various applications. As an application in gas sensors, for the enhancement of gas sensitivity, full depletion of electrons through the catalyst structure is advantageous. For this reason, various nanostructures have been studied, with nanoparticles, nanowires, nanotubes, nanosheets, and nanocubes. It has proven that the response of gas enhances significantly when the particle sizes are smaller than several nm. (Debye length)[15]. For the electrochemical sensor, it is well known that the decisive factors in the electrochemical performance of the electrode are the active reaction sites, transport or diffusion paths, accessibility of electrolytes, and the kinetics of the reaction. [16] Li et.al.[16] described those factors are significantly dependent on the morphologies of materials; hence it can be deduced that the electrochemical properties of catalyst can be modified by controlling the morphology. This shows the importance of the morphology-controlled synthesis of catalyst material. The issue is that the uniform distribution of nanoparticles is not easily made since the aggregation between the nanoparticles due to the van der Waals attraction is inversely proportional to the size of the particle. [17] When the aggregate becomes dense and also large, only the particles near the surface region react with an analyte, and the inner region remains inactive. [18]

1.1.2 Hollow sphere structure

The rational morphology design plays a pivotal role in advanced electrocatalysts. [19] When considering the fact that the reaction of electrocatalyst occurs at the surface of the material, generally, it is essential to think deeper about the design with more exposure of the active sites. [20] For this reason, from many applications the hollow structure materials have been studied. Many researchers take advantage of enhanced surface area by introducing hollow spheres from various applications. (Table 1-1)

Table 1-1 Benefits of hollow structure depending on the application

Application	Benefit
Dye-Sensitized Solar Cells (DSSC)	Enhanced surface area
	Scattering and reflection effect
UV photodetector	Enhanced surface area
Gas sensors	Enhanced surface area
Supercapacitor	Enhanced surface area
Sodium ion battery	Enhanced surface area
	Enough spaces to buffer the strain induced by the volumetric change

Zhu et. al., synthesized a mesoporous $NiCo_2O_4$ hollow sphere for the application of supercapacitor, which shows high BET specific surface area ($189.7 m^2g^{-1}$) than that of nanoparticles ($61.15 m^2g^{-1}$), nanorods ($71.65 m^2g^{-1}$), and nanosheets ($112.6 m^2g^{-1}$) reported in other literature. Due to the large specific surface area from the hollow sphere, the electrode could provide more electroactive region for faradaic redox reaction and lead to improving specific capacitance. [21]

The hollow structure can be prepared by hard templates [22] [12] [23], soft templates [24], and template-free methods [25]. Among them, the hard template is straightforward and easily reproducible; hence it is most widely accepted as a preparation method. Generally, solid particles in various morphologies are prepared at first as a template. In the next step, the guest chemical is coated on the surface of the prepared hard template. And lastly, the hard template is removed selectively depending on the type of hard template. It has the advantage of uniform morphology and narrow distribution in size. However, the removal process can affect the guest coating material. SiO_2, polymers such as polystyrene, and carbon spheres are common hard template materials. The

removal process of polymer is usually achieved by the combustion process.[26] Silica-based templates are removed by bases and acids generally, and the most common etching agents are NaOH solution and HF solution [27]

Table 1-2 The literature using hard templates of foam for the synthesis of hierarchical structure

Catalyst	Structure	Template	Application	Ref.
NiO	Nanosheet	Ni foam	Urea sensor	[28]
SnO_2	Hollow sphere	Polymer bead	lithium storage	[29]
TiO_2	Tubular structure	ZrO_2 fibers	-	[30]
SnO_2	Hollow sphere	Silica	-	[22]
$Ni(OH)_2$	nanocup array	PS sphere	electrolysis of urea	[12]
FeOOH	Hollow sphere	SiO_2	water remediation	[23]

To fabricate those complex hierarchical structures, generally complicated multistep processes are followed, nano cup array using PS-bead [12] and hard template using Ni foam as a scaffold. [31]

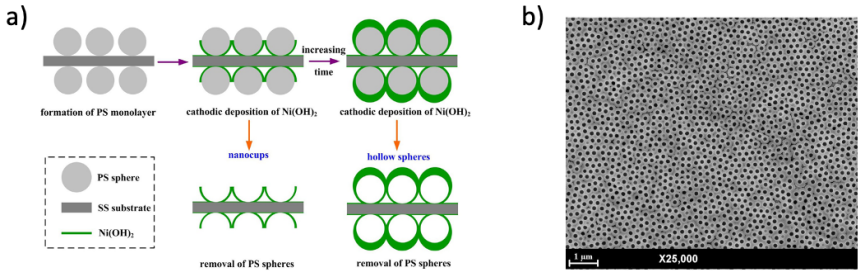

Figure 1-2 Schematic electrochemical formation of nickel hydroxide electrodes with a monolayer of nanocup arrays and hollow spheres. [12]

Wu et al. [12] utilized the polystyrene spheres as a template material to form nano cup-like pore arrays, which provide much better electrocatalytic performance than just film electrodes during urea reaction. However, to make the structure, additional steps to deposit polystyrene (PS) beads as a template should be preceded, and the template removal step for PS sphere should be followed (immersion in toluene for 10m, rinsing with DI water, and drying at 100°C for 30min)

The soft templates have less rigid and more deformable in the form of liquid or gas, such as micelle and bubble. Unlike hard templates, the process for template preparation is not independent due to the thermodynamically metastable structure of it. It is highly influenced by the chemical and physical conditions during the synthesis step. Precise process optimization is required for the accurate control of morphology or composition. [32] For the removal process, the soft template can be easily removed during the separation process of catalyst material, or no need to remove it purposely.

Self-template methods are usually comprised of one or two steps, a template preparation step and a transformation step. In general, it can be categorized into two, selective etching and outward diffusion (Ostwald ripening and Kirkendall effect). It has the advantage of simplicity, high efficiency in processing, and low cost. [33]

For selective etching, by using interior nonhomogeneity, the inner core region is removed. Another strategy is a surface-protected etching, the protective agent enhances the stability of the near area, and selectively inner is etched. As an example, Yang et al. synthesized hollow structured CeO_2 with PVP as a protective agent by 12M HCl etching solution. During etching, a microchannel was made, and through the channel, the HCl penetrates and is etched inside. [34]

1.1.3 Hydrothermal synthesis of Nickel Oxide

Among various synthesis methods of metal oxide nanostructures, the hydrothermal technique has been the most popular, gathering interest from scientists. The term “hydrothermal” usually refers to any heterogeneous reaction in water solvents with or without mineralizers under the condition of high temperature and high pressure in order to dissolve materials and recrystallize them which are insoluble in normal conditions.

In other words, the chemical reaction with heterogeneous material in the water or non-aqueous solvent at higher than room temperature and at greater than 1 atm in a closed system. [35] It is known that this method provides good crystallinity and selectivity toward morphology to oxide-based materials. The factors that are reaction temperature, reaction time, the remaining space in the container, and dissolved salt play a pivotal role in the final morphology of metal oxide. The main advantage of hydrothermal is that it avoids the use of hazardous catalysts and provides highly monodispersed particles with controllable size and morphology, and also has high product purity. [36]

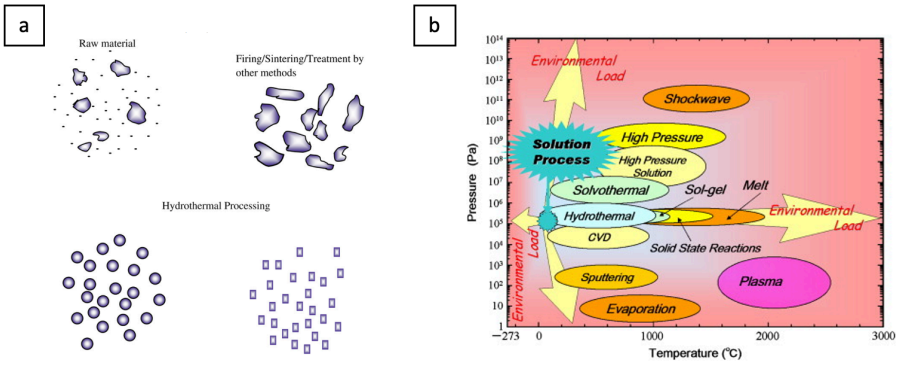

Figure 1-3 a) schematic of the advantage of the hydrothermal method and b) Pressure temperature map of materials processing techniques [37]

The recent advancement of the hydrothermal method has opened a new trend in materials synthesis. The materials prepared under the significant pressure and temperature conditions in

earlier days could now be synthesized at much lower pressure and temperature conditions. This advantage accelerates the speed of synthesis in processing advanced nanomaterials, thus having significant potential in the nanotechnology of the 21st century.

1.1.4 Hydrothermal synthesis of hierarchical structure

As a non-enzymatic metal-based material, Ni-based nanomaterials exhibited excellent catalytic activity over urea originating from the catalytic effect for forming the redox couple of Ni(II) and Ni(III) on the surface. The nickel catalysts showed higher current densities and lower oxidation potentials for the electro-oxidation of urea than those of the noble metal catalysts [1]. However, there is a potential gap between the theoretical electro-oxidation potential of urea (−0.46 V vs. SHE) and the observed oxidation potential using pure Ni catalysts (ca. 0.45 V vs. SHE). The existence of a large overpotential, and therefore high potential, for the oxidation of urea not only decreases the efficiency of the urea electrolysis process (Eq.(4)), but also causes a certain degree of the oxygen evolution reaction (OER) in alkaline media. The OER in alkaline media will lead to an extra energy loss for urea electrolysis and make a negative impact on the stability of the nickel electrode. Therefore, novel catalysts need to be synthesized to decrease the urea oxidation potential, to promote urea electrolysis, and to reduce the interference of the OER.

$$CO(NH_2)_{2(aq)} + 6OH^- \rightarrow N_{2(g)} + 5H_2O_{(l)} + CO_{2(g)} + 6e^- \quad (1\text{-}1)$$

$$Ni(OH)_{2(s)} + OH^- \rightarrow NiOOH_{(s)} + H_2O_{(l)} + e^- \quad (1\text{-}2)$$

$$6H_2O_{(l)} + 6e^- \rightarrow 3H_{2(g)} + 6OH^- \quad (1\text{-}3)$$

$$CO(NH_2)_{2(aq)} + H_2O_{(l)} \rightarrow N_{2(g)} + 3H_{2(g)} + CO_{2(g)} \quad (1\text{-}4)$$

The high-performance UOR (urea oxidation reaction) catalysts are required to promote the reaction rate. Compared with precious metal catalysts (Pt, Pt-Ir, etc.), the inexpensive earth-abundant nickel metal has exhibited highly efficient catalytic performance for UOR in an alkaline

medium. Moreover, several kinds of Ni-based catalysts, including nickel hydroxides [4], nickel cobalt bimetallic hydroxides[38], alloys (binary Ni-Rh, Ni-Co [39], and ternary Ni-Zn-Co field [40]), nickel oxide [28] and bimetallic oxides ($NiCo_2O_4$ [41], nickel manganese oxides [42] and $NiMoO_4 \cdot xH_2O$ [31]) have also been developed to efficiently electro-oxidize urea in alkaline medium. An efficient catalyst for urea electrooxidation is usually required to achieve high current densities at low over-potentials. As revealed by the literature, the introduction of bimetallic catalysts electrode could improve the electro-catalytic activity due to the lower $Ni(OH)_2$/NiOOH peak potential, increased electrode conductivity, and a higher oxidation state of Ni with the coexistence of other metal oxides. [38]

Table 1-3 The recent literature about the hierarchical NiO

Material	Shape	Size (μm)	Described Mechanism	Detail	Application	Yr	Ref
NiO	Hollow sphere (1-3 or 0-3)	0.2 - 0.8	Ethylene glycol-mediated self-assembly	Solvent effect - without PEG - nano rod. / w PEG solid sphere complex between Ni^{2+} and PEG + OH^- form $Ni(OH)_2$ nano sheet and the spontaneously attached together to form aggregates of nanosheets to minimize surface E by reducing the exposed areas.	Photocatalytic Properties	08	[43]
NiO	Hollow flower (1-3)	2~6	Citrate from (Trisodium citrate) as a directional agent for building block, and lead to hollow as the condensation-polymerization. the nanosheets polymerize into spheres driven by a minimum of total surface energy	Without Trisodium citrate - NiO like flower no hollow 0.1g Trisodium citrate - Hollow sphere (2-3) 0.3g - nanosheet size increase and no hollow structure trisodium citrate can control the growth direction of crystals by coordinating with Ni^{2+} to form a nickel citrate complex anion the nanosheets polymerize into spheres driven by a minimum of total surface energy condensation–polymerization Not Ostwald ripening (time controlled experiment shows hollow at first)	Gas sensor	21	[44]
NiO	Hollow sphere (2-3)	2~3	glycine and strong alkaline condition Self-assembly and core evacuation (like Ostwald ripening)	1st : assemble together to form loosely attached aggregates 2nd : grow and to form a sphere with a solid core 3rd : interior cavity is gradually formed via a core evacuation process (similar to Ostwald ripening) aggregate → solid core → hollow sphere Glycine functions as morphology control agent. without glycine - solid sphere minor effect toward temperature	-	05	[45]
NiO - CeO2	Hollow sphere (2-3)	2~3	Self-assembly and core evacuation (like Ostwald ripening	Solverthermal method	electrocatalytic methanol oxidation	18	[46]
NiO	Hollow sphere	2~3	CO_2 microbubble soft template from Urea	Under the action of high temperature and high pressure, urea formed microbubbles, and $Ni(OH)_2$ generated by the reaction with Ni^{2+} and OH^- was driven by the decreasing interface energy and adhered to the surface of microbubbles.	Gas sensor (Ethanol)	22	[47]
NiO	Fluppy hollow sphere (0-3)	1~1.5	CO_2 microbubble soft template from Urea	Ni^{2+} ions were absorbed around the urea molecule by the Coulomb forces due to the single bond NH2 and C double bond O hydrolysis reaction of urea - bubble Aggregation of $Ni(OH)_2$ - for the decreasing of interfacial energy Gas release leads to forming the fluffy surface	Gas sensor	18	[48]

NiO	Fluppy hollow sphere (0-3 , 2-3)	3~5	CO_2 microbubble soft template from Urea	a fluffy surface with pores and a flower-like surface which is made of nanoplates. Flower like - EtOH & water/ SDS/ urea was used. There was no explanation from different surfactant and solvent. Rather ununiform about the size and structure.	Gas sensor	18	[49]
NiO	Hollow flower (2-3)	0.8~1.2	CO_2 microbubble soft template from Urea	CBD method The CO2 microbubbles act as the soft templates	Adsorptive removal of Congo red	19	[50]
NiO	Hollow sphere (0-3, 2-3)	1~3	CO_2 microbubble soft template from Urea CTAB for structure directing agent	For 2-3, CTAB functions as structure-directing agent, nano sheets formed on the bubble.	Gas sensor (Ethanol)	11	[51]

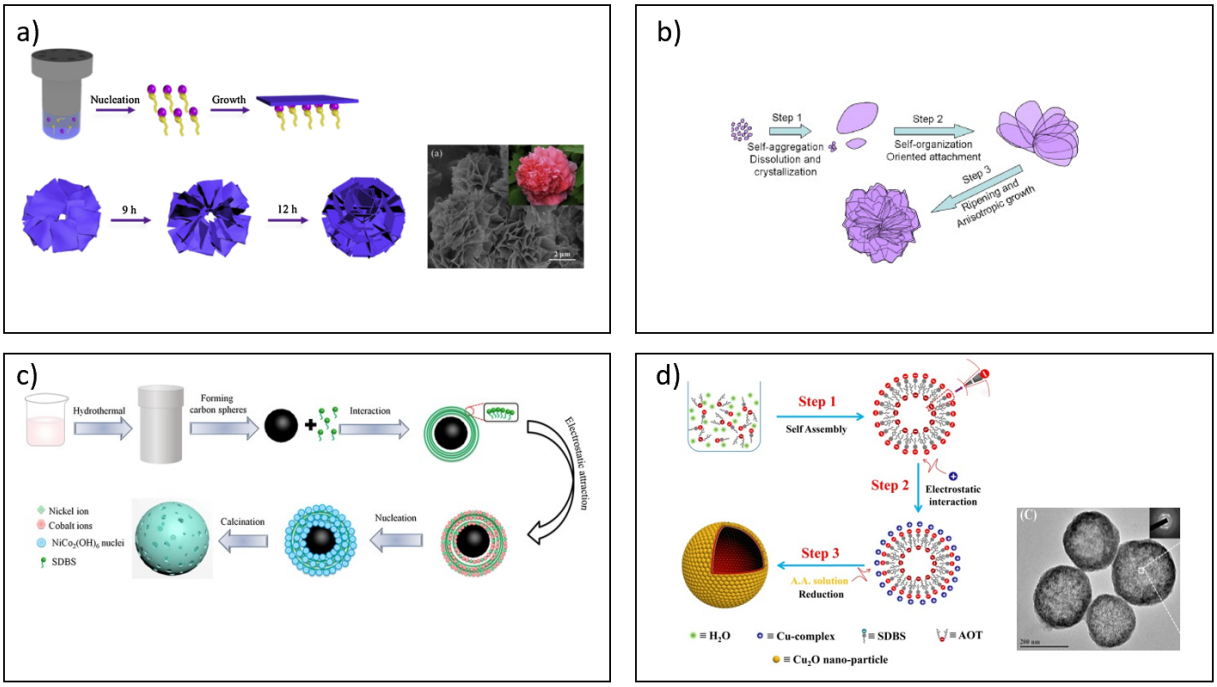

Figure 1-4 Schematic illustration of the mechanism of different types of sphere by hydrothermal method. [126], [127], [128], [94]

1.1.5 Nickel oxide

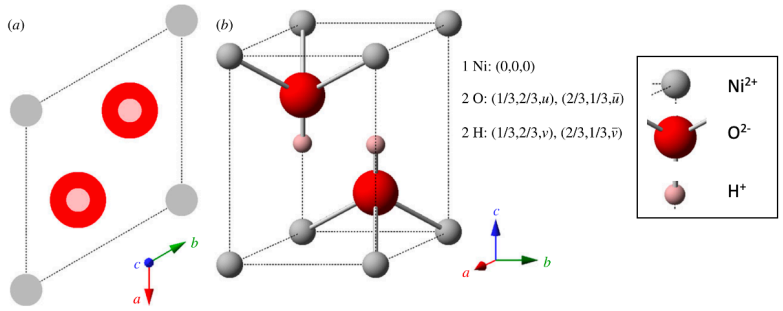

Figure 1-5 The crystal structure of ß-$Ni(OH)_2$ described by a) the projection of the unit cell, b) the unit cell [52] a- and b- axis are not orthogonal (trigonal symmetry)

The application of nickel hydroxide has been made in diverse fields such as physics, chemistry, and materials engineering. As an electrode material of battery, $Ni(OH)_2$ has been widely utilized since the first half of the 20^{th} century. It is also essential in the surface layers that form electrochemically or by the corrosion of Ni metal or alloys.

In the 1960s, Bode et al. explained the reported behavior of the electrochemical oxidation and reduction between Ni(II) to Ni(III). [53] The description remains a good overall agreement about the process at $Ni(OH)_2$ battery electrode.

Bode et al. identified two pseudo-polymorphs of Nickel hydroxide as α- and β-$Ni(OH)_2$. The β-phase $Ni(OH)_2$ occurs naturally, and it has the same structure as brucite, $Mg(OH)_2$.

As the polymorph of nickel hydroxide, the α-$Ni(OH)_2 \cdot xH_2O$ consists of layers of β-$Ni(OH)_2$, and are intercalated by water. The degree of hydration is from 0.41 to 0.7. Though this material is hydrated, the water molecules are generally omitted from the formula. (denoted α-$Ni(OH)_2$)

1.1.6 Synthesis of NiO by hydrothermal method

For Hydrothermal or solvothermal synthesis, the precursor materials and solvent are mixed together, transferred into a pressure vessel (autoclave), and then heated. A typical range of reaction

temperature is 120 - 200°C, generally above the boiling temperature of the water. Since the vessel has a fixed volume, the pressure inside the vessel increases with temperature. Hence, the increase in pressure leads to an increase in the boiling point. As a result, the precursor solution remains liquid, and the precursor materials are fully dissolved. Depending on the size of the vessel, the scale can be larger to the industrial level, such as on the order of hundreds of liters. So, the hydrothermal methods can be said to be beneficial toward scale from the lab to industrial size for the production of $Ni(OH)_2$. The β-$Ni(OH)_2$ is the general phase of the hydrothermal synthesis. However, α-$Ni(OH)_2$ also can be synthesized with the introduction of an intercalation agent [54] into the precursor solution [55], reduced reaction time, and low-temperature [56].

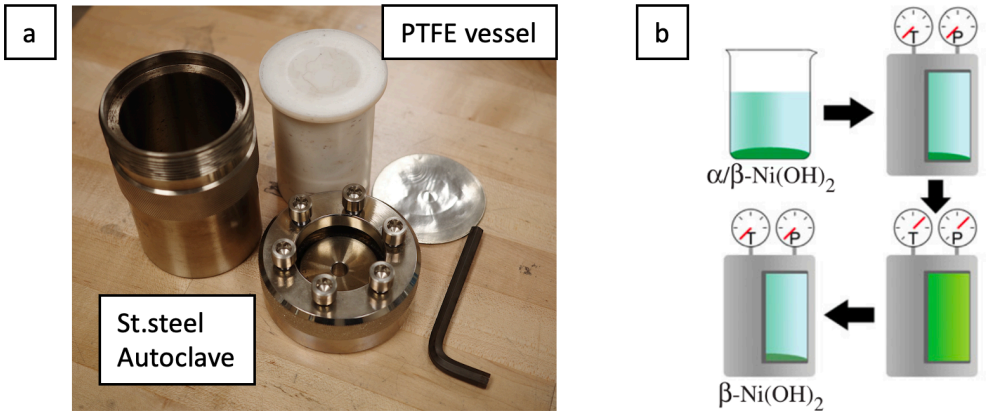

Figure 1-6 a) pressure vessel (autoclave), b) schematic mechanism of hydrothermal method

1.1.7 Amphiphilic organic compound

Hydrophilic compounds are soluble in polar solvents, and hydrophobic compounds are also soluble in non-polar solvents. However, the non-polar (hydrophobic) compound is not soluble in a polar solvent. When a chemical compound has both hydrophilic and hydrophobic groups, it is called amphiphilic. The hydrophilic(polar) part is named as 'head,' and the hydrophobic part (non-polar) part is called ‘tail.’ Since they can naturally exist at the surface between two different media, they are called 'surface-active agents' or 'surfactants.'

As the charge of the head group, the surfactant can be categorized into cationic, anionic, and nonionic surfactants. The surface activity of these surfactants is based on the chain length of hydrocarbon and the property of the head group. Amphiphilic surfactants with longer hydrocarbon chains are considered to be more surface-active comparing those having a shorter tail. [57] The micelle is the most common aggregate in polar solvents. The hydrophilic head groups are positioned outside the micelle and in contact with the circumferent water. Alkyl tails are positioned inside the micelle.

For a surfactant in solution, the hydrophobic tails are hydrated, hydrogen bond interactions are increased, and freedom is lost for the hydration of water molecules compared to bulk water. During the micellization, the Van der Waals interaction among hydrophobic tails led to a significant decrease in hydrophobic hydration. The removal of the extra hydrogen bonds leads to the unfavorable enthalpy effect. This is compensated by the gain of entropy because of the increased freedom of water molecules. The favorable entropy effect is compensated with two effects: the loss of entropy by the tails and the increase in enthalpy by head-group repulsion. (especially for ionic surfactants) The presence of a counter-ion can relieve the repulsion by neutralizing the overall charge. [57] [58]

Critical micelle concentration (CMC) is the concentration where the formation of micelle occurs significantly. The structure of the surfactant, the types of added electrolytes in the solution, the property of counter-ion, the presence of an organic compound, and the temperature of the solution are the essential factors that affect the CMC in an aqueous solvent. The temperature effect on CMC is rather complicated. First, CMC decreases with temperature, but after a certain point, it increases with temperature. Temperature increase leads to the prevention of hydration of the hydrophilic group, which helps micellization. However, it also disrupts structured water

surrounding the hydrophobic tail group, reducing micellization. Those two opposite effects determine the increase or decrease in CMC. [59]

Depending on the structure of the surfactant, the shape of the aggregate can be changed. The simplest type is a spherical micellar structure. It is comprised of 50-100 molecules of surfactant for a micelle (aggregation number) and has a 5~10 nm average diameter.

The worm-like or cylindrical micelle can be formed by the addition of counterions or a mixture of cationic and anionic surfactants. They reduce the effective area of the head group and result in closer packing. The worm-like micelles may increase the viscosity of the solution.

The third type is the bilayer, which is the base of the vesicle. Two non-polar tails face each other, and the pairs are stacked continuously and form a bilayer. The vesicle is the bilayer with small curvature and is closed at the ends. The vesicle can be comprised of a uni- or multi-lamellar structure having a diameter ranging from 10 nano to several microns.

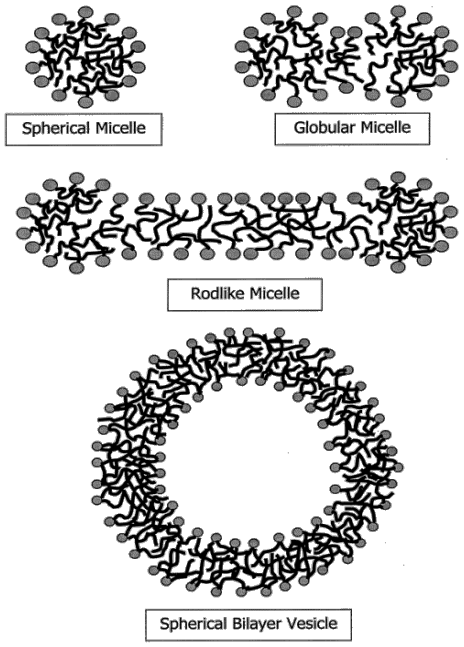

Figure 1-7 Schematic of surfactant aggregates in solution. [60]

1.1.8 Packing factor

The self-assembly behavior of surfactants in solution has been researched theoretically and experimentally, and the advantage of it has been widely utilized in various applications. The aggregate's structure affects the properties of mixed solution, such as the solubility of hydrophobic substance, viscoelastic property, and their application. It is important to understand how the molecule aggregates to get the desired morphology, such as spherical, globular, rodlike, or vesicles.

The concept of the packing parameter of molecules has been widely accepted in the chemistry, biology, and physics literature due to the simple insight of the self-assembly phenomenon. The equation of the packing factor is described as below:

$$p = \frac{v}{al}$$

, where v is defined as the volume of the hydrophobic portion of surfactant and l is the length of the hydrophobic chain, and a is the area of the headgroup.[61]

Table 1-4 The range of packing factor based on the micellar structure

Spherical micelles	$\mathbf{0 < p \leq \frac{1}{3}}$
Globular micelles	$\frac{1}{3} < p \leq 0.406$
Worm like micelles	$0.406 < p \leq \frac{1}{2}$
Vesicles	$\frac{1}{2} < p \leq 1$

Based on the concentration or complexing surfactant or interaction with other ions, the packing factor can be varied, which leads to the change in the structure of aggregate from micelles to vesicles.

1.2 Electrophoretic deposition as a coating process of metal oxide

1.2.1 Electrophoretic deposition (EPD)

Electrophoretic deposition (EPD) is one of the processes for making thin or thick film colloidally. It has the advantages of short formation time, needs simple apparatus, little restriction of substrate shape, and no requirement for binder burnout as the green coating contains few or no organics. Compared to other advanced shaping techniques, the EPD approach is quite versatile since the process can be controlled easily based on a specific application. For example, deposition can be applied to various shaped substrates, such as flat, cylindrical, and porous. In particular, though EPD is a wet process, this technique offers easy control of the thickness of a deposited layer by means of simple adjustment of the applied voltage and the deposition time. During the EPD process, charged particles, dispersed in a liquid medium (called suspension), are attracted and deposited onto a conductive substrate with oppositely charged on the application of a DC electric field. The term 'electrodeposition' is sometimes used to refer to both electroplating and electrophoretic deposition; however usually refers to electroplating more. The table below is a comparison of both processes.

Table 1-5 Characteristics of electrodeposition techniques

Property	Electroplating (ED)	Electrophoretic deposition (EPD)
Moving species	Ions	Solid particles
Chargetransfer on deposition	Ions reduction	None
Required conductance of liquid	High	Low
Preffered liquid	Water	Organic

The primary difference between the two processes is that ED uses ionic species in solution, but EPD uses solid particles such as ceramic in solution. We can know which electrode the deposition may occur depending on the particle charge. If the particle has a positive charge in the solution, the deposition occurs on the cathode, which is called cathodic EPD. On the other hand, if the particle has a negative charge, the deposition occurs on a positive electrode (anode), anionic EPD. By appropriate modification of the surface charge of the particles, any of the two types of deposition is possible. For technological application, the potential of EPD as a materials processing is being increasingly recognized academically and industrially. Further traditional applications, EPD has been applied to various applications: nontoxic ceramic coatings, functional films for electronic devices, coatings for SOFC, and bioactive coatings for the medical implant. The EPD also provides important advantages in the coating of complex compounds and ceramic layers. Stoichiometry in the resultant deposition can be controlled by the stoichiometry in the particle used.

1.2.2 Steric and Electrosteric forces

Steric stabilization provides an alternate route of controlling colloidal stability in aqueous and nonaqueous systems. This approach uses adsorbed organic molecules (often polymeric in

nature) to induce steric repulsion. The adsorbed layers must have sufficient thickness and density to overcome the van der Waals attraction between particles and prevent bridging flocculation. Such species should be firmly anchored to avoid desorption during particle collisions. The conformation of adsorbed layers can vary significantly, depending on solvent quality, molecular architecture, the number of anchoring groups, active surface site density, and colloid and organic concentrations in solution. For example, schematic illustrations of such layers adsorbed on ideal ceramic surfaces are shown in Figure 1-8 for varying molecular structures, including homo-polymers, di-block copolymers, comb-like copolymers, and functionalized short-chain dispersants.

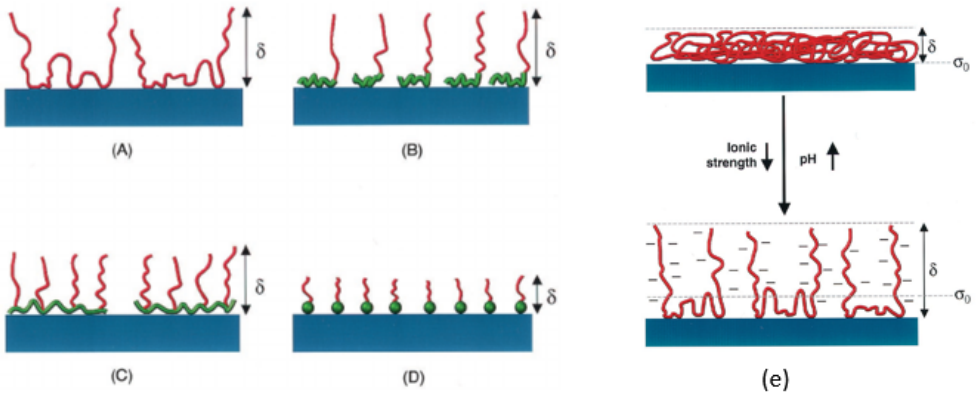

Figure 1-8 Schematic illustrations of adlayer conformation on an ideal ceramic surface varying molecular architecture [62]

Colloidal dispersions are commonly stabilized electrostatically and sterically with polyelectrolyte species. The term electrosterically stabilized is often used to describe such systems. Polyelectrolytes are polymers containing one or more ionizable groups (e.g., carboxylic or sulfonic acid groups), with molecular architectures ranging from homopolymers, such as poly(acrylic acid), to block copolymers with ionizable segments. Adsorption of polyelectrolytes is strongly influenced by the chemical and physical properties of the solid surface and solvent medium. In the case of polyelectrolyte species and colloid surfaces of interest carrying opposite charges,

adsorption is strongly favored.[63] By neutralizing surface charges or bridging mechanisms, these species can promote flocculation at small adsorbed amounts. Due to electrosteric interactions, particle stability increases with higher adsorbed amounts. Modulating solvent conditions (such as pH and ionic strength) may affect polyelectrolyte adsorption behavior and conformation. Anionic polyelectrolytes are ionized more strongly with increasing pH. They adopt a compact coil configuration in solution at low pH and adsorb in a dense layer of large mass and low adlayer thickness, as shown in Figure 1-8 (e). [64] As a result of intersegment repulsion, anionic polyelectrolytes adopt an open coil configuration in solution when fully ionized. The highly charged species would adsorb in an open layer and in a high layer (d), also shown in Figure 4 (e). Intersegment repulsion can be mitigated by screening effects at high ionic strengths, but the structure of adlayers will be altered.[63]

1.2.3 Zeta potential

If the particles in suspension carry a charge, they will move only in response to the electric field. In order to develop a charge on a particle, four mechanisms have been identified: (a) selective adsorption of ions from the liquid onto the solid particle, (b) dissociation of ions from the solid phase into the liquid, (c) adsorption or orientation of di-polar molecules at the particle surface, and (d) electron transfer between the solid and liquid phases due to differences in work function. In a suspension, an ion with an opposite charge surrounds a charged particle in a concentration greater than the bulk concentration of these ions. This is called a double layer (Figure 1-9). In the presence of an electric field, these ions as well as the particle should move in opposite directions. However, the particle also attracts ions. This results in a fraction of the ions surrounding the particle moving along with it instead of moving in the opposite direction. Therefore, the speed of a particle is determined by the net charge enclosed in the liquid sphere, not by its surface charge. Zeta-potential

or electrokinetic potential is the potential at the shear surface. Generally, particles with a negative surface charge will have a positive zeta potential. It occurs when the charge of specifically adsorbed ions exceeds the surface charge, for example.

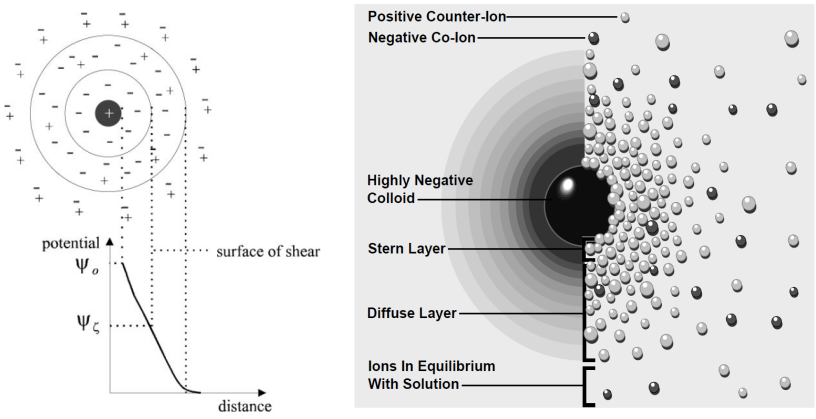

Figure 1-9 Schematic of the double layer surrounding a charged particle and evolution of the electric potential from the surface potential to zero far from the particle.[65]

The equilibrium speed of a particle is determined by four forces acting on it. The first, which accelerates the particle, is the force caused by the interaction of the surface charge with the electric field. All other forces slow the particle: viscous drag from the liquid following Stoke's law, electric fields exerting forces on counterions in the double layer (retardation), and, when a particle moves, the distortion in the double layer caused by a displacement between the centers of the negative and positive charges, (relaxation).[65]A colloidal suspension's zeta potential determines its stability. As long as all the particles have large negative or positive charges, the suspension will be stable. Flocculation is more likely to occur at low zeta potentials. Another essential consideration when discussing zeta potentials is pH; in fact, quoting a zeta potential without an accompanying pH is almost meaningless. For most suspensions of materials, a plot of zeta potential versus pH shows an isoelectric point, a point at which there is no net charge on the particles.

1.2.4 Governing equations of EPD

EPD kinetics were first described by Hamaker in 1940 for electrophoretic cells with planar geometry (Eq. 1-5).[66] It relates the deposited mass per unit area, m (g), with slurry properties, such as suspension concentration, C_s (g cm^{-3}), and electrophoretic mobility, μ (cm^2 s^{-1} V^{-1}), with physical and electrical conditions imposed on the system such as electric field, E (V cm^{-1}), deposition area, S (cm^2), and deposition time, t (s):

$$m = C_s \mu S E t \tag{1-5}$$

The linear variation of deposited mass with deposition time requires that Eq. (1) parameters remain unchanged with time.

Hamaker equation also can be described as eq. (1-6), where the deposit yield (w) to the electric field strength (E), the electrophoretic mobility (μ), the surface area of the electrode (A), and the particle mass concentration in the suspension (C) through the following equation:

$$w = \int_{t_1}^{t_2} \mu \cdot E \cdot A \cdot C \cdot \mathrm{d}t \tag{1-6}$$

Ishihara et al. [67] and Chen and Liu used the following equation (1-7) for the weight (w) of charged particles deposited per unit area of the electrode in the initial period, ignoring the charge carried by the free ions

$$w = \frac{2}{3} C \cdot \varepsilon_0 \cdot \varepsilon_\mathrm{r} \cdot \xi \cdot \left(\frac{1}{\eta}\right) \cdot \left(\frac{E}{L}\right) \cdot t \tag{1-7}$$

where C is the concentration of the particle, ε_0 is the permittivity of vacuum, ε_r is the relative permittivity of the solvent, ξ is the zeta potential of the particles, η is the viscosity of the solvent, E is the applied potential, L is the distance between the electrodes, and t is the deposition time. The above equation often termed as Hamaker equation, suggests that the deposition weight of the charged particles under ideal electrophoretic deposition depends on the above parameters.

However, if the solvent, the particles, and the apparatus for EPD are fixed, the factors ξ, ε_r, η, and L in the above equation are constant. Consequently, the weight of the deposited particles (w) in the EPD method is a function of E, t, and C. Therefore, the mass of the deposited particles, namely, the thickness of the films, can be readily controlled by the concentration of the suspension, applied potential, and deposition time in the EPD method.

$$m(t) = m_0(1 - e^{-t/\tau}) \tag{1-8}$$

This equation (1-8) for EPD kinetics has been widely applied by Sarkar and Nicholson. It completes the first description proposed by Zhang et al.[68] in 1994 concerning the incorporation of changes in particle concentration in EPD kinetics. Eq. (1-8) can be reduced to the Hamaker model for a short time, and it is widely accepted in the literature. In recent years several authors have proposed different mathematical models based on this equation to describe the deep electrophoretic penetration and deposition of ceramics in porous substrates, to determine deposit thickness, or to control the homogeneity of the porous distribution in a ceramic membrane.

1.2.5 Parameters relating to suspension

a) Particle size

Although there is no general rule of thumb to specify particle sizes suitable for electrophoretic deposition, good deposition for a variety of ceramic and clay systems has been reported to occur in the range of 1–20 μm. But this does not necessarily mean that deposition of particles outside this size range is not feasible. For homogeneous and smooth deposition, the particles must remain dispersed and stable. For larger particles, the main problem is that they tend to settle due to gravity. Ideally, the mobility of particles due to electrophoresis must be higher than that due to gravity. It is difficult to get a uniform deposition from the sedimenting suspension of large particles. When a vertical deposition electrode is placed over a settling suspension, EPD will

cause a gradient in deposition, resulting in a thinner layer of deposit above and a thicker layer at the bottom. Additionally, larger particles need either a powerful surface charge or a larger electrical double-layer region in order to undergo electrophoretic deposition. Particle size has also been found to have an apparent influence on controlling the cracking of the deposit during drying. [69] Sato et al. investigated the effect of $YBa_2Cu_3O_{7-\delta}$ (YBCO) particle size reduction on crack formation, and their results are shown in Figure 1-10. Crack in films deposited from a suspension consisting of a relatively smaller particle (0.06 μm) was much less than that in films deposited from the suspension containing larger particles (3 μm). [70]

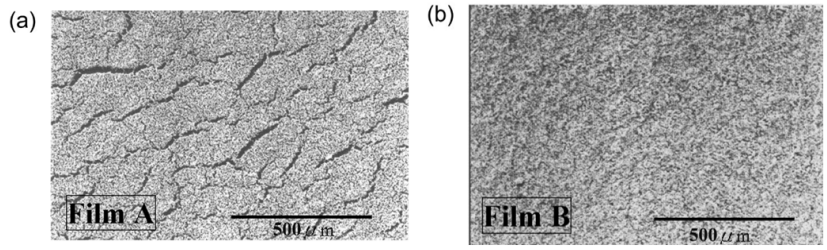

Figure 1-10 SEM images of sintered films. The images of (a) and (b) show films fabricated from colloids consisting of micron-sized particles and submicron-sized particles, respectively. [19]

b) Dielectric constant of the liquid

Powers investigated beta-alumina suspensions in numerous organic media and determined the incidence of deposition as a function of the dielectric constant of the liquid and the conductivity of the suspension. A sharp increase in conductivity with dielectric constant was noted, which apparently refers to the liquid in its pure state. As a consequence of dissociative or adsorptive charging modes, impurities, especially water, affect the conductivity where the conductivity of milled suspension differs greatly from the pure liquid. Thus, a liquid with a low dielectric constant will have a low ionic concentration. Generally, the dielectric constant is the product of the relative dielectric constant and the vacuum dielectric constant. [71]

c) Stability of suspension

The electrophoresis is a process by which particles are in motion in a colloidal solution or suspension under the influence of an electric field. Generally, it occurs when the distance over which the double-layer charge falls to zero is larger than the particle size. When an electric field is applied, the particles will move relative to the liquid phase. Colloidal particles with 1μm or less in diameter tend to remain in suspension for long periods due to Brownian motion. Particles larger than 1μm require continuous hydrodynamic agitation to remain in suspension. It is unlikely that the electric field can overcome the repulsive forces between the particles if the suspension is too stable. The stability of the suspension is evidently its most influential property, but this is a somewhat empirical property not closely related to fundamental parameters. [69]

1.2.6 Parameters relating to the process

a) Effect of deposition time

There is no doubt that the deposition occurs linearly during the initial stages. Nevertheless, as more and more time is allowed for deposition, the rate of deposition decreases and reaches a plateau at very high levels of deposition. ZnO coating on a copper electrode is shown in Figure 1-11 at different potentials and with increasing deposition time. [72] As a result, in a constant voltage EPD, electrophoresis is reduced since the electric field influencing electrophoresis decreases with deposition time (Figure 1-11) due to the formation of an insulating layer of ceramic particles on the electrode surface. [73]

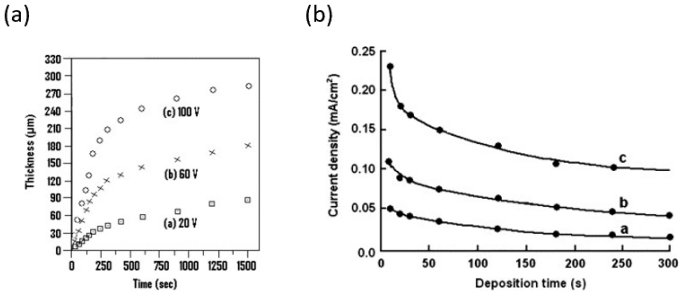

Figure 1-11 a) Relationship between deposit thickness and time of deposition for ZnO coatings on the copper electrode at the different applied potential. [21] , and b) Current density versus deposition time for deposition of hydroxyapatite at different applied voltages

b) Applied voltage

In general, the amount of deposit increases as the applied potential is increased. Because the formation of a particulate film on an electrode is a kinetic phenomenon, the accumulation rate of the particles influences their packing behavior in the coating. Higher applied fields may cause turbulence in the suspension, causing the coating to be disturbed even during deposition by flows in the surrounding medium. In addition, particles can move so fast that they cannot find enough time to sit in their best positions to form a closed-packed structure. As a result of the higher applied potential exerting more pressure on particle flux and movement in high field situations, particles are also restricted in their lateral motion once they have been deposited; the applied field affects the deposition rate and deposit structure.

c) Concentration of solid in suspension

In multi-component EPD, the solid volume fraction in the suspension plays an important role. In some cases, although each particle species has the same surface charge sign, they could deposit at different rates depending on the volume fraction of solids in the suspension; if the volume fraction of solids is high, the powders deposit at an equal rate. As long as the volume fraction of solids is low, the particles may deposit at a rate proportional to their individual electrophoretic mobility. [74] It is pretty evident from the above discussion that the kinetics of electrophoretic deposition and the quality of the deposit formed depend on many parameters. Electrophoretic deposition requires careful control of these parameters. However, many of the parameters are interconnected. The quality of electrophoretically deposited layers is heavily

influenced by the suspension conditions. An EPD deposit is generally better with a well-dispersed stable suspension than an unstable or agglomerated powder suspension. Zeta potential is an essential parameter that relates to suspension stability and mobility. In general, the higher the absolute value of the measured zeta potential, the better the dispersion of the particles in the suspension. Additionally, the ions in the suspension carry most of the current when an electric field is generated during EPD; as a result, the electrical conductivity of the suspension plays an important role in the process. [69]

1.3 Paper-based electrode

1.3.1 Paper as a Point of Care Devices

The majority of technological advances in measurement science is aimed at increasing sample throughput and/or reducing detection limits for samples. [75] Despite the fact that such technological advances have enhanced our understanding of chemistry and biology, they are usually limited to laboratory use by highly trained scientists. Consequently, there is a growing awareness of the need to enhance modern analytical tools with low-cost methods designed for point-of-need applications. [76] Often, point-of-need measurement technologies are simple and inexpensive, but they sacrifice detection limits, specificity, and speed for sensitivity, specificity, and speed. [77] It is also attractive to use point-of-need technologies because they are low-cost and require little training from the user. The technology of this kind can have a significant impact on science and society as a whole. Litmus paper and home pregnancy tests, for example, have diffused into everyday society.

Capillary-based flow is a common feature of these point-of-need devices. A paper-based analytical device (PAD) is a type of point-of-need technology that uses porous cellulose (like filter

paper) to store reagents and utilizes capillary action to generate flow via capillary action. The flow path is controlled by hydrophobic materials printed on the paper. [78] These devices are more functional than traditional analytical techniques that use paper as a substrate. There are several advantages to using paper as a substrate over traditional materials. (e.g., polymers, glass, or ceramics)

a) It is lightweight and flexible, making it easy to transport and store.
b) By capillary action, it can passively move fluids.
c) Due to its microfiber composition, it has a very high surface area, which favors adsorption.
d) It is porous and biocompatible, allowing reagents to be immobilized and stored in active form.
e) It is capable of filtering and then separating microscopic components.
f) It is available in a wide range of thicknesses, porosities, and compositions (for instance, metallic or carbon-modified).
g) A wide range of printing technologies can be used with it.
h) It can be easily modified to become hydrophobic, conductive, etc.
i) A 3D structure can be created by stacking and folding it.
j) It is easy to dispose of by incineration.

As evidenced by the large number of articles describing applications of PADs in clinical, food, and environmental fields, the paper is very appealing as a substrate for designing analytical platforms. [79] [80] Materials and reagents, instrumentation, personnel, and analysis time all influence the cost of the analysis. The use of low-cost materials, the low volume of reagents required, the use of inexpensive instrumentation, the simplicity of procedures by non-qualified personnel, and the considerable reduction in the analysis time (facilitated by the miniaturization of

devices, integration of steps, reduction of complexity, etc.) reduces the cost enormously. In addition, disposal management expenses can be woven in, and mass production of devices reduces the cost per unit. Furthermore, low-cost devices are democratizing analysis, bringing equal opportunities to developed and developing countries. By adding colorimetric reagents to specific zones of the paper, analytes are detected and quantified by changes in color hue and intensity. Despite its simplicity, this method has limitations, including user variability when detecting changes in reagent hue and intensity. It is possible to observe color changes caused by reactions on paper with the naked eye, providing semi-quantitative results for some assays. Color intensity is integrated using an imaging tool and image processing software to obtain quantitative results. In contrast, colorimetric detection is limited by low background surfaces, a limited dynamic range, low sensitivity, and variable lighting conditions. [81]

Thus, even with PADs, precise and accurate quantification may require the use of peripheral technologies such as digital scanners, cameras, or other optical techniques. It is also possible to improve PAD performance by using instrumented techniques, such as electrochemistry. Paper-based devices can benefit from electrochemical sensing due to their low cost, high sensitivity, and high selectivity, especially for detecting blood analytes. [82] For these sensors, high surface area with electrically conductive electrodes made from electrochemically stable materials are required, such as glassy carbon electrodes, highly oriented pyrolytic graphite (HOPG), or other microstructured surfaces. Electrochemical detection is very suitable for paper-based analytical devices (PAD) because of the fact below. [83]

a) It does not require complex/expensive materials or instruments
b) Electrodes can be easily miniaturized and fabricated onto paper
c) On-site analysis is already possible with portable potentiostats.

The combination of electrochemical detection and PADs allows for the development of inexpensive, mobile, and sensitive devices. In 2009, Henry and coworkers reported the first example of PAD using screen-printed carbon electrodes. [84]

Furthermore, they have gathered attention in the biomedical field by being capable of matching the ASSURED criteria established by World Health Organisation, where ASSURED represents the benchmark criteria: Affordable, Sensitive, Specific, User-friendly, Rapid and robust, Equipment-free, and Deliverable to end-users for identifying the most appropriate diagnostic tests for resource-constrained settings. [85]

The publication of research works in this field has experienced an almost exponential progression, and it seems to have leveled off during the last year. A bibliographic search on the Web of Science portal, using the topic "paper-based electrochemical device," reported 812 papers since 2009. Of those 812 works, 225 described "point-of-care" applications distributed in time, as seen in the bar chart (Figure 8). Among them, around 70% were paper-based electrochemical devices for biomedical point-of-care applications. [86]

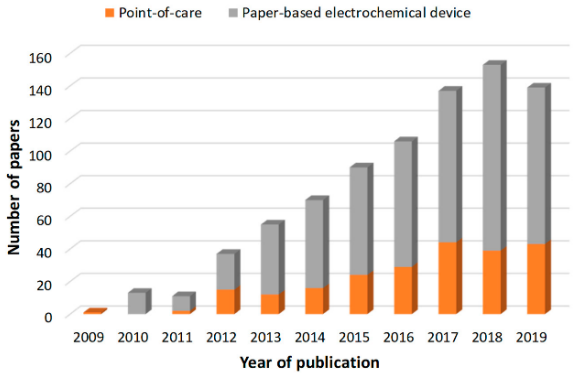

Figure 1-12 Annual trend in the number of publications for "paper-based electrochemical device" (grey) and "point-of-care" applications (orange) from 2009 to 2019. Database: Web of Science Core Collection.

1.3.2 Carbon Nano Tube

Electrochemical sensing is one of the most attractive opportunities for paper-based devices, especially for detecting various blood analytes, owing to its low cost, high sensitivity, and high selectivity. These sensors require high surface area electrically conductive electrodes made out of electrochemically stable materials such as glassy carbon electrodes, highly oriented pyrolytic graphite (HOPG), or other micro-structured surfaces. Among these, carbon nanotubes (CNTs) have been used as transduction materials in a number of applications as they have a high surface area, are electrically conductive, chemically inert, and have been used as transduction materials in a variety of sensor types, including resistive, [87] colorimetric, and electrochemical sensors. [84] Furthermore, CNT powders are now regularly fabricated at an industrial scale, and protocols have been established to make large-volume suspensions that enable integration into devices. [88]

Carbon nanotubes (CNTs) have attracted considerable attention since their discovery due to their unique properties, such as thermal, electrical, mechanical, and current-carrying capability, which are helpful in various fields of material science and technology. In addition to its exceptional strength and stiffness, the considerable length-to-diameter ratio of 132,000,000 : 1 is just peculiar to CNTs. Nanotubes are the family member of fullerene structures and are divided into two categories as single-walled nanotubes (SWNTs) and multi-walled nanotubes (MWNTs). In fact, the SWNTs can be considered as one layer of graphene, which is wrapped into an integrated cylinder, and multi-layered graphene rolled up concentrically forms the MWNTs, Figure 1-13. [89]

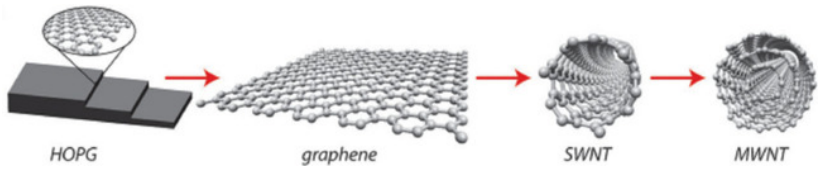

Figure 1-13 The structural connection between HOPG, graphene, SWNTs, and MWNTs. HOPG and MWNTs are 3D structures, while graphene and SWNTs are only surface atoms [89]

Due to their chemical and dimensional compatibility with biomolecules, CNTs are widely used in the construction of biosensors. These features facilitate electron transfer between the electrode surface and biomolecules and catalyze the reaction. In addition to their small diameter and long length, carbon nanotube-derived electrodes appear to be as fine or even better than other carbon-based electrodes in terms of electroactivity, as well as their high surface area compared to other carbon-based electrodes. The preparation and use of carbon nanotube-modified electrodes, however, remain challenging. The nanotubes must be processed in a controlled manner so that the electrode can be modified. One of the most commonly detected analytes using enzyme–CNT electrodes is glucose. Several strategies were used to immobilize the necessary enzymes. Through polypyrrole or even CNT inks, glucose oxidase (GOx) has been immobilized onto CNTs. [89]

Due to CNTs' exceptional electrochemical properties, they can be used in Faradaic reactions (e.g., their fast electron transfer kinetics resulting from edge plane graphite sites in their walls and ends) or in non-Faradaic processes, such as the significant changes in conductance that occur when CNTs accept or withdraw charges from or to molecules in their nearest chemical environment due to the cloud of electrons surrounding their walls. A degree of maturity has been demonstrated for electroanalytical methods using electrodes modified with CNTs for sensing and biosensing. It is still necessary, however, to investigate the suitable integration of such devices into miniaturized systems suitable for more relevant applications (e.g., point-of-care clinical multiplexed analysis). There are still many possibilities for imaginative CNT-functionalization strategies in this context.

1.3.3 Paper electrode fabrication

In the early stages of the development of electrochemical paper-based analytical devices (ePAD), electrode materials and fabrication methods were adapted from traditional microfluidic and biosensor systems. Carbon electrodes are commonly made with screen printing, which was

the first electrode fabrication method for ePADs. It is popular due to its advantages of ease of fabrication, low cost, large-scale production, and reasonable electrode-to-electrode reproducibility. Carbon electrodes are manufactured using an open mask or stencil, just as they are in screen printing. Stencils are easily made from solid films, including adhesive tape and transparent film, using craft or laser cutters. Key advantages of this fabrication technique are facile mask generation for rapid prototyping and low cost. Inkjet printing, stencil printing, and pencil drawing were among the new electrode fabrication methods introduced for ePADs. Still, screen printing electrodes remained the most popular fabrication technique and were further developed with more complicated and multiplexed ePAD designs.

A screen printing technique is a simple method of fabricating electrodes by printing electrodes onto screens made from silk or nylon. Using computer software, these meshes are designed and created using an emulsion process, producing a negative cut-out of the electrode geometry. Upon placing these screens on the substrate, conductive ink is spread onto them. After printing, most inks are thermally cured at 60–90 °C for several minutes. Often these electrodes involve multiple applications of different inks and meshes that must be aligned (e.g., one ink for the working and counter electrodes and one for the reference electrode). Due to low cost and ease of fabrication, screen printing allows for convenient incorporation in ePADs. SPEs have been incorporated into complex designs such as 3D origami. SPEs fabricated with screen printing machinery tend to be reproducible since the fabrication is automated, and screen printing can also be scaled up for mass production. [90]

Using different conductive inks, screen-printing allows for both simple fabrication and simple modification of electrodes. Adding catalysts to the ink adds versatility without requiring complicated post-modification steps. It is possible to use a variety of commercially available

carbon and metallic inks with screen printing equipment, and many groups prepared their own inks. The low cost and availability of carbon inks have made them a popular choice for electrode fabrication in ePADs. Carbon-based electrodes have wide potential windows and are less prone to fouling than precious metals, allowing them to detect various analytes. Generally, Ag/AgCl ink is used as a reference electrode because it is low-cost, low-toxic, and stable. SPEs often use pseudo-reference electrodes like carbon or silver, where thermodynamic equilibrium is not maintained and the reference potential can drift. Recently, SPEs have been modified with inks such as carbon black/Prussian blue nanocomposite-modified graphite, graphene-modified carbon, Co(II)phthalocyanine-modified carbon, and Au nanoparticle ink to improve detection. The electrochemical properties of SPEs are not as good as traditional metallic and conductive carbon electrodes with regard to electron transfer kinetics and electrode resistance, even with such modifications.

Chapter 2 Research Motivation

The research aims to develop the processes that can be utilized to fabricate highly performing urea sensors by investigating the mechanism of the synthesis of catalysts, the coating of the catalysts, and their properties. The research tasks focus on developing non-enzymatic catalysts for urea sensors with an emphasis on the increase of sensitivity of devices fabricated via a facile synthesis approach on a flexible substrate. The following objectives and tasks are proposed to complete my research.

2.1 Hydrothermal synthesis of a hierarchical structure of NiO catalyst for urea detection

This chapter is focused on the development of catalyst synthesis for a higher sensitivity sensor. Non-enzymatic catalyst materials have been widely examined to resolve the problems associated with enzyme-based sensors, such as high fabrication costs, complex enzyme immobilization processes, and a lack of long-term stability due to enzyme denaturation, which may occur due to high temperature and low or high humidity. [6]

Table 2-1 Pros and cons of enzymatic and non-enzymatic sensor

	Sensitivity	Selectivity	Lifetime	Application	Cost
Enzymatic	High	Good	Limited	Limited	High
Non-enzymatic	Low	Bad	Unlimited	Unlimited	Low

Although noble metal is widely used, it ie expensive and susceptible to poisoning in long-term contact with physiological fluids. Nickel metal, a potential non-noble metal catalyst, is unstable and easily oxidized in air and solution, which leads to a gradual change of its catalytic

activity. Therefore, metal oxides are widely used for the electrochemical detection of urea because of their stability against enzymatic-based catalysts, excellent electrochemical properties, and chemical stability, as well as their abundance and affordability. There are a number of nickel oxide-based catalysts that have demonstrated excellent electrocatalytic properties on urea oxidation through the formation of a redox couple of Ni(II) and Ni(III). [7]

Table 2-2 Comparison of the price of catalyst

Compound	**$NiCl_2$**	$PtCl_2$	$PdCl_2$	$AuCl_3$	$RhCl_3$
Price in USD (per 1mmol)	**0.1**	32.2	5.8	35.6	51.8

One of the most popular methods for the synthesis of metal oxide nanostructures among the various synthesis methods has been the hydrothermal method, which has gained the attention of scientists and technologists from a wide range of disciplines, particularly within the last fifteen years. [35] This method can be effective in improving the crystallinity and shape selectivity of oxide-based materials. The main advantages of hydrothermal processing are the absence of hazardous catalysts, the production of highly monodispersed particles with controlled size and morphology, and the high purity of the product. [36]

Because the Faradaic electrochemical processes occur only on the surface and near the surface of NiO, which is a pseudo-capacitance material, surface properties, including the morphology, the surface area, and the pore size distribution, play a crucial role in this process. [91]] Since the electrochemical performance of NiO is closely correlated with its porosity and surface area, recent research has focused on synthesis methods and morphology studies. Therefore, hierarchical synthesis can contribute to enhancing the detection capabilities of urea electrochemical sensors. The electrochemical reaction occurs only at several surface layers, which

makes it difficult to achieve an ultimate theoretical sensitivity due to its intrinsically low conductivity. An effective way to synthesize NiO nanostructures with abundant surface-active sites must be developed to address this problem. In order to address these challenges, NiO morphologies ranging from mesoporous nano-urchins to porous nanotubes to hollow core-shell microspheres were investigated. To create the hierarchical structure, many complex morphologies and processes have been introduced.

In a study by Wu et al. [12], nickel hydroxide electrodes with cup-like pore arrays were developed that are capable of serving as an effective catalyst layer for the electrolysis of urea on stainless steel foil by cathodic electrodeposition using a monolayer of polystyrene spheres.
By using a cup-like pore array, more active sites were exposed to the electrolyte during the electrolysis of urea, which resulted in improved electrocatalytic performance over a film electrode. The desired structure, however, required the assembly of a monolayer of PS spheres on SS substrates prior to nickel hydroxide deposition. In the next step, nickel hydroxide was electrochemically deposited. Despite the two steps, the nickel hydroxide electrode containing PS spheres was immersed in a toluene solution several times to remove the PS hard template completely. Although these processes enhance the electrocatalytic performance, post-process steps such as hard template deposition, removal, and cleaning are tedious and difficult to prepare, as well as the risk of catalyst degradation or poisoning during removal. These complex hierarchical structures are achieved through complicated multistep processes, such as nano cup arrays using PS beads[12], hard templates using SBA-15[92, p. 15], and hard templates using Ni foam as a scaffold. [31]

For the purpose of overcoming the challenge of fabricating a hierarchical structure, I propose to use a soft template with a hydrothermal method, which can result in increased catalytic

efficiency and a simpler catalytic preparation process than the hard template method. In my research, sodium dodecyl benzene sulfonate (SDBS) surfactant was employed as a soft template for the synthesis of hierarchical hollow nickel hydroxide spheres.

A soft template has been used in some studies for the nucleation and growth of metal oxides using a hydrothermal method. On top of the vesicle of multilayer SDBS, several micron-sized spheres were fabricated using the hydrothermal method by Qin et al. [93] Luo et al. synthesized hollow Cu_2O spheres with 300 nm diameter using anionic vesicles as templates. [94] Soft templates may come from vesicles, but the mechanism is still unclear, especially for large vesicle structure.

An amphiphilic surfactant, SDBS has a hydrophilic head and a hydrophobic tail. There is a well-established relationship between concentration and the degree of aggregation into micelles, vesicles, and bilayer sheets that reduce surface area. Accordingly, I assumed that the morphology of the synthesizing particles would follow the shape of the aggregate if they nucleated and grew on top of it during the hydrothermal process.

Throughout this chapter, the hierarchically structured catalyst is the key focus. It was discussed in the chapter how the structure was synthesized, its benefits, and its mechanism. The effect of hierarchical structure on current response and sensing performance was observed by comparing other shaped NiO particles.

2.2 Alternating current (AC) EPD for morphology control

The electrophoretic deposition (EPD) technique has recently gained increasing attention both in academia and in the industrial sector due to its broad range of novel applications in the processing of advanced ceramic materials and coatings. In addition, due to its versatility and cost-

effectiveness, the apparatus can be used with a wide range of different materials and their combinations. Although the basic phenomena involved in EPD are well known and have been the subject of extensive theoretical and experimental research, the governing equation for EPD was first proposed by Hamaker [66] in the 1980s. Researchers continue to focus on developing more accurate quantitative models or fundamental mechanisms of EPD, so that the working parameters of EPD can be optimized for broader applications in materials processing. [69] The EPD technique has been used successfully for a thick film of silica[95], nano-size zeolite membrane[96], hydroxyapatite coating on the metal substrate for biomedical applications [97], luminescent materials [98], high Tc superconducting films[99], gas diffusion electrodes and sensors [100], multi-layer composites [101], glass and ceramic matrix composites by infiltration of ceramic particles onto fiber fabrics [102], oxide nanorods, carbon nanotube film [103], functionally graded ceramics [104], layered ceramics [105], superconductors [106], piezoelectric materials [107], etc. In fact, EPD has intrinsic disadvantages when compared to other colloidal processes (such as dip coatings and slurry coatings), which include that water cannot be used as a liquid medium because the application of voltage to water causes the evolution of hydrogen and oxygen gases at electrodes, adversely affecting the quality of the deposits formed. This limitation can, however, be mitigated by using a number of non-aqueous solvents. In the first place, a preliminary result examines how DC-EPD behaves with the protective coating applied to PEMFCs. By parametric study, including voltage, time, and particle size, the experimental results investigate and compare the reported EPD equations.

It was found that alternating current (AC) instead of direct current (DC) was more effective in controlling the morphology of anisotropic nanostructures when coated with EPD. A

hypothesized effect of controlling deposit morphology by AC-EPD is that it can increase electrochemical signals by increasing the reaction area of the catalyst surfaces on sensor surfaces.

In the literature, alternating current (AC) was utilized for electrolysis suppression when the EPD process uses water (aqueous) as a solvent. [108], [109] The formation of oxygen or hydrogen bubbles during water decomposition can be avoided by AC fields. AC–EPD allows electrophoretic deposition from aqueous suspensions rather than organic solvents (such as ethanol), which is a significant advantage from a safety, economic, and environmental perspective, while maintaining the surface quality and processing rate of DC–EPD using organic solvents. Regarding ionic mobility, it is known that the reduction of protons to molecular hydrogen and the oxidation of hydroxyl ions to molecular oxygen have sluggish reaction rates as they involve the transfer of more than one electron and involve significant molecular rearrangement upon electron transfer. Because of this, when the frequency of the applied AC field is sufficiently high, nearly all of the current flows through the double-layer capacity, so there is no gas bubble formation from water decomposition. In accordance with the concept above, Neyrinck et al. implemented AC-EPD to suppress electrolysis in an aqueous solvent. [108] In an asymmetric AC-EPD, electrophoretic deposition from aqueous suspensions at high voltages is possible, and AC-EPD avoids the formation of gas bubbles on the electrode when electrolyzing water.

Several studies have attempted to control the deposition morphology using AC-EPD. Kollath et al. compared EPD under AC and DC field conditions. [110] At similar thicknesses, AC-EPD provides denser and less cracked coatings than DC-EPD. According to their conclusion, AC-EPD is advantageous for depositing powders with broad particle size distributions since it can control particle migration according to wave asymmetry and frequency. The coating characteristics can be improved by fine-tuning the asymmetry of the AC wave and the frequency. Riahifar et al. [111]

investigated the influence of AC electric field on electrohydrodynamic fluid flow. At frequencies between 10 Hz and 1000 Hz, the combined effect of induced fluid flow (AC electroosmosis) and electric forces can be used to demonstrate sorting nanoparticles. Calzavarini et al. [112] reported anisotropic particle behavior in convective turbulence flow. According to the simulation, particles with small-scale turbulence align more preferentially. If the particle shape is oblate (more like a disk shape), it tends to tumble much faster than if it is prolate (more like a rod shape).

In light of the above reports, I hypothesize that rotations, tumbling, and spinning of suspended particles under turbulence, especially with anisotropic shape material, may induce particle alignment. The AC EPD changes the bias between the anode and cathode periodically, which results in periodic changes in the direction of the suspended particles. When the duty cycle or waveform is adjusted asymmetrically, it can lead to the net movement toward the substrate while the suspended particles repeat moving forward and backward.

As far as I know, AC-EPD is only used for preventing electrolysis in aqueous solvents [109] [108], and sorting [111], but no one discussed utilizing the AC field to control the morphology of deposition when using anisotropic catalyst material and examining their electrochemical properties. The organic solution(ethanol) was used as a solvent to minimize the possibility of water electrolysis in the preliminary results. To utilize more effective and environmentally friendly process, the aqueous solvent was also dealt with AC-EPD.

2.3 Paper-based sensor fabrication for highly sensitive urea sensor.

First introduced in 2007 by the Whitesides group, paper-based analytical devices (PADs) use porous cellulose to store reagents, with water adding capillary action to generate flow. Flow paths are controlled by hydrophobic materials printed on paper. [78] The use of patterning in these

devices improves their overall functionality in contrast to traditional analytical techniques using paper as a substrate.

It is obvious from the many articles describing applications of PADs in clinical, food, and environmental fields that the paper is very attractive as a substrate for designing analytical platforms. PADs and electrochemical detection offer a good combination for developing inexpensive, portable, and sensitive devices. A majority of electrochemical biosensors utilize the enzymatic method. However, enzymes have a limited shelf-life, are expensive, and require complicated operating conditions. In order to overcome these limitations, a non-enzymatic urea sensor has been attracted because of its good stability, re-usability, simplicity, and low cost. As a non-enzymatic catalyst, NiO has excellent catalytic activity when it forms the redox couple Ni(II) and Ni(III) to detect urea. Although NiO has many advantages over enzymatic catalysts, it still doesn't have the same sensitivity as enzymatic sensors. Several approaches for increasing the reaction surface area of the non-enzymatic sensor were investigated vigorously, including hierarchical structures and support matrices. Nevertheless, it is accompanied by a series of complicated steps.

Accordingly, from an engineering perspective, the incorporation of NiO into paper is beneficial to the urea sensor. This will take advantage of its complex porous structure and simplify preparation processes due to the capillary action of paper. By combining NiO and the utilization of paper as a substrate, an improvement in the sensitivity of the sensor can be achieved.

The major challenge is to overcome the limitations of a non-enzymatic catalyst, low sensitivity, and increasing reaction surface area by taking advantage of the paper's cellulose structure. In addition to the main problem, there are also other problems with using paper as a substrate. Firstly, the paper has to be modified so that the electrode area on the paper becomes conductive. A widely

used method for making it conductive is to apply carbon paste with a screen printing technique on the paper substrate. The paper is easily coated with screen printing, but the porous cellulose network of the paper is diminished. Therefore, NiO is applied on top of a flattened carbon pasted layer. In order to make use of the paper's porous network, a different but simpler dip-coating method was used. As a fabrication method, dip coating is perfectly suited when using paper due to its capillary action. If the paper substrate is soaked in a mixture containing NiO catalyst and CNT conductive medium, the mixed solution can easily penetrate into the fibrous structure of the paper. As the paper dries, NiO and CNT are placed on top, which provides a higher surface area of reaction for the urea and NiO reactions thanks to the higher porosity of the paper, as well as a high conductivity to transfer current during the reaction between the two. As a matter of fact, the process is much simpler than screen printing. Simple drop casting, for instance, distributes catalyst solution through the pores in cellulose fiber structures with the flow of solvent (di water). Based on my investigation of the #1 chromatography paper with SEM, it has an average fiber diameter of 14 μm and an average pore size of 43 μm (defined as the space between fibers on top). In other words, the catalyst can penetrate inside the pores and be deposited on top of the fiber as long as the size is several microns or lower. And the stability and mechanical strength of prepared paper during reaction should be considered for the application of flexible sensing devices.

Paper is a very suitable choice for flexible device applications. It is also worth noting that if the complex network of paper is utilized well, then the capability of enhancing the sensitivity, and thus overcoming the limitations of the non-enzymatic sensor, could be achieved. As part of the engineering aspects of this project, parametric studies will be carried out in order to enhance sensitivity by means of paper.

Chapter 3 Experimental

3.1 Hydrothermal Synthesis of metal oxide

To synthesize NiO particles using a hydrothermal system, 4 mmol of nickel chloride hexahydrate ($NiCl_2$•$6H_2O$) (Alfa Aesar), 8 mmol of ammonia solution (26%) (Alfa Aesar), and different concentrations of SDBS (Sigma Aldrich) were dissolved in 40 ml of deionized water. After stirring all chemicals vigorously for 2 hrs, the solution was transferred into a Teflon-lined steel autoclave and kept in the oven for 6 hrs at 160°C. The product was washed with DI water and ethanol several times, centrifuged, and dried for 10 hrs at 80°C, and dried powders were collected. The powders were calcinated at 400°C for 2 hrs. After calcination, NiO nanoparticles were obtained. The synthesized NiO was added in ethanol (2g/L), and then the suspension was ultrasonicated for 1 hr to break agglomerates prior to EPD process.

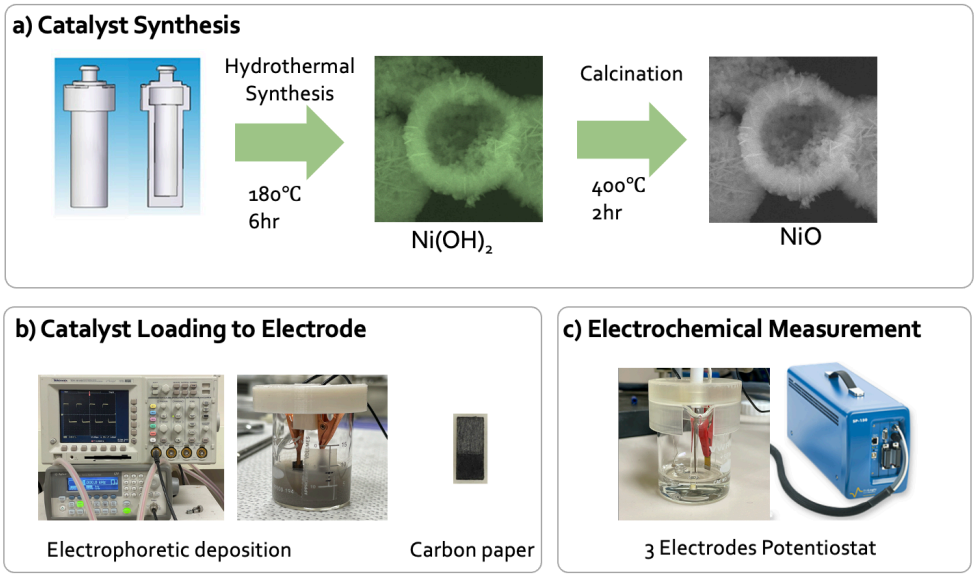

Figure 3-1The experimental process of fabrication of urea sensor

3.2 Electrophoretic deposition of NiO

3.2.1 Parametric study of DC EPD with TiN

Commercially available titanium nitride (TiN) powders with different particle sizes of 20 nm, 800 nm (US Research Nanomaterials, Inc), and 3 μm (Sigma-Aldrich) were used to prepare suspensions in anhydrous ethanol (Fisher Scientific). Polyethyleneimine (PEI, molecular weight : 25,000, Alfa Aesar) and Poly(diallyldimethylammonium chloride) (PDADMAC, low MW : ~100,000 , med MW : 200,000 ~ 350,000, Sigma Aldrich) were added as a charging agent. For most experimental conditions, 0.253 wt% of TiN and 0.006 wt% of the PDADMAC were used. To investigate the effect of pH on the suspension and coating layer, the pH level of the suspensions was adjusted by adding ammonium hydroxide (Sigma-Aldrich) for the basic condition and acetic anhydride (Sigma-Aldrich) for the acidic condition. The suspensions were ultrasonicated for 1 hour to break agglomerates before EPD process. All stainless steel substrates were cleaned with ethanol and DI water by ultrasonication prior to EPD. The 316 stainless steel was used for the working and counter electrode. The DC power supply (Agilent 6645A) and power amplifier (Trek PZD 700) were used to generate electric fields for the EPD process. The area of each electrode was set as 1 cm^2, and the distance between the two parallel-plate electrodes was kept at 1 cm. The working and counter electrodes were connected to the power supply and then submerged into the prepared suspension. Varying voltage and time were applied for the EPD process. After deposition, the coated substrates were dried in air for 12 hours at room temperature, and the weight change was measured.

3.2.2 AC-EPD for Non-enzymatic Urea sensors

To synthesize the NiO nanoplates using a hydrothermal system, 4 mmol of nickel chloride hexahydrate ($NiCl_2{\cdot}6H_2O$) (Alfa Aesar), 8 mmol of ammonia solution (26%) (Alfa Aesar), and 2

mmol of cetyltrimethylammonium bromide(CTAB) (Sigma Aldrich) were dissolved in 40 ml of deionized water. After stirring all chemicals vigorously for 2 hrs, the solution was transferred into a Teflon-lined steel autoclave and kept in the oven for 24 hsr at 160°C. The product was washed with DI water several times, centrifuged, and dried for 24hr at 50°C, and dried powder was collected. The powder was calcinated at 400°C for 2 hrs. After calcination, NiO nanoparticles with hexagonal plate structure were obtained. The synthesized nanoplates were added to ethanol (1.67g/L), and then the suspension was ultrasonicated for 1hr to break agglomerates prior to an EPD process. For EPD, carbon paper and stainless steel were used as the working and counter electrodes. The distance between the two electrodes was kept constant at 1 cm. To set up the waveform of the electric field, a function generator (Agilent 3320A) and amplifier (PZD 700) were used.

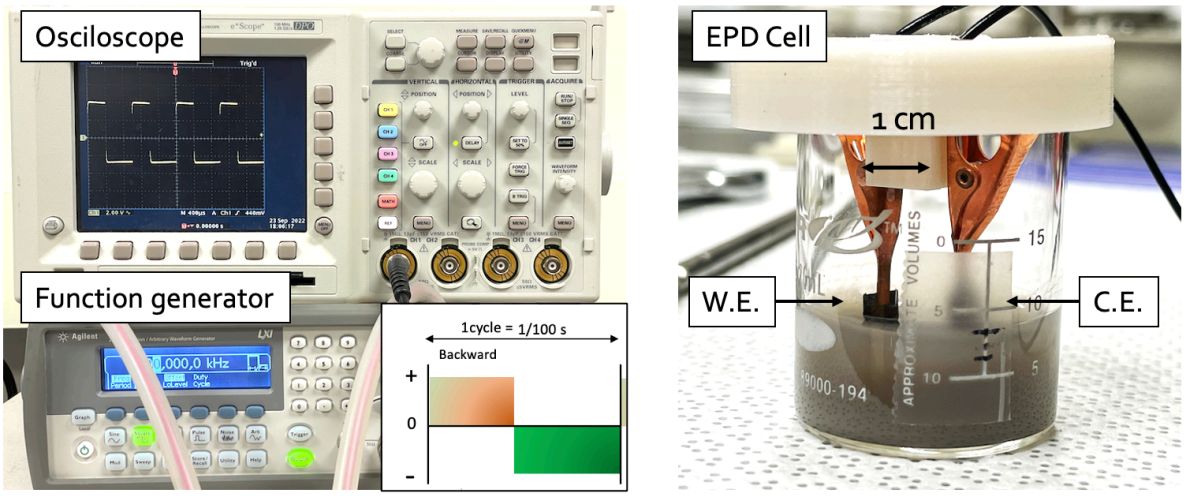

Figure 3-2 Experimental configuration of AC-EPD

3.3 Paper-based sensor fabrication

3.3.1 Fabrication of screen-printed paper substrate

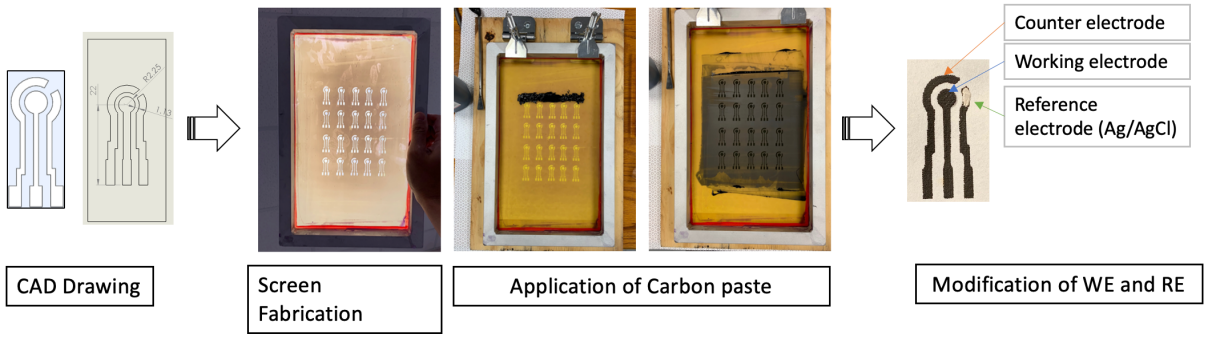

Figure 3-3 Fabrication process of a paper-based substrate by a screen printing method

As part of the process of making three electrodes system into the paper, the entire circuit, suitable for the point-of-care, was designed using Solidworks, a CAD program. The image was printed on transparent PET paper in order to mask the light. After applying the photosensitive polymer to the screen, the masking was attached to the screen. It was lit to solidify the photosensitive polymer and washed until the masked polymer was removed. Through the designed open part of the screen, the carbon paste can penetrate. The paper was located under the screen frame and the carbon paste was squeezed on it. The coated paper was dried for 6 hrs to ensure loading of the catalyst material on the working electrode area. A pseudo reference electrode was created by using Ag/AgCl ink as a reference electrode. Throughout all experiments, Wattman #1 chromatography or filter paper was used.

3.3.2 Fabrication of paper strip from dip coating

For strip fabrication, Wattman filter paper No.1 was cut into 0.5 mm x 3 mm strips. In order to prepare the strip, it was cut into 0.2 mm x 0.5 mm and attached on the working electrode to the catalyst circuit. MWCNT was used as a conductive medium for the general strip and NiO nanopowder (20 nm, Sigma Aldrich) as the catalyst. In the mixing solution, SDBS was added as a

surfactant. The first step was to mix NiO, MWCNT, and SDBS in DI water vigorously for 10 minutes with a stirrer. For strong dispersion of CNT and MWCNT in solution, a tip-ultrasonicator was used. (100W, 10 min)

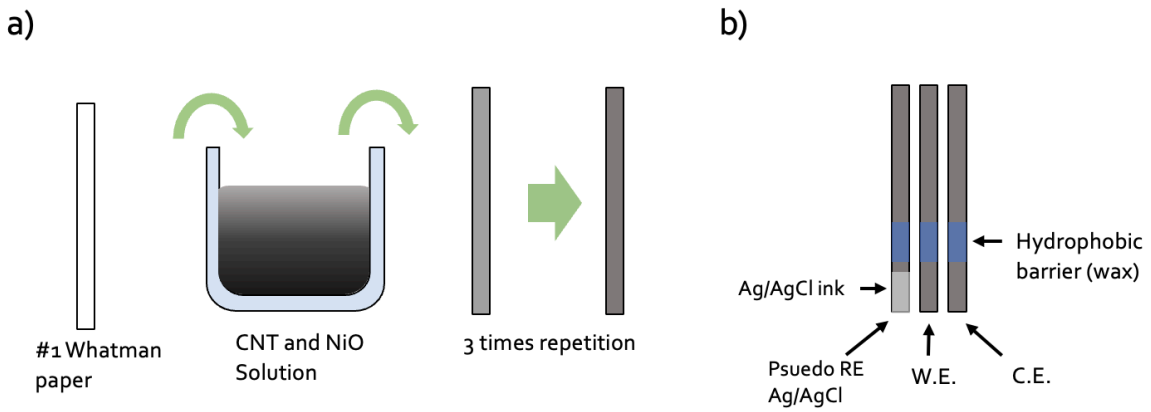

Figure 3-4 Fabrication process of strip electrode by dip-coating method

3.3.3 Characterization

The structure of NiO was characterized by using an X-ray Diffractometer (XRD, Bruker D8 Discover) with Cu Kα radiation in the 2θ range from 20° to 80° with a step size of 0.02°. The morphology of the NiO layer deposited by EPD was investigated by a field emission scanning electron microscope (FESEM, JEOL JSM-7000F). The electrochemical oxidation of urea was investigated by cyclic voltammetry in a three-electrode configuration with 1 M KOH and 0.33 M urea. Ag/AgCl and Pt wire were used as the reference and counter electrodes, respectively. The NiO-deposited carbon paper was used as the working electrode (5 x 5 mm). The cyclic voltammetry was measured by a potentiostat (Biologic SP-150). The scan rate varied from 10 to 100 mV/s, and the range of potential was set from -0.2 to 0.7V.

Chapter 4 Hierarchical nickel oxide for urea detection

4.1 Introduction

With various synthesizing techniques, nickel oxide has been synthesized in various morphological structures including nanoflakes, nanosheets, nanoflowers, nanoballs, nanowires, nanorods, nanotubes, nanoneedles, and nanospheres. These include wet chemical synthesis, hydrothermal synthesis, sol-gel synthesis, thermal decomposition, microwave synthesis, and many others. Among them, the hydrothermal method uses a heterogeneous reaction taking place under high temperature and pressure under aqueous solvents to synthesize or recrystallize nanomaterials. Using hydrothermal methods, high-purity nanostructured NiO can be obtained by varying reaction temperature, pH, and pressure. [113]

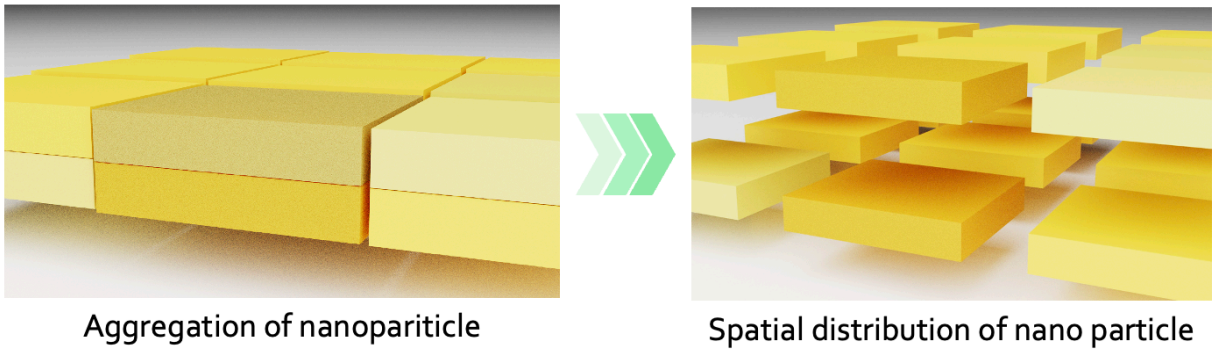

Figure 4-1 Schematic of an analogue of hierarchical structure

Despite the wide use of nanoparticles for research, they have drawbacks: nanoparticles aggregate easily due to the inverse relationship between particle size and the van der Waals attraction. As the aggregate becomes larger, only the primary particle near the surface participates in catalysis, while the inner part remains inactive. The hollow structure, however, has well-defined voids within, which corresponds to the high specific surface area, making species transportation

easier. At the interface between solids and liquids, electrolytes or ions are transported. It is possible for active catalyst materials to easily access urea molecules because of those interior voids. When repeated measurements are conducted, hollow structures can withstand large volume changes and structural strain, which leads to better cyclability and stability.

The low utilization of active materials resulting from electrochemical reactions, which only occur at surface layers, makes it difficult to achieve high theoretical sensitivity with electrochemical sensors. A way to resolve this issue is to synthesize NiO nanostructures with abundant surface active sites and short transport pathways for analytes. For this reason, a variety of NiO morphologies have been investigated in the literature, including mesoporous nano-urchins, porous nanotubes, and hollow core-shell microspheres. As another means of improving NiO's electrochemical performance, highly conductive materials can be incorporated into it.

Table 4-1 The literature using hard template of foam for synthesis of hierarchical structure

Catalyst	**Structure**	**Template**	**Application**	**Ref.**
NiO	Nanosheet	Ni foam	Urea sensor	[28]
SnO_2	Hollow sphere	Polymer bead	lithium storage	[29]
TiO_2	Tubular structure	ZrO_2 fibers	-	[30]
SnO_2	Hollow sphere	Silica	-	[22]
$Ni(OH)_2$	nanocup array	PS sphere	electrolysis of urea	[12]
FeOOH	Hollow sphere	SiO_2	water remediation	[23]

It is usually a multistep procedure to fabricate those hierarchical structures, using PS-bead arrays [12] and Ni foam scaffolds as hard templates. [31]

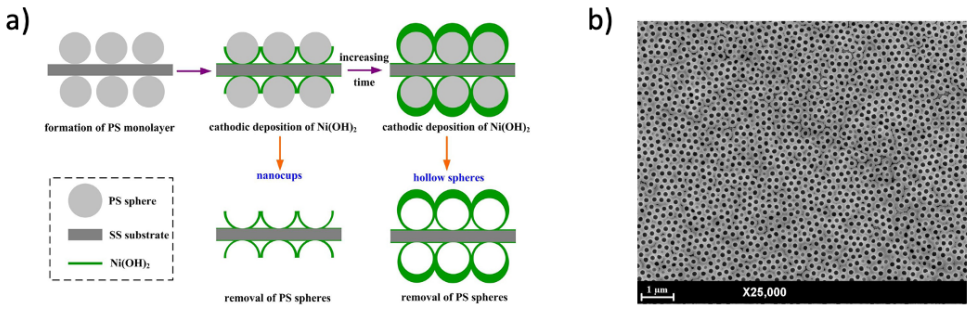

Figure 4-2 Schematic electrochemical formation of nickel hydroxide electrodes with a monolayer of nano cup arrays and hollow spheres. [12]

Many researchers have attempted to make more exposed active sites on catalysts by using hard templates, a process well-known in the field. For example, Wu et al. [12] fabricated nano cup-like pore arrays from polystyrene spheres, which are much more effective for urea oxidation reactions than films. It is, however, necessary to proceed with additional steps to deposit PS beads as a template, and to remove the template for PS spheres after immersion in toluene for 10 minutes, to rinse it with DI water, and to dry it at 100°C for 30 minutes.

In spite of the fact that the fabricated catalyst enhances the electrocatalytic performance, pre-processing such as hard template deposition, and post-processing such as removal and cleaning require additional steps to prepare the electrode. As a resolution to this issue, one-pot hydrothermal was introduced with additives as soft templates. Afterward, those prepared catalysts can be cast on desired paper substrates. To synthesize the hierarchical hollow sphere nickel oxide, sodium dodecyl benzene sulfonate (SDBS) was introduced to achieve the desired properties in this work. It was possible to prepare a hollow sphere shape of $Ni(OH)_2$ using one-pot hydrothermal synthesis, but it is composed of thin nanosheets that are spaced widely apart. (Figure 4-3) As part of this chapter, the morphological modification of the catalyst through synthesis was addressed in addition to the benefits and mechanism of hierarchical catalysts. As a result of the structural benefit,

the enhanced performance was demonstrated considering calcination temperature, SDBS concentration, sensitivity, LOD, and selectivity. All experiments in this chapter are conducted with hierarchical hollow NiO (2-3).

4.2 Characterization of hierarchical NiO

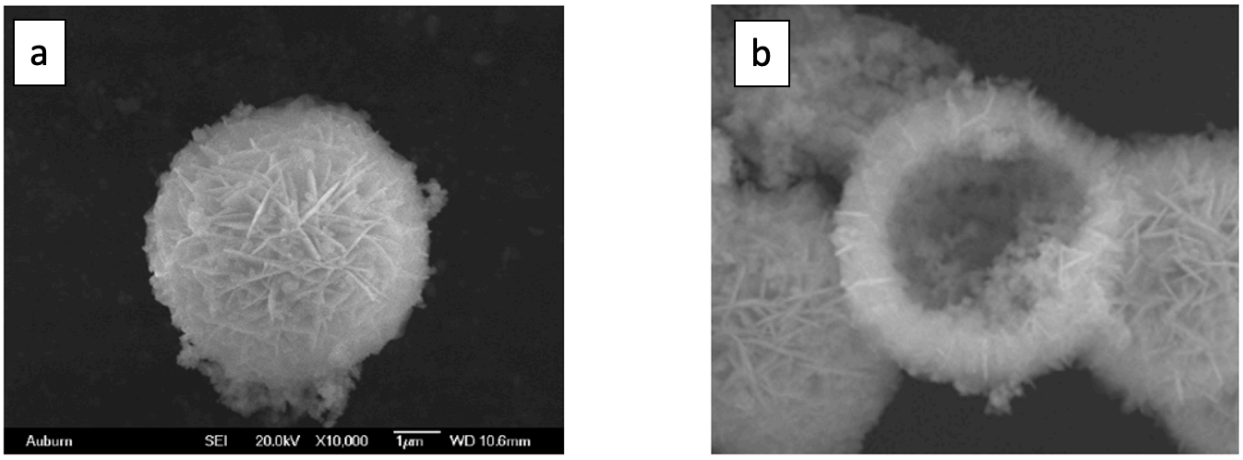

Figure 4-3 SEM results of a) hierarchical NiO hollow sphere, b) hollow structure from the broken sphere

The SEM results confirm that the hierarchical spheres of NiO were well synthesised by the hydrothermal method using SDBS soft template. By investigating the broken sphere, it was possible to confirm the hollow interior, and it was observed that 2D nanosheets of 15 ~ 25 nm comprised the 3 ~ 5 μm-sized 3D sphere.

NiO and $Ni(OH)_2$ (as prepared) samples with varying calcination temperatures were prepared and characterized. Calcination was processed for 2 hrs in an air environment with a heating rate of 5°C/min. The patterns for 'as prepared $Ni(OH)_2$' and calcined at 200°C shows diffraction peaks of $Ni(OH)_2$ and are confirmed by standard JCPDS 14-0117: 33.2°, 38.5°, 52.1°,

and 59.2° corresponding (100), (101), (102) and (110). 200°C is below the temperature of the dihydroxylation reaction ($Ni(OH)_2 \rightarrow NiO + H_2O$), hence the pattern of $Ni(OH)_2$ is still observed.

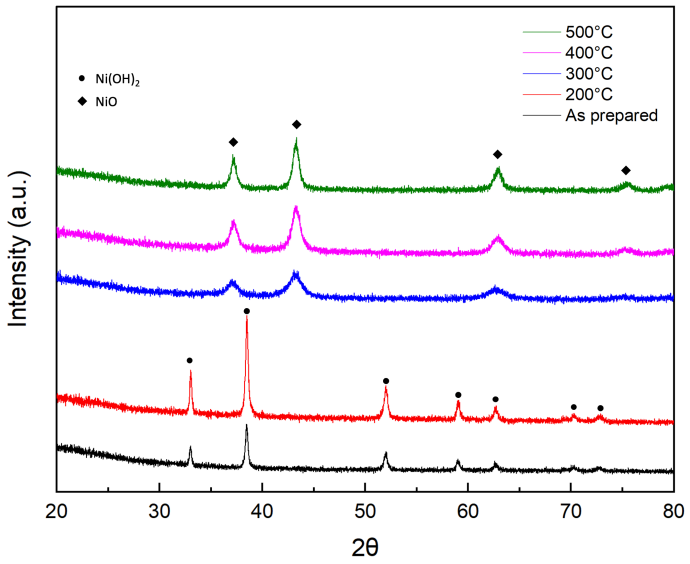

Figure 4-4 XRD patterns of hierarchical NiO with varying annealing temperature

At around 350°C the dihydroxylation process is finished from the TGA result. The sample at 300°C is under the dihydroxylation process, so the peak intensity is rather lower than others annealed at higher temperatures. The patterns of the materials annealed at 400°C and 500°C show clear diffraction peaks and are well matched with the standard powder diffraction pattern of NiO. (JCPDS 47-1049: 37.2°, 43.3°, 62.9°, 75.4°, and 79.4° correspond to the (111), (200), (220), (311) and (222) planes of NiO, respectively)

Peak intensity of NiO increases with calcination temperature, reaching a maximum at 500°C. Depending on the annealing temperature, the intensity of the peaks varies. A high calcination temperature provides highly intensive diffraction peaks, which indicates an increase in the degree of crystallization with increased crystallite size.

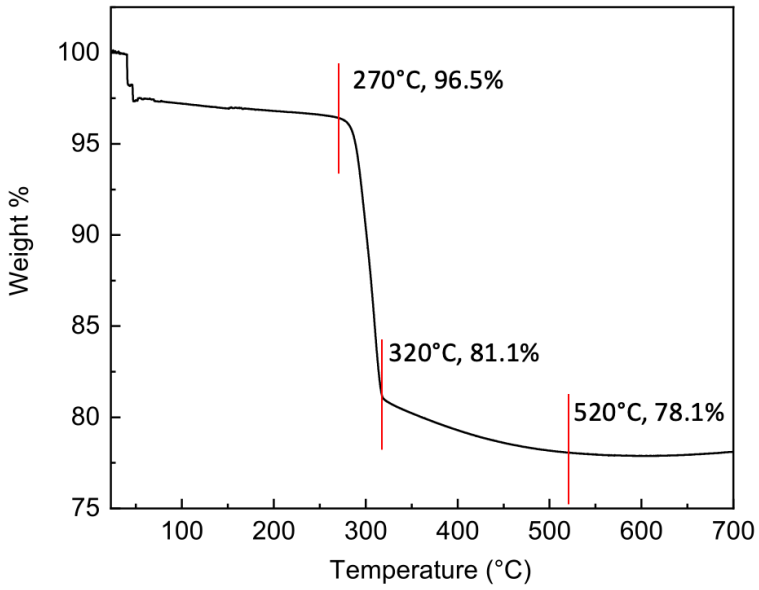

Figure 4-5 TGA result of hierarchical NiO sphere

Figure 4-5 shows the thermal gravimetric analysis (TGA) result of hierarchical $Ni(OH)_2$. As-synthesized particle from hydrothermal synthesis is nickel hydroxide ($Ni(OH)_2$). After calcination at 400°C for 2 hr, hierarchical NiO was prepared. In this TGA analysis, the $Ni(OH)_2$ 'as synthesized' particle was used.

The first step of weight loss of 3.5% below 270°C is due to the removal of surface and interlayer water molecules. In the second step, a weight loss of 15.4% at the temperature between 270°C and 320°C comes from the de-hydroxylation of hydroxide layers in nickel hydroxide. After two steps, a slight change in weight was observed, which implies that the formation of NiO nanoparticles is almost complete. The observed thermal stability result is in good agreement with those repored in the literature. [114]–[117]

4.3 Effect of concentration of SDBS

As reported in the literature, vesicle structure forms as SDBS concentration increases. [118] [119] It also serves as a soft template, and nucleation is preferable on the surface of SDBS due to the electrostatic absorption. In Figure 4-6, the increase of SDBS concentration results in the reduction of nanosheet thickness from 20 nm to less than 10 nm, probably due to a stronger steric effect from combined SDBS between nanosheets. With a further increase in amount of SDBS, the inhomogeneous rod shape was observed. As the concentration of SDBS is raised, the vesicle structure is deformed, and can be transformed into a long fiber structure.[118] As the SDBS structure in solution transforms, the resultant synthesized particle follows the structure since it functions as a soft template during hydrothermal synthesis.

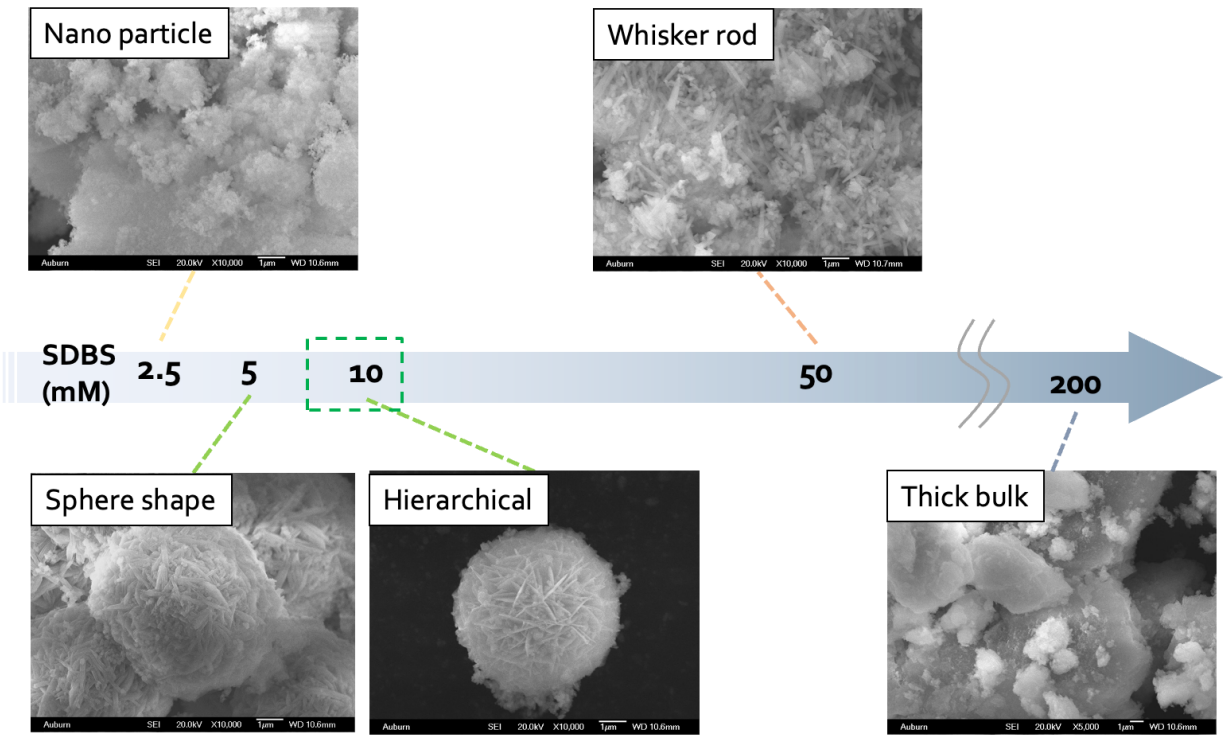

Figure 4-6 Effect of SDBS concentration from 2.5 to 200 mM

4.4 Effect of the ratio between Ni^{2+} and SDBS

From the default condition (forms hierarchical structure), the ratio between Ni^{2+} and SDBS was controlled. SDBS amount was kept. Ni salt ($NiCl_2$ $6H_2O$) was varied during synthesis.

Table 4-2 The ratio between Ni^{2+} and SDBS where hierarchical structure is observed

Precursors	Concentration	Ni^{2+}/ SDBS
$NiCl_2$ $6H_2O$	100 mM	10
SDBS	10mM	

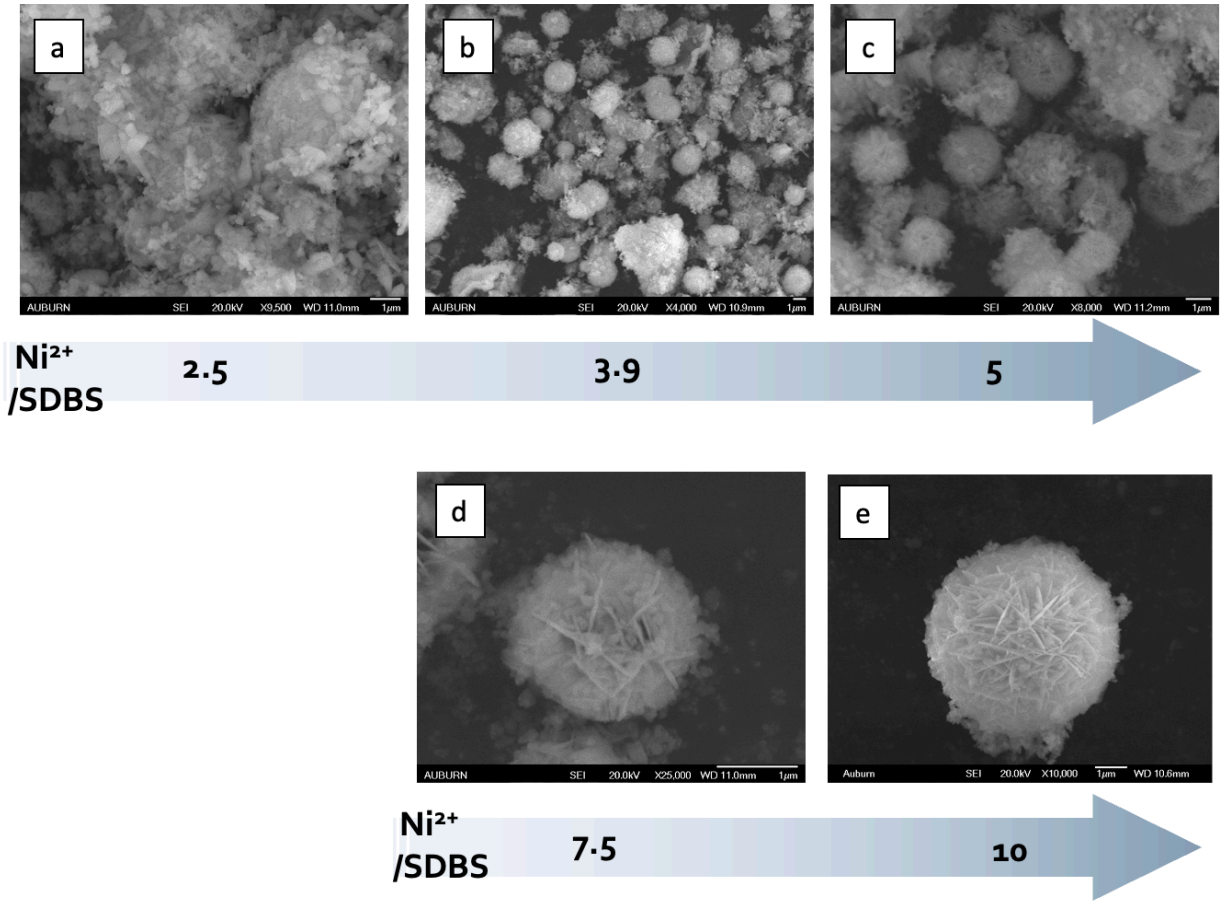

Figure 4-7 The effect of the ratio of Ni^{2+}/SDBS (Ni^{2+} salt concentration) from 2.5 to 10

If concentration of Ni^{2+} is lower, the hierarchical hollow sphere was not occured, though SDBS was kept same.

The concentration of SDBS may not be only factor for the vesicle formation. The combination of Ni^{2+} ion and SDBS together comprieses the vesicle sphere (soft template), and nucleation and growth occurs.

4.5 The mechanism of SDBS-assisted hierarchical hollow sphere

The mechanism for the synthesis of NiO hierarchical hollow sphere structure was proposed on the basis of the experimental result above and analysis. SDBS is an anionic amphiphilic surfactant comprised of sulfate hydrophilic and hydrocarbon hydrophobic segments. To lower the surface energy, they aggregate and the form the sphere shape. Depending on the property of counter-ion, the presence of an organic copound, and the temperature of solution, their aggregation shape is different.

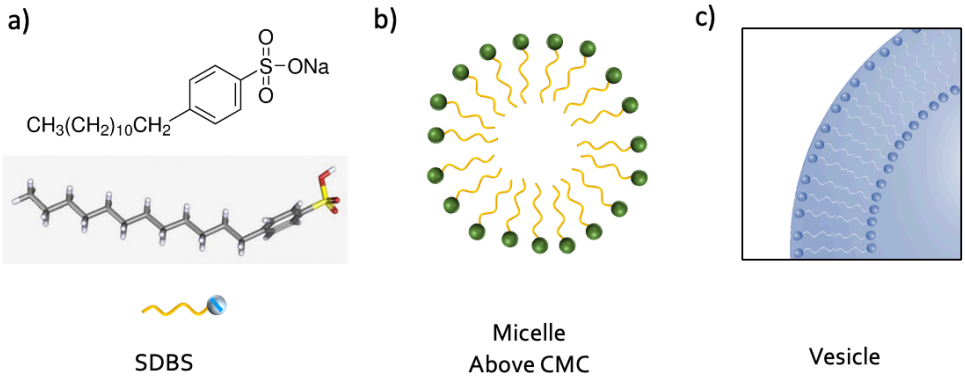

Figure 4-8 Schematic of a) SDBS, b) micelle, and c) vesicle structure by amphiphilic surfactant

The concentration of SDBS is definitely an important factor for the evolution of aggregation shape in solution. The study of the effect of concentration (chapter 4.3, Figure 4-6) shows that the morphology of $Ni(OH)_2$ is transformed depending on the concentration of SDBS when other conditions are kept the same. There is only a certain range of SDBS concentration that produces

the hierarchical structure, and that is presumed to be the reason that the bilayer vesicle soft template is formed through the aggregation of SDBS in the synthesis solution at a certain temperature and pressure. And then, the nucleation and growth could happen at the soft template. Since the vesicle has a void interior, when the nucleation and growth of $Ni(OH)_2$ occurs, the resultant synthesized particle has a hollow structure. A further increase in SDBS concentration makes it difficult to maintain sphere shapes, leading to the extended rod shape or deformed bilayer aggregate, which results in the rod shape or bulk $Ni(OH)_2$. The mechanism should be amended to include a counter-ion factor. In our case of hierarchical structure, the concentration of SDBS was not the only factor determining the soft template shape. The experiment about the effect of the ratio between Ni^{2+} and the SDBS (chapter 4.4, Figure 4-7) would more clarify the mechanism.

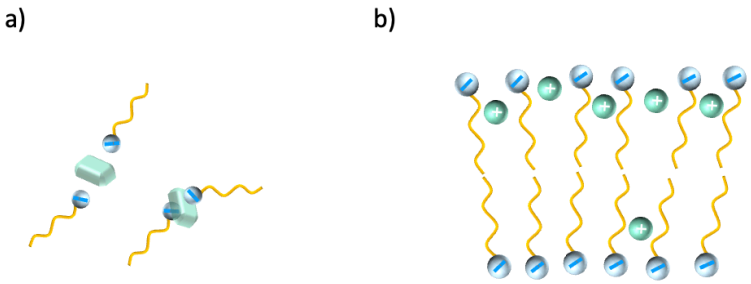

Figure 4-9 Schematic of steric repulsion between nucleate of $Ni(OH)_2$ by absorbed SDBS, and b) complex of SDBS and Ni^{2+}

At first, it was assumed that the vesicle soft template would be formed by SDBS self-assembly in order to lower its surface energy at a certain concentration. Afterward, nucleation and growth occur on the vesicle structure. If the assumption above is correct, the hollow structure should be synthesized even at the low concentration of Ni^{2+} salt (when the SDBS concentration is set at the condition hierarchical structure observed. I will name this condition as a default condition.) However, as shown in Figure 4-7, when the concentration of Ni^{2+} salt is lower than the

default condition, the hollow structure was not observed, which is pivotal evidence that the SDBS concentration is not the only factor determining soft template shape.

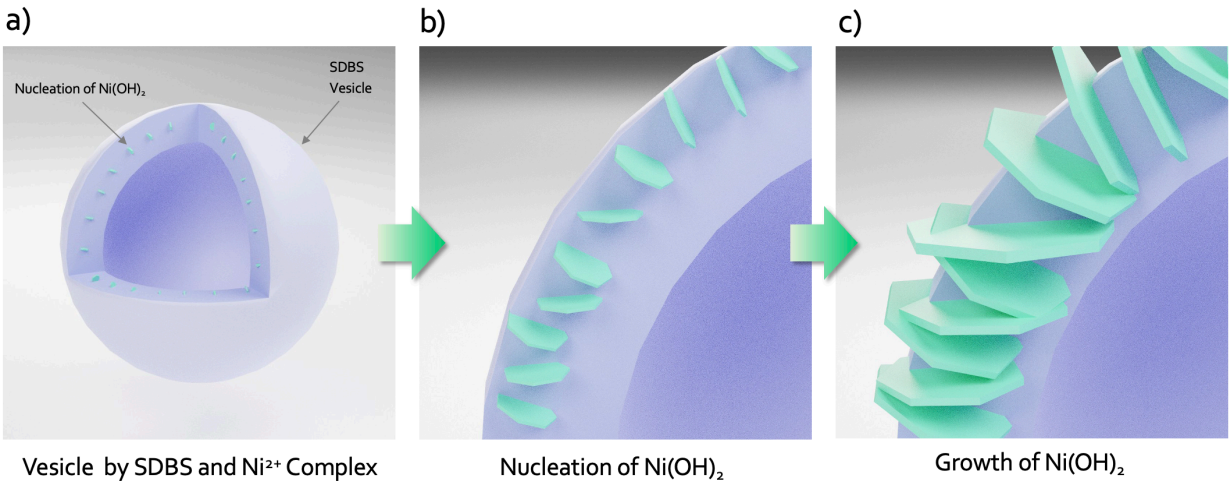

Figure 4-10 Schematic of development of hierarchical structure

A modified mechanism is that the ratio between Ni^{2+} and SDBS plays a crucial role in forming vesicle soft template structure and synthesizing hierarchical structure. The size of the vesicle of amphiphilic surfactant is known to be up to several hundred nm generally. Considering the size of the synthesized hierarchical sphere at several μm, another factor contributed to the aggregation of SDBS, namely the presence of counter-ion (Ni^{2+}) and the anionic surfactant ($SDBS^-$). When the complex of Ni^{2+} and SDBS was made by charge neutralization, the presence of a Ni^{2+} relieves the repulsion between SDBS, which affects the packing factor of the SDBS. Reducing the effective area of the head group results in closer packing. [57]]

In our synthesis case, the Ni^{2+} functions as the counter-ion. From the complex, much larger vesicle structure is formed in the reaction solution, and then growth within the SDBS layers occurs. The steric repulsion from the long alkane group of SDBS helps nucleation to overcome the van der Waals attraction [130], and they will have a spatial distribution between them. Eventually, the

growth (the sheet shape) intertwines with each other, resulting in the final 2-3 hierarchical structure. Figure 4-10 illustrates the mechanism graphically.

4.6 Effect of scan rate

For the electrochemical tests for UOR, the hierarchical NiO (2-3) was used. The effect of the scan rate was investigated in 1M KOH with the presence of 0.33M urea. This CV result shows that the anodic current for urea oxidation increases rapidly with increasing the potential scan rate.

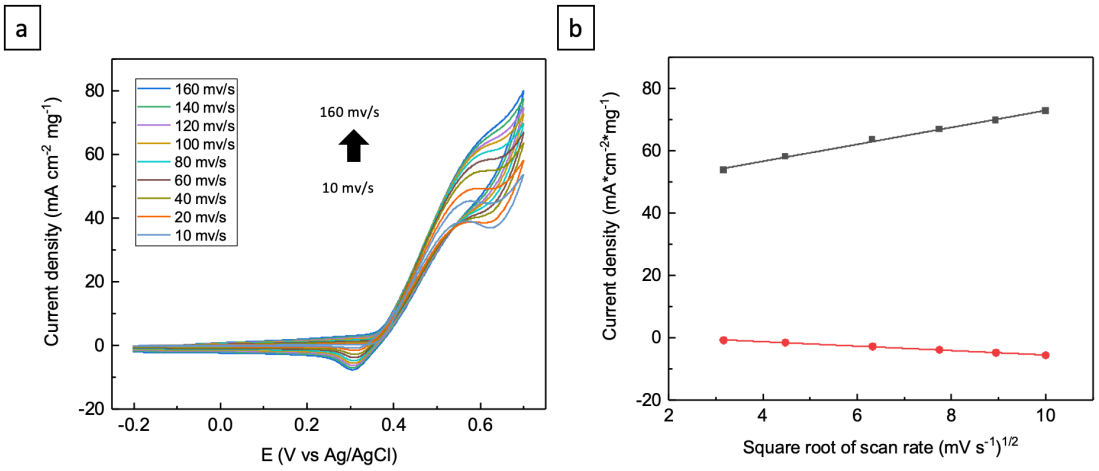

Figure 4-11 Cyclic voltammetry of NiO at 1M KOH + 0.33M urea varying scan rate from 10 to 160 mV/s

Figure 4-11 exhibits that the anodic peak currents at 0.7V are linearly proportional to the square root of scan rate up to 160 mVs^{-1}, which shows a diffusion-controlled process according to Randles-Sevcik equation. The Randles-Sevcik equation describes how the peak current I_p increases linearly with the square root of the scan rate υ ($V\ s^{-1}$).

$$i_p = 0.4463nFAC^0\left(\frac{nFvD}{RT}\right)^{1/2} = \left[0.4463nFAC^0\left(\frac{nFD}{RT}\right)^{1/2}\right]v^{1/2} \quad (4\text{-}1)$$

i_p	peak current (A)
n	number of electrons
A	electrode surface area (cm^2)
C^0	analyte concentration (mol cm^{-3})
v	scan rate (V/s)
D	diffusion coefficient (cm^2 s^{-1})
F	Faraday's constant (C mol^{-1})
R	gas constant (J K^{-1} mol^{-1})
T	temperature (K)

In diffusion-controlled reactions, the formation of products from the catalytic reaction is much faster than the diffusion of analytes. In diffusion-controlled reactions, the reaction rate is equal to the rate of transport of the reactants through the reaction medium. The observed rate of chemical reactions is the rate of the slowest or "rate-determining" step. For this reason, CV result exhibits that the rate-determining step is the mass transport of urea to the electrode governed by the concentration gradient, and the urea oxidation reaction by NiOOH is faster than the diffusion of urea molecules.

4.7 Effect of morphology

Several morphologies of NiO were prepared in order to support the importance of hierarchical structure in electrocatalysts.

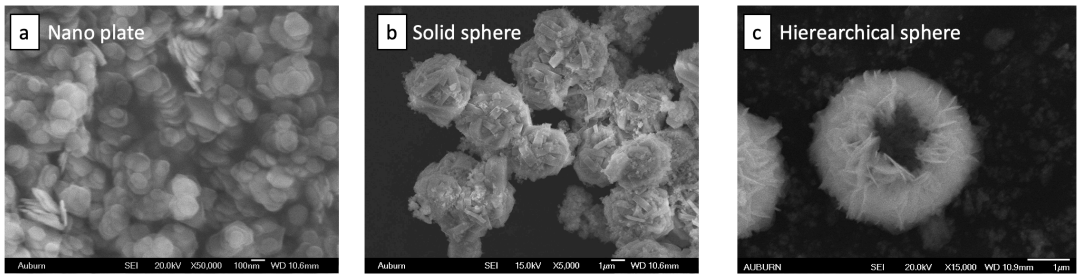

Figure 4-12 SEM images of synthesized three different morphology of NiO: a) nanoplate, b) solid sphere, and c) hierarchical hollow sphere

In this study, a hierarchical hollow sphere was compared with a NiO nanoplate and solid sphere. Because our hierarchical sphere consists of nanosheets, we selected NiO nanoplates for comparison. The solid sphere, which is similar in size to a hollow sphere, was also chosen as the counterpart.

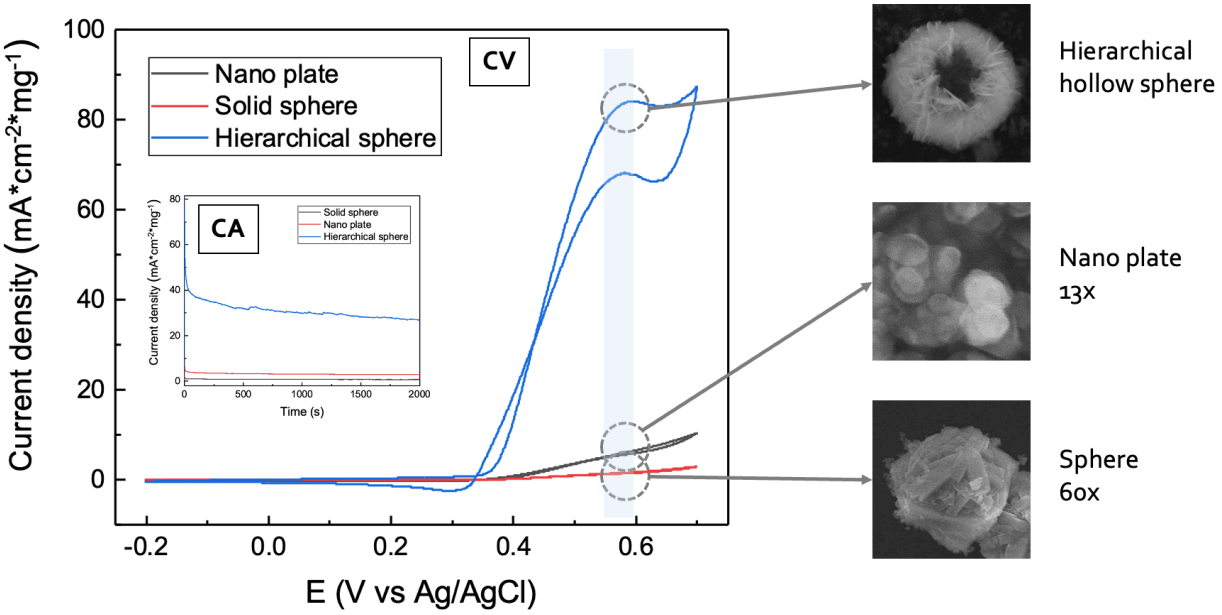

Figure 4-13 Comparison of CV and CA of nanoplate, solid sphere, and hierarchical hollow sphere NiO (1M KOH + 0.33M Urea, CV :20mV/s, CA: 5.5V)

A much higher current response can be obtained from a hierarchical sphere than from a nanoplate or solid sphere NiO, according to the CV results. This is a 13-fold increase over nanoplates and a 60-fold increase over solid spheres at 0.59V. Due to the spatial arrangement of each nanoparticle into a 3D sphere, there is a quite big difference in current density (the deposited weight is also considered for current density). Comparing nanosheets with nanoplates, despite their similar size, hierarchically structured nanosheets will provide more reaction sites, while nanoplates will aggregate. Since the interior cavity is utilized to catalyst reaction, the current response of the hollow structure is superior to that of the solid sphere. Compared to just nanoplates or solid

spheres, hollow spheres with 2D nanoplates have a much higher current density, which emphasizes the need to modify catalyst morphology, which results in a hierarchical structure, in order to develop highly sensitive electrochemical sensors.

4.8 Effect of calcination temperature

After hydrothermal synthesis, $Ni(OH)_2$ is under the calcination process. The effect of calcination was investigated to understand the origin of specific surface area and process optimization. From CV, calcination at 400°C shows the highest current response, and then as increasing temperature current response decreases.

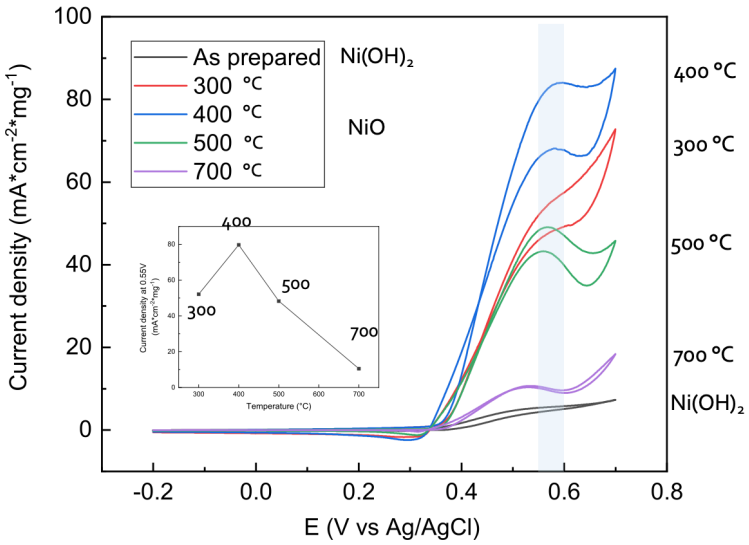

Figure 4-14 a) CV response depending on the calcination temperature, and current density at 0.55V as a function of temperature (inset)

Based on XRD results, as temperature increases peak intensity increases, while peak broadness decreases, which is associated with crystallinity. During the calcination process, de-hydroxylation of water molecules makes mesopores within the structure, which will increase the specific surface

area also. At high temperatures, however, the mesopores and micropores within NiO particles can collapse, increasing the crystallite size of the particle corresponding to decreasing the reaction surface area. A CV response decreases at a high temperature above 400°C for this reason.

4.9 Sensitivity and limit of detection(LOD)

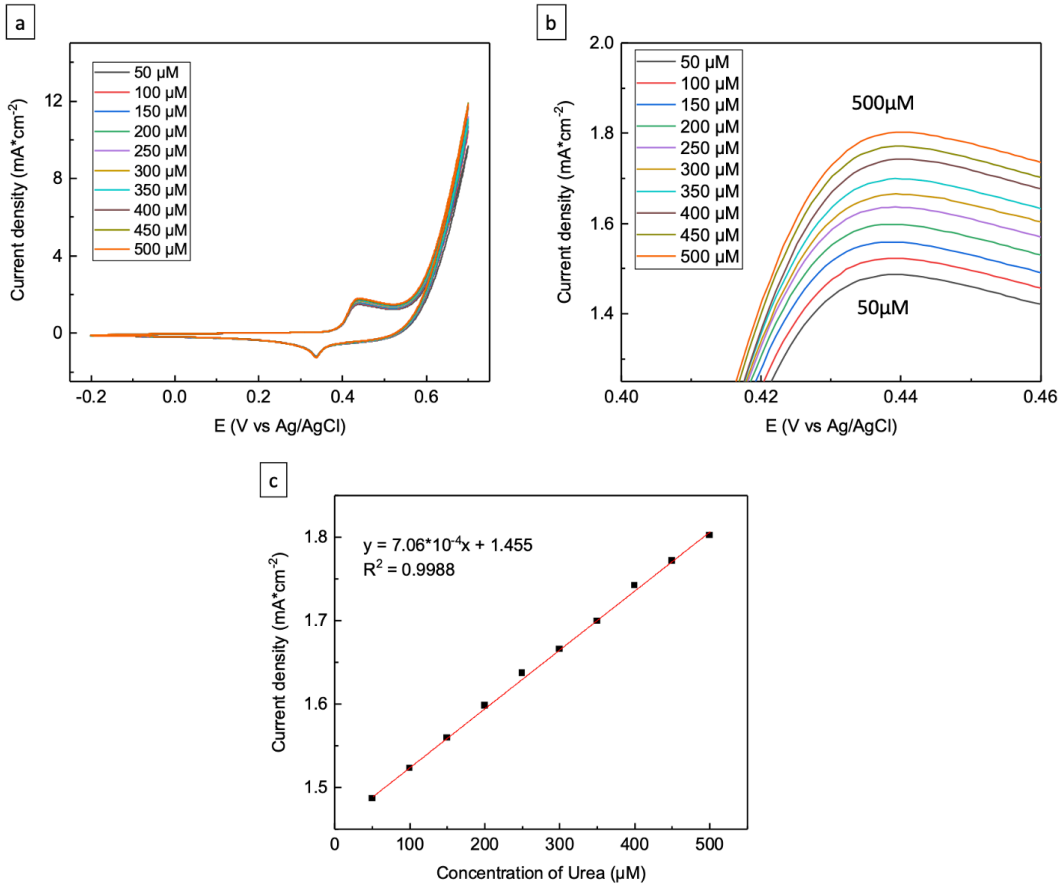

Figure 4-15 CV response as a function of the concentration of urea in 1M KOH

Figure 4-15 is the CV response as a function of concentrations of urea ranging from 50 µM to 500 µM. The corresponding calibration curves show that anodic peak current densities increase with urea concentration, as depicted in Figure 23 c. The corresponding R^2 value for the calibration is 0.9988, which demonstrates a good linear behavior of the curve. The sensitivity of the

hierarchical NiO electrode is calculated to be 706 μA mM^{-1} cm^{-2} from the calibration curve, which is an outstanding value when comparing other literature results. The limit of detection (LOD) can be achieved with the formula below:

$$\mathrm{LOD} = \frac{3S_d}{s} \tag{4-2}$$

'S_d' represents the standard deviation of the values from the blank solution (without urea) on the responding CV curve. The 's' represents the slope of the calibration curve above. The LOD was calculated as 8.04 μM, and the value is quite comparable to other literature data. (Table. 4-3)

The high sensitivity and low detection limit are attributed to the morphological property of hierarchical structure that maintains spatial arrangement between nanosheets and facilitates mass transfer, hence significantly enhances specific reaction surface area.

Table 4-3 Comparison of analytical performance of electrode

Electrode	Type	Electrolyte	Electrochemical Type	Linear range (μM)	LOD (μM)	Sensitivity ($\mu AmM^{-1} cm^{-2}$)	Ref.	Yr
Ni-MOF/MWCNT	Non-enzymatic	3 M NaCl	CA (0.45V)	10-1120	3	685	[120]	2017
Ag−ZnO/GCE	Non-enzymatic	1 M KOH	CV	26.3–427	13.98	162.2	[121]	2017
PVdF-HFP/Ni−Co	Non-enzymatic	1M KOH	CA (0.26V)	20-2000	12	2.4	[122]	2017
Ni-MOF	Non-enzymatic	0.1 M KOH	CA (0.45V)	0.5–832.5	0.471	1960	[123]	2021
NiO	Non-enzymatic	PBS	CV	100–1100	10	-	[124]	2016
ZnO NRs	Urease	PBS	CV	1 - 26	10	41.64	[125]	2014
Hierarchical NiO	**Non-enzymatic**	**1M KOH**	**CV**	**50 - 500**	**8.04**	**706**	**This work**	

4.10 Selectivity

The influence of other organic species on the detection of urea with the modified NiO electrodes was examined. The presence of some interference substances in biological systems, such as uric acid (UA) and glucose, may affect the detection of urea in real samples. Analyte solutions containing the substance may result in incorrect sensing, which is why interference studies are important.

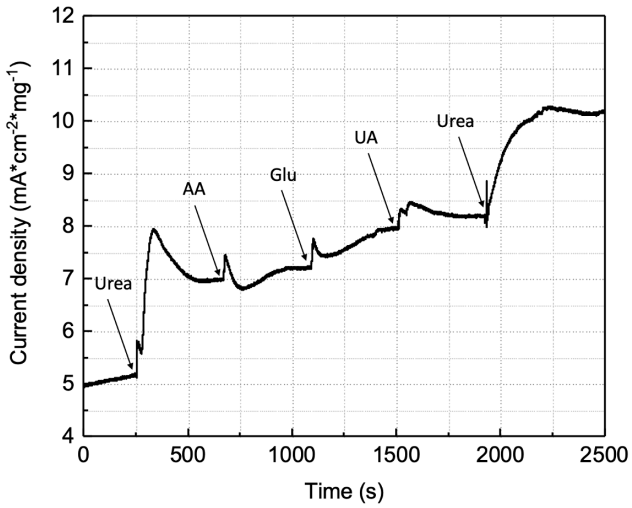

Figure 4-16 Current response of the sensor to the addition of 1mM urea, 100μM ascorbic acid (AA), 200 μM glucose, 100 μM uric acid (UA), and 4.5 mM of urea. (0.55V)

Figure 4-16 shows CA responses with successive addition of organic compounds such as ascorbic acid, glucose, and uric acid that are considered the major interferents during the detection of urea. The current response significantly changed when urea was added for the first time. As subsequent additions of AA, glucose, and UA, they only produce a slight change in response. Lastly, the current response increased significantly when the urea was added again. The result proves that hierarchical NiO modified electrode provides good selectivity toward other interferents for urea detection.

4.11 Bimetallic comparison

A similar size of sphere NiO was prepared to examine the effect of hierarchical hollow structure on electrochemical properties. In Figure 4-17a, the hollow sphere was comprised of nano sheet as a building block as observed from cross-sectional microstructure from a broken sphere.

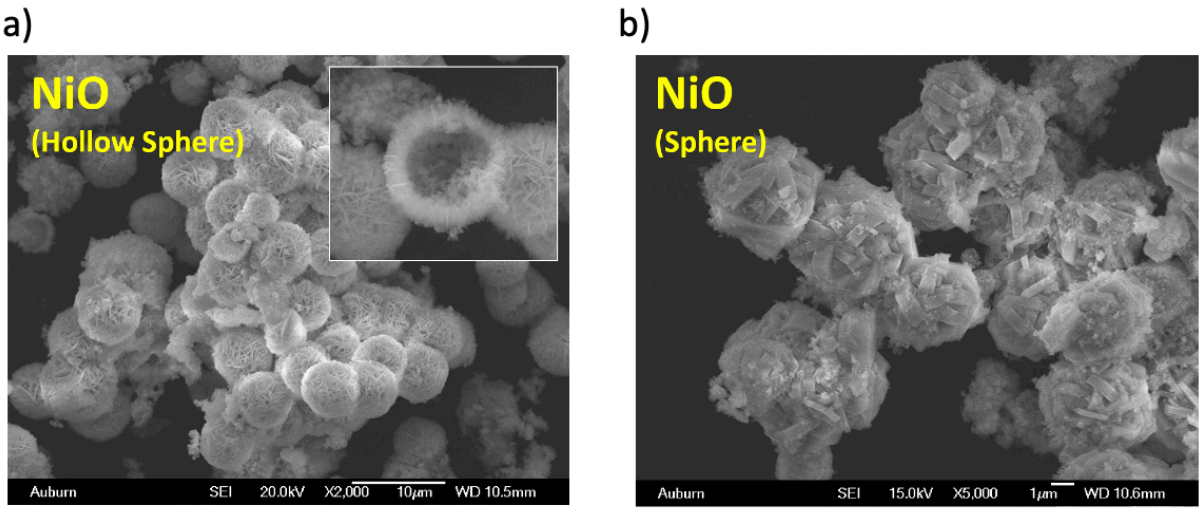

Figure 4-17 a) NiO hollow sphere, b) NiO sphere prepared by hydrothermal.

The utilization of soft template was expanded by adopting other combinations of materials. Using a catalyst composed of nickel and manganese oxide can be very beneficial because bimetallic catalysts are said to downshift the onset potential and to reduce the activation energy of nickel oxyhydroxide formation, thereby facilitating urea oxidation at a lower potential. [42] Thus, Mn salts were introduced together with Ni salts in the solution for hydrothermal synthesis, and Ni-Mn-O hollow spheres were synthesized using SDBS.

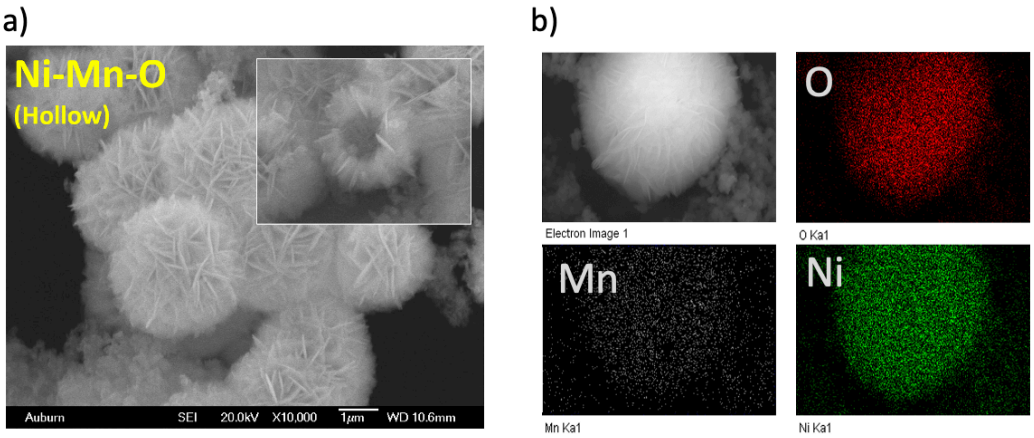

Figure 4-18 a) Ni-Mn-O hollow sphere, and b) EDS of Ni-Mn-O

As observed in the NiO hollow sphere, the compound catalyst has nanosheet building block and shows 2-5 μm hollow sphere structure. The EDS result confirms that Ni and Mn are distributed uniformly. The similar morphology of synthesized Ni-Mn-O with NiO implies that the potential application of SDBS soft template for bimetallic synthesis to introduce a synergistic effect.

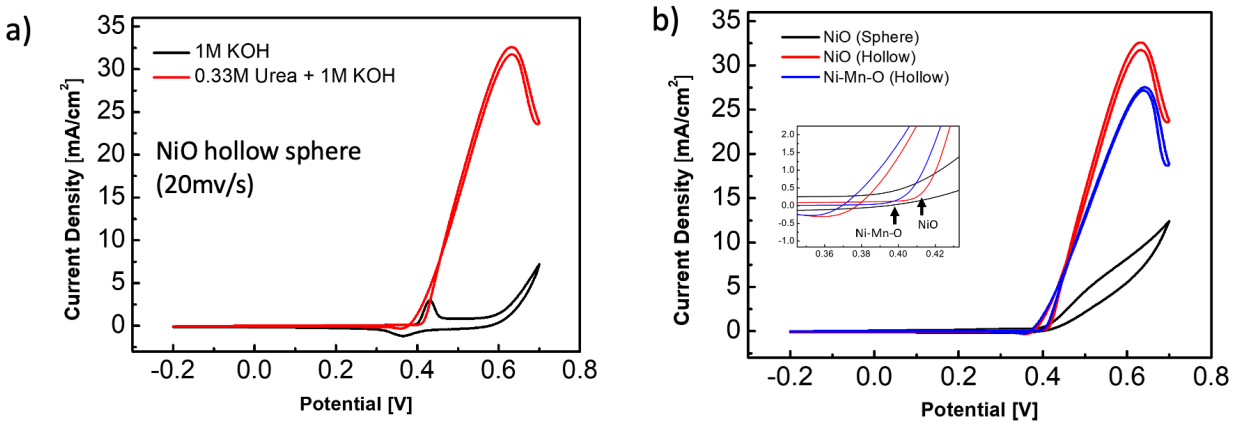

Figure 4-19 CV result of a) NiO hollow sphere, b) comparison of CV of NiO hollow, NiO solid, and NI-Mn-O hollow sphere.

The electrochemical measurement was conducted for the detection of urea. Figure 4-19a shows the result of cyclic voltammetry (CV) of the NiO hollow sphere. When adding 0.33M urea, the current density was significantly increased compared with the sample without urea (1M KOH). Figure 4-19b presents the comparison of CV results of NiO hollow, NiO solid, and Ni-Mn-O hollow sphere with the presence of urea. First of all, when comparing the solid sphere(black) and hollow sphere(red), there is a significant increase in current density (3.2 times at 0.6V), which confirms hierarchical hollow structure led to an increase in the sensitivity for urea biosensor. Such improvement can result from facile transport channels through electrolyte that exploits its inner and outer surfaces as the active site while the structural stability of the catalyst is maintained. When comparing samples between NiO hollow and Ni-Mn-O hollow sphere, the level of current density was similar, but the onset potential of Ni-Mn-O bimetallic sample was relatively lower (0.415V

vs 0.390V). The result indicates that at a more lower potential, a reaction of urea oxidation occurred by introducing Mn. The introduction of multivalent manganese in the bimetallic oxide and redox property of MnO_2 would downshift the onset potential as well as reduce the activation energy of the formation of NiOOH: thus it accelerates the urea oxidation at lower overpotentials. [42]

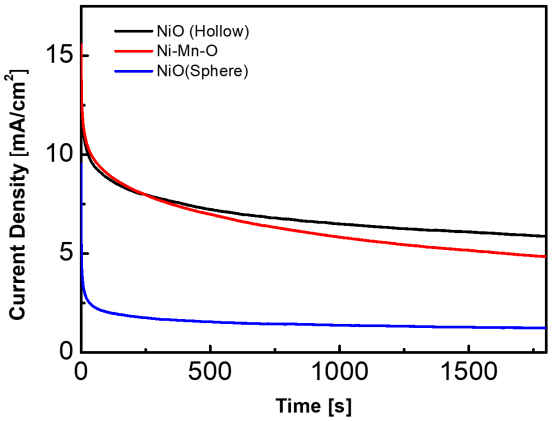

Figure 4-20 Chronoamperometric(CA) experiments of NiO and Ni-Mn-O

In Figure 4-20, the chronoamperometric experiments were performed to evaluate the stability of synthesized particles. The result represents the current transients recorded on particles polarized at a potential of 0.5 V (vs Ag/AgCl) during 1500 consecutive sec. It shows a constant current was maintained in the presence of 0.33 M urea during 1500 s, which indicates prepared hollow structure is stable during urea electrolysis.

4.12 Summary

Nickel oxide hierarchical structure was synthesized by hydrothermal method for a highly sensitive non-enzymatic urea sensor. With the SDBS soft template, the synthesis process became simpler; however, the current response became much higher than that of nanoparticles or spheres.

2D building block nanosheets comprise a 3D hollow structure, which prevents aggregation of nanoparticles and provides the abundant pathway for an analyte solution. From the effect of SDBS and Ni ion concentration, the ratio between them plays a critical role in forming the hierarchical structure. The complex between SDBS and Ni^{2+} forms the giant vesicle structure from hydrothermal synthesis, and further growth within the vesicle leads to the final hierarchical structure. A highly sensitive electrochemical urea sensor has been fabricated due to the hierarchical structure's abundance of electrochemical reaction sites.

Chapter 5 Parametric study of DC EPD with TiN for a protective coating

Firstly, the general parametric study of the EPD was conducted as the application of the TiN coating to the bipolar plate of the PEM fuel cell in order to ensure effective urea detection was performed based on AC-EPD. The DC-EPD was utilized throughout chapter 5.1, and based on the general behavior of the EPD and the importance of the parameters for the EPD, for example, the effects of time, potential, and surfactant. This parametric study is focused on the application of EPD coating for the protective coating of a bipolar plate that is used for proton-exchange membrane fuel cells (PEMFC). The AC-EPD was utilized throughout chapter 5.2.

5.1 Characterization

The XRD patterns of TiN powders (20 nm) and TiN-coated stainless steel by the EPD process are compared in Figure 5-1 (a). There were three peaks of TiN and two peaks of stainless steel in the case of TiN-coated stainless steel. SEM was used to verify the morphology of the EPD TiN layer. The stainless steel substrate is coated densely and uniformly with TiN particles in Figure 5-1 (b).

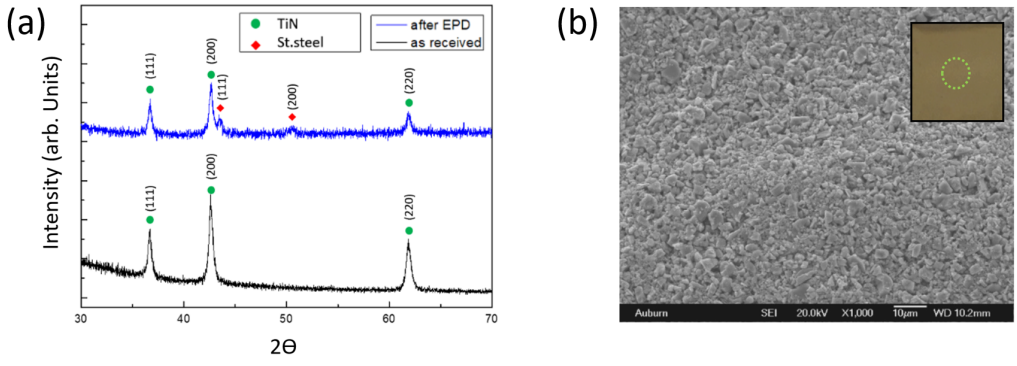

Figure 5-1 (a) XRD patterns of the as-received TiN Powder and TiN-coated stainless steel, and (b) the morphology of TiN coated layer by EPD at 100 V for 1 min (800 nm).

5.2 Effect of applied time, potential, and size of particle

During the investigation of the kinetics of EPD TiN, the well-known kinetic equation proposed by Hamaker [66] was used in equation 1 where μ is the mobility, V is applied voltage, d is the distance between electrodes, A is an area of the electrode and C is the mass concentration.

$$W = \int_{t_1}^{t_2} \mu \left(\frac{V}{d}\right) AC \, dt \tag{5-1}$$

$$\mu = \frac{\varepsilon \xi}{\eta} \tag{5-2}$$

Equation 2 shows that mobility (μ) is proportional to zeta potential (ξ) and permittivity (ε), and inversely proportional to viscosity (η).

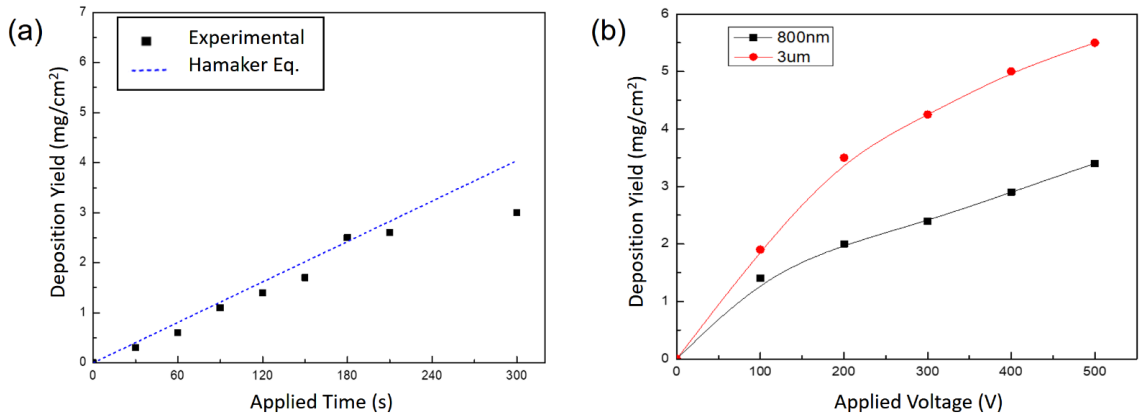

Figure 5-2 The deposition yield (mg/cm^2) as a function of (a) time (800 nm) and (b) voltage (800 nm and 3 μm)

As predicted by Hamaker's equation, deposition yield increases as time and voltage are applied. In Figure 5-2, PDADMAC deposition yields for 800 nm TiN powders are shown as a function of time and voltage. The deposition yield increases with time at 100V of applied voltage. Based on the comparison of the yield with equation 1 (blue dash line in Figure 5-2 (a)), it can be concluded that the Hamaker equation presents well-fitted yields in the EPD TiN process. When

the deposition time is long, there is a reduction in the deposition rate. As a result of the decrease in particle concentration between substrate and counter electrode during the EPD process, as well as the insulative effect that deposited TiN has on the counter electrode, there is a voltage drop through the TiN layer [69]. Figure 5-2 (b) compares different sizes of TiN particles (800 nm and 3 m), and the voltage is varied while the EPD time is kept for the same period of time (60 s). Deposition yield increased with both applied time and electric field, but 3 μm TiN powders showed higher yield than 800 nm powders. As a result of different zeta potentials, different yields can be observed. The zeta potential of 3 μm (61.3 mV) was measured to be higher than that of 800 nm (48.2 mV). As described in equation 2, a higher zeta potential increases electrophoretic mobility and deposition yield. The electrophoretic mobility also depends on the protonation of additives at the pH level of the working solution. Adding a pH agent affects the ionization state of the charging agent, resulting in zeta potential.

5.3 Effect of polyelectrolyte for EPD

PEI and PDADMAC were compared in Figure 5-3 for their pH dependence. To adjust pH, acetic acid and ammonium hydroxide were used. PEI and PDADMAC produced similar yields of maximum deposition during the test process. In spite of this, the pH values where maximum yield was achieved in PEI and PDADMAC were different. This may be due to the different zeta potential of suspension in PEI and PDADMAC. Since the pH agent dissociates at a higher conductivity level, the yield decreases when an excessive amount is added.

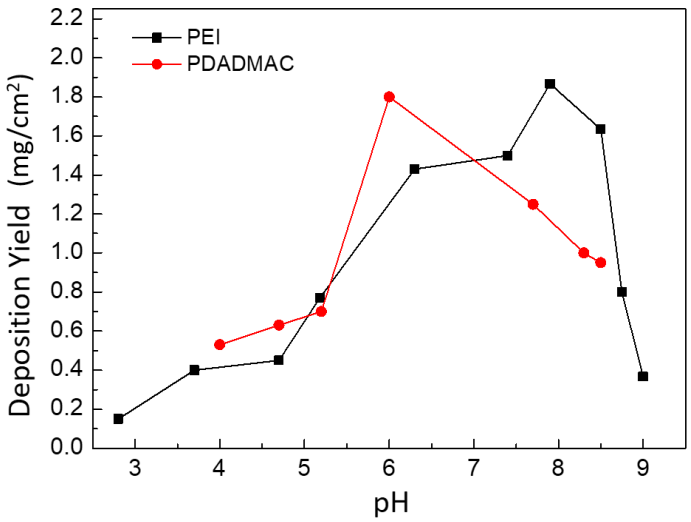

Figure 5-3 Deposition yields of TiN as a function of pH when PEI and PDADMAC were used as an additive in TiN suspension.

When anode and cathode couples are submerged in a suspension containing electrolyte, electrolytic corrosion may occur. For example, Lau et al. reported electrolytic corrosion during EPD when PEI and PDADMAC were used as charging agents for coating Ti on stainless steel. Using PEI resulted in more pitting corrosion on the electrode surface. The reason for this is that PEI contains a higher amount of anion (OH^-) than PDADMAC does. Due to this, PDADMAC could be beneficial for corrosion-resistant coatings, even though the maximum yield values are similar between PEI and PDADMAC. [132]

5.3.1 The difference in deposition depending on MW of polyeletrolyte

Figure 5-4 compares the deposition yields of two different PDADMACs, namely 'low' molecular weight (MW) (~100K) and 'med' MW(200~350K). Deposition yield was calculated as a function of the added PDADMAC amount. When PDADMAC is incorporated at lower concentrations, the deposition yield shows a rapid logarithmic increase up to the maximum yield.

Then a slower logarithmic decline was followed by further addition of PDADMAC. Due to the fact that the PDADMAC charging agent was not fully saturated, a rapid increase in yield was observed from 0% to 2.5 wt% PDADMAC. Consequently, an increase in the addition of PDADMAC resulted in an increase in deposition yield. The maximum deposition yield was reached with 2.5 wt.% PDADMAC addition, and the TiN particle mobility was the highest. However, an excessive amount of PDADMAC showed adverse effects on EPD. In view of the large polymeric size of the PDADMAC molecules between TiN particles, a shielding effect is likely to occur between the PDADMAC molecules and the electric field, resulting in a lower deposit yield. A variation in the amount of PDADMAC may also result in a variation in conductivity in suspensions. The particle motion is slowed when the suspension is too resistive or conductive, since the conductivity is directly proportional to the amount of polyelectrolyte. In this way, PDADMAC will reduce deposition yields over the optimum conductivity range as the conductivity increases.[133].

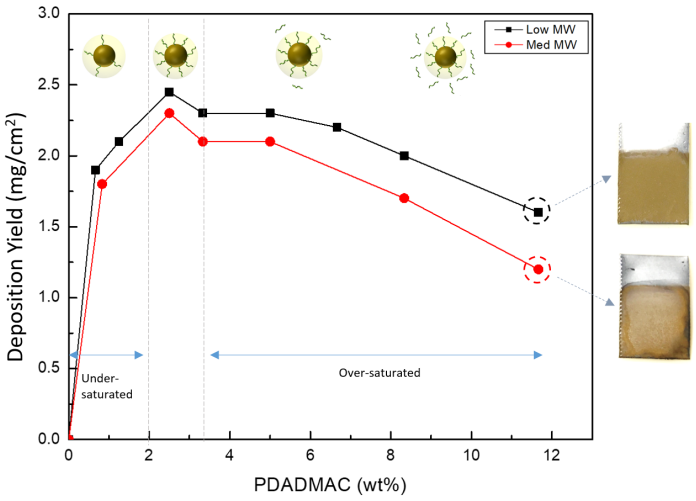

Figure 5-4 The deposition yields as a function of the addition of PDADMAC as a charging additive. Wt% of PDADMAC is based on the amount of TiN.

The low MW polymer (shorter chain of polymer) of PDADMAC shows a higher yield than the medium MW polymer (longer chain of polymer) in Figure 5-4. After adding PDADMAC past its optimal range, both MWs of PDADMAC showed a decrease in deposition yield and coating uniformity. As shown in Figure 5-4, the layer with a medium MW (bottom) showed lower uniformity than the layer with a low MW (top). The surface of the coated stainless steel even shows uncoated areas when a large amount of medium MW is used. A PDADMAC interface causing shielding of the electric field or dislodging of a particle attached to the coating surface is more likely to occur when the polymer chain is longer (medium MW cases). Therefore, higher length of polymeric chain would deteriorate coating uniformity more than shorter polymeric chain of PDADMAC. Those prepared samples were into the application of PEMFC bipolar plate.

5.4 Application of TiN deposited SS for PEMFC

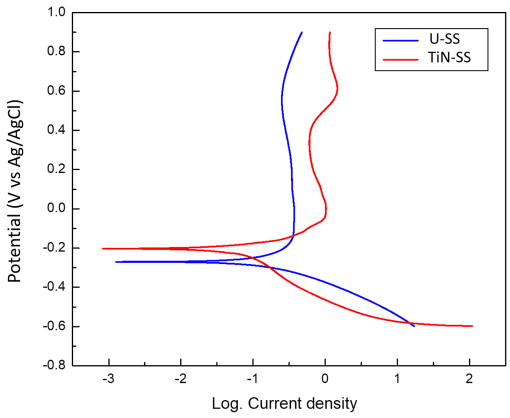

Figure 5-5 Polarization curves of uncoated stainless steel and TiN-coated stainless steel

Stainless steel coated with TiN has a conductivity of 1.48 X 10^6 S/m, which is higher than the conductivity of stainless steel uncoated (1.334 X 10^6 S/m). As part of the evaluation of EPD TiN layers, electrochemical corrosion tests were also conducted. In Figure 5-5, the potentiodynamic polarization results were obtained in the simulated PEMFC operating

environment (0.5 M H_2SO_4 solution purged with air at 70°C). In a corrosion potential comparison, the corrosion potentials of uncoated 316 stainless steel (U-SS) and TiN-coated stainless steel (TiN-SS) have been found to be -263 mV for U-SS and -203 mV for TiN-SS, respectively. The corrosion current density of the U-SS and TiN-SS were 134 $\mu A/cm^2$ and 64 $\mu A/cm^2$, respectively. Following TiN coating, the corrosion current density was reduced, which implies that this coating is more corrosion resistant, and that the protection provided by TiN deposition through EPD is more effective. A protective coating prepared by EPD may need to improve to achieve a lower corrosion current density compared to a coating prepared by PVD or CVD [134]. However, it is worth investigating, considering the simplicity of the process and the economic apparatus that can enable mass production, and based on the parametric investigation, the AC-EPD is going to be dealt with to next chapter.

Chapter 6 AC-EPD of NiO for Non-enzymatic Urea Sensors

In the literature, alternating current (AC) was utilized for electrolysis suppression when the EPD process uses water(aqueous) as a solvent. [108], [109] The formation of oxygen or hydrogen bubbles during water decomposition can be avoided by AC fields. AC–EPD allows electrophoretic deposition from aqueous suspensions rather than organic solvents (such as ethanol), which is a significant advantage from a safety, economic, and environmental perspective, while maintaining the surface quality and processing rate of DC–EPD using organic solvents. The research objective of this chapter starts with the possibility of AC electric field could induce the modified fluid flow above substrate due to the periodic changes in the direction of the suspended particles.

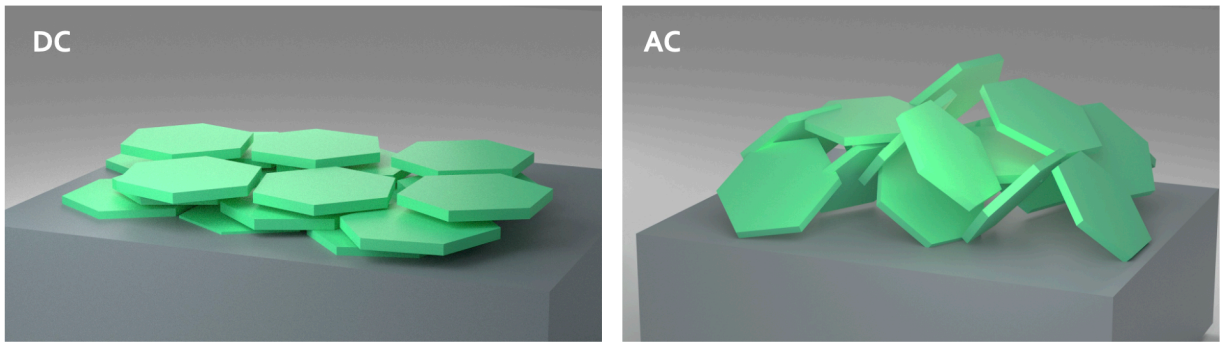

Figure 6-1 Schematic comparison of the resultant coating from DC and AC-EPD

6.1 Characterization

Powder synthesized by the previously described hydrothermal method was characterized by XRD and SEM to find information about the crystalline nature and morphology of the powder. Figure 6-2 (a) shows the XRD patterns of the synthesized nanoplates before and after calcination. The XRD pattern of as-synthesized nanoplates presents the diffraction peaks at the angles of 2θ = 33.1°, 38.5°, 52.1°, 59.1°, 62.7°, 70.4°, and 72.7°. Major diffractions peaks were indexed as (101),

(100), (102), (110) crystal planes with $Ni(OH)_2$ hexagonal structure (JCPDS 14-0117). The nanoplates after calcination at 400°C for 2 hrs show NiO crystal. The diffraction peaks at the angles of 2θ = 37.2°, 43.3°, 62.9°, 75.4° and 79.4° corresponding to (1 1 1), (2 0 0), (2 2 0), (3 1 1) and (2 2 2) planes confirm FCC structured NiO (JCPDS 47-1049). Although different shapes of NiO nanostructures are available, the anisotropic plate shape of NiO was used in this study to maximize the effect of the AC electric field during the EPD on the deposited morphology to investigate the difference between DC and AC fields. The SEM image in Figure 6-2 (b) confirms that the synthesized NiO powder has a hexagonal nanoplate shape with a diameter range of 100 ~ 300 nm and a thickness of about 10 nm.

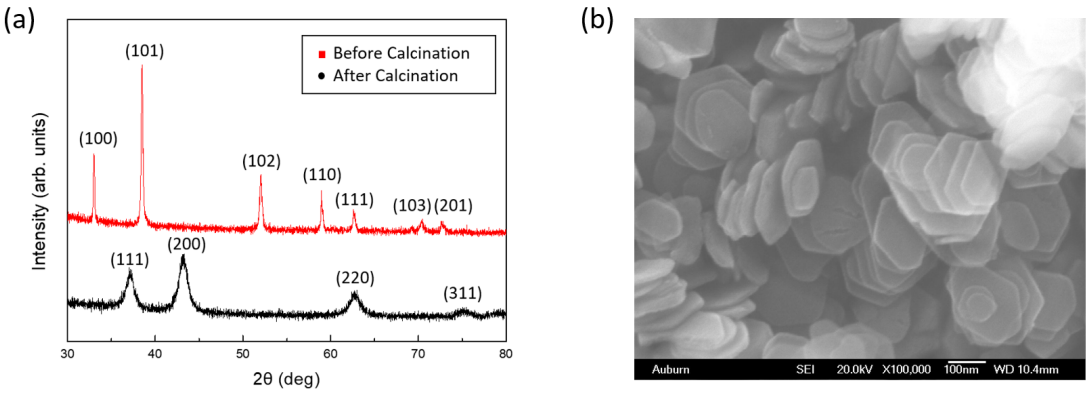

Figure 6-2 (a) XRD patterns of Ni(OH)2 and NiO, (b) SEM image of the NiO plate-like nanostructure.

6.2 The optimization of AC-EPD parameters

The direct current(DC) and the alternating current(AC) EPD processes are illustrated in Figure 6-3 (a) and (b). NiO powder exhibits positive zeta potential in an ethanol solution, which means that it has a positive charge. An electric field moves positively charged particles along the carbon electrode anode when it is applied. A DC electric field is constantly one directional; however, an AC electrical field involves the movement of charges that change their direction constantly, rather

than being continuously one-directional. The waveform of the AC field that is being set up at the function generator is shown in Figure 6-3. There is a periodic change in the direction of the electric field between the electrodes due to this asymmetric square wave, which alternates from positive to negative with a 4 to 6 ratio.

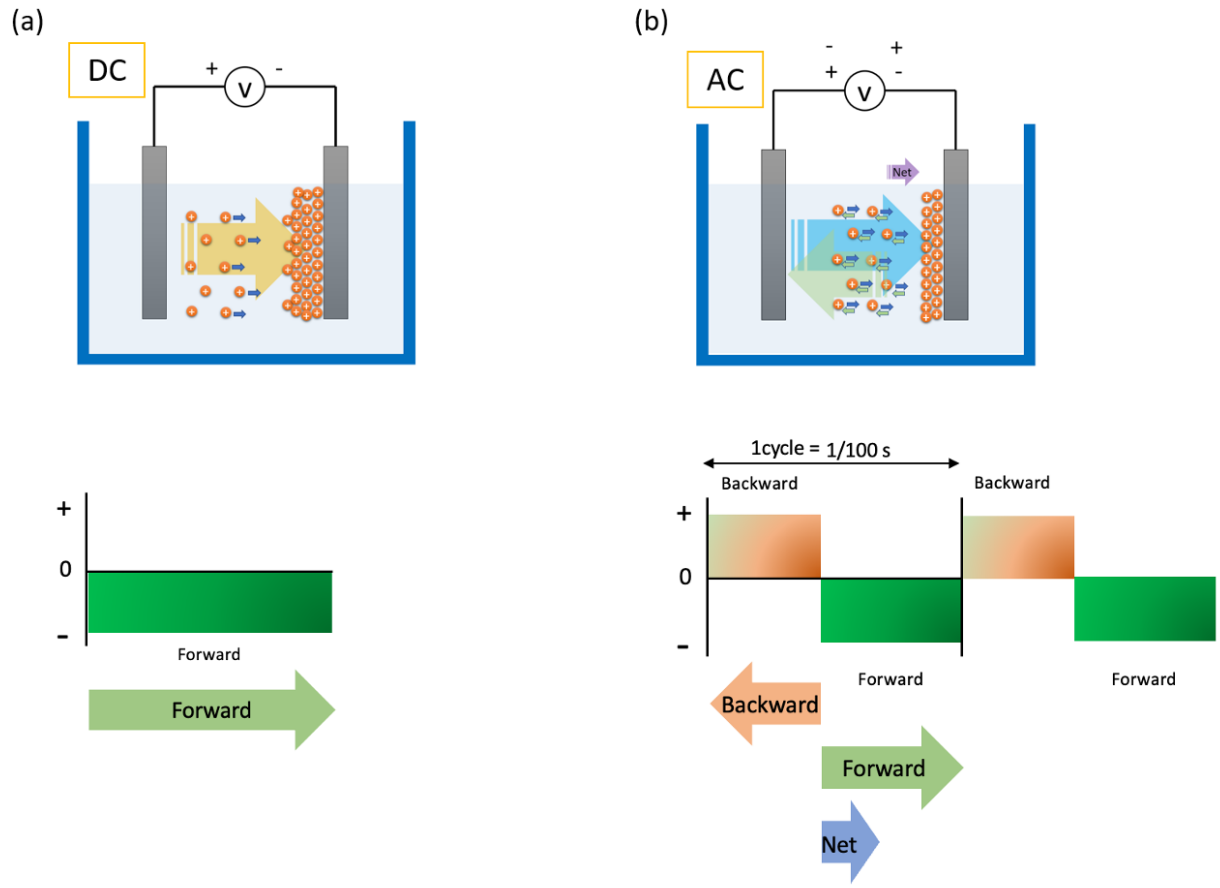

Figure 6-3 The schematic of (a) DC, (b) AC EPD, and their waveform for AC EPD.

A periodic change in the source of the electric field between the cathode and the anode also results in a periodic change in the direction of the electric field as well. This results in charged NiO plate particles following the field direction in real-time, i.e., the particles are moving forward and backward with the magnitude of the waveform in the field generator. The negative portion of the electric field is higher than the positive portion; therefore the net electric field is negative, resulting

in a net flow of particles to the anode surface. As a result, the NiO particle moves and is deposited onto the carbon substrate. Several ratios of waveforms were applied, but the DC behavior becomes more apparent when the portion of the negative charge (that moves NiO to the substrate) is higher. When using more negative ratios, such as 1:9 and 3:7, the surface morphology and electrochemical behavior are similar to standard DC. As a result, in this work, the ratio for AC electric field was set to 4 to 6 to see the difference between DC and AC electric fields. An article reported that yields of deposition increase up to 100 Hz, then plateau before decreasing with further increases in the frequency [135].

Table 6-1 The effect of the periodic ratio of AC-EPD

Duty cycle (+) : (-)	Result
1:09	Show similar behavior with DC
2:08	
3:07	
4:06	AC behavior

Table 6-2 The optimized parameters of AC-EPD

Applied Voltage	60 Vrms
Applied Time	5min
Wave form	Square form (40%+ : 60%-)
Frequency	100, 200Hz

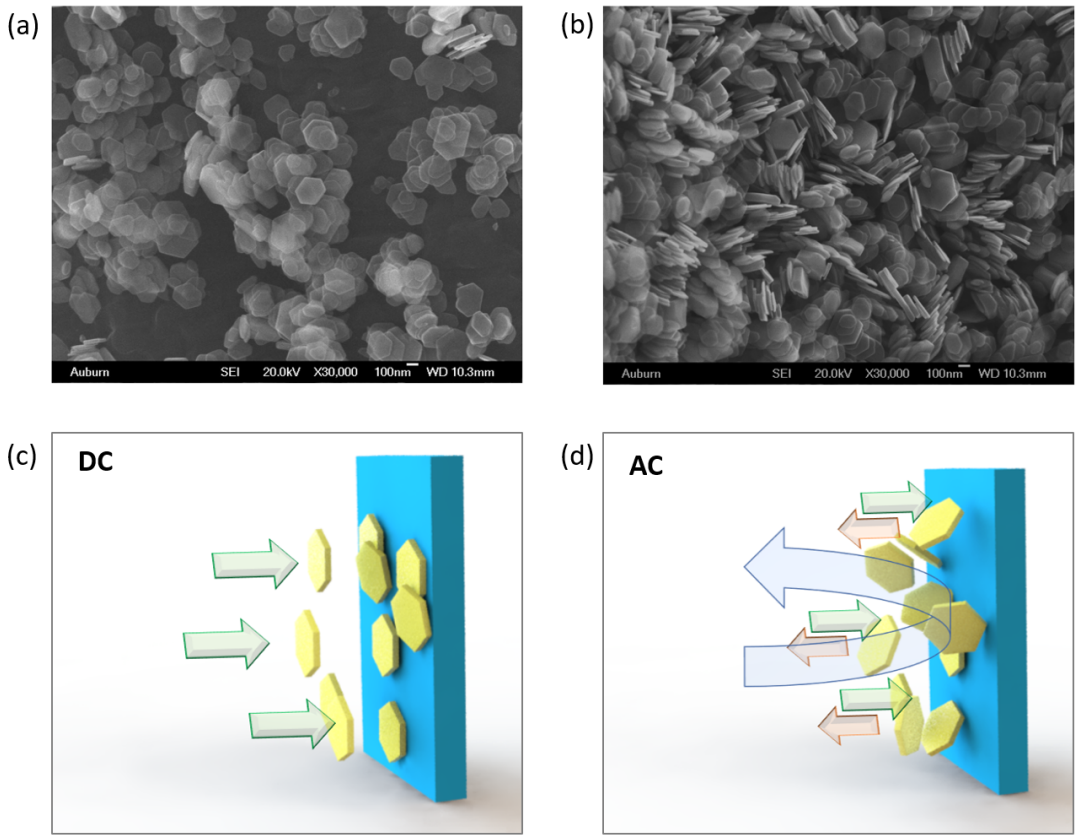

Figure 6-4. The SEM image of NiO-coated electrode surface of (a) DC and (b) AC and the schematic of electric field effect by (c) DC and (d) AC.

SEM images of NiO nanoplates deposited on the surface of carbon paper are shown in Figure 6-4 (a) and (b). A perpendicular alignment of nanoplates is more observed in Figure 6-4 (b) when NiO is deposited under AC electric fields. In contrast, when DC electric fields were applied, as shown in Figure 6-4 (a), NiO nanoplates were more laid down on the electrode's surface. Figure 6-4 (c) and (d) illustrate this phenomenon schematically. In the DC field, the plate particles lay down on the substrate due to the continuous one-directional electric field. As the AC electric field was applied, the particles moved back and forth periodically. As a result of this oscillation on the surface induced by an AC field, convective turbulence flows developed. Turbulence can cause particles to tumble, rotate, and spin depending on their shape. Simulated results from Calzavarini

et al. [112] show that oblate spheres tumble much more quickly than prolate spheres (more like rods) in turbulence. Although it is not the same case, the simulation suggests that anisotropic particles tend to behave differently. The plate-like shape of the suspended particles in AC-EPD may create more convective turbulence on the substrate, thereby altering NiO plate packing as EPD progresses. Even in oscillations, since the negative portion of the waveform is greater than the positive portion in waveforms of AC fields, there is a net flow of the charge toward the target electrode, resulting in different packing characteristics. In the course of the further deposition, this results in a more porous packing because of the vertical alignment to the electrode.

The mechanism of urea oxidation by Ni-based catalysts in alkaline media can be expressed with the following reactions [136]

$$NiO + OH^- \leftrightarrow NiOOH + e^- \quad (6\text{-}1)$$

$$CO(NH_2)_2 + 6OH^- \xrightarrow{NiOOH} N_2 + 5H_2O + CO_2 + 6e^- \quad (6\text{-}2)$$

Figure 6-5(a) shows CVs of NiO electrodes (catalyst) as functions of scan rate from 10 to 100mV/s in 1M KOH containing 0.33M urea. The peak current density of urea oxidation is linearly related to the square root of scan rate. The linear relationship implies that the electrochemical oxidation is dependent on the diffusion of the analyte on the surface of the NiO catalyst [124].

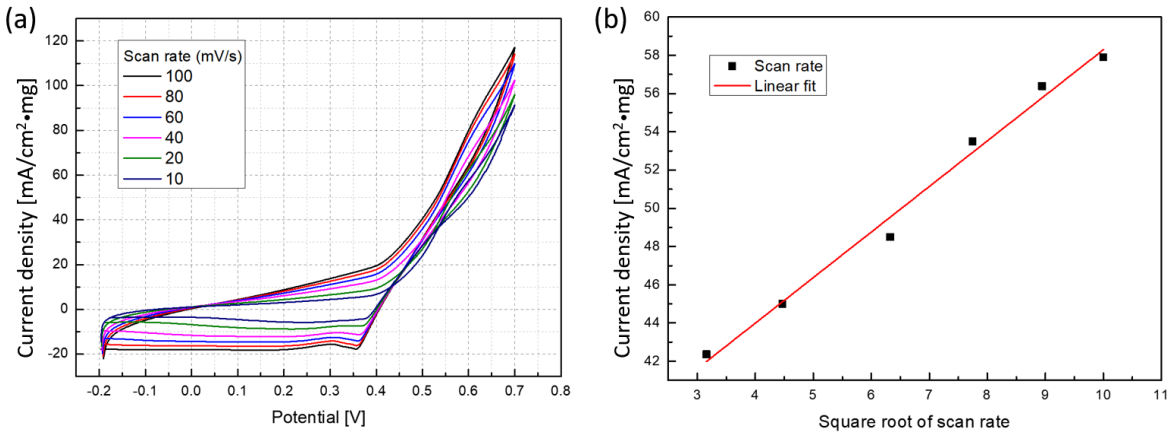

Figure 6-5 The scan rate effect on peak current density (a) CVs of NiO electrode in 1M KOH with 0.33M urea at a scan rate from 10 to 100 mV/s and (b) square root of scan rate.

In figure 6-5, NiO-coated carbon paper is used as an electrode for cyclic voltammetry (CV). To examine urea electrooxidation, Pt wire counter electrode and Ag/AgCl reference electrode were used as a three-electrode electrochemical set.

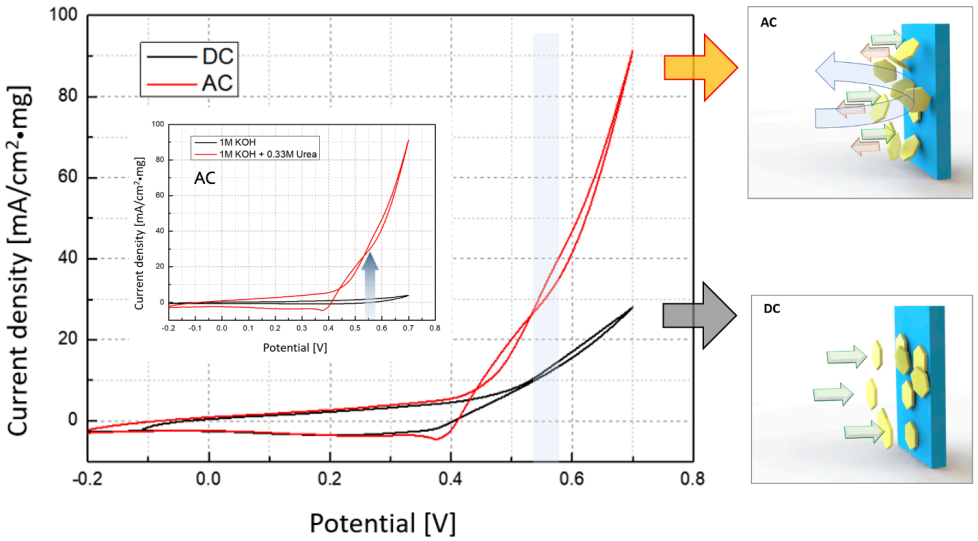

Figure 6-6 CVs of NiO electrodes in the absence and presence of urea (inset), and the CVs comparison of NiO electrode using AC-EPD and DC-EPD in 1M KOH with 0.33M urea at a scan rate of 20mV/s

The results of comparing with and without urea in KOH solution are shown in Figure 6-6 (inset). Based on this result, it can be concluded that synthesized NiO is able to detect urea well, which is related to the reversible transformation between Ni^{2+} and Ni^{3+}, which can be seen in equations (6-1) and (6-2).

In the presence of urea, NiO electrodes show a high oxidation current density starting at 0.42 V (onset voltage), suggesting NiOOH forms at 0.42V and is involved in the oxidation of urea. Figure 6-6 compares the CV result by DC and AC EPD. The onset potential, which is starting voltage for the formation of Ni^{3+} was observed at 0.42 V. At the potential of 0.5V, NiO is characterized by current densities of 20.17 and 7.85 mA/cm^2•mg by AC and DC, respectively. According to the results, the current density in AC electrodes is 2.57 times higher than in DC electrodes at 0.5V, which indicates that such a change in current density is mainly due to the higher specific surface area of NiO-deposited electrodes. The vortex and oscillation caused by the AC electric field are believed to be responsible for the vertical alignment of NiO nanoplates on the electrodes, which in turn resulted in more spatial distribution of the NiO plates when the nanoplates were further deposited during the EPD process. Those exposed standing NiO and the porous space that allows electrolyte smear might increase the active surface area for urea oxidation, thus increasing the electrochemical activity. As a result of the porous spaces created by the AC-EPD, analyte solution can penetrate into the NiO film and increase the number of reaction active sites.

6.3 Effect of Solvent

For environmental and economical perspective, the water is superior solvent for the process than non-aqueous (organic solvent). However, In the case of aqueous media, bubbles are formed as a result of water electrolysis. Most studies used AC-EPD to prevent bubble formation and

achieve quality coating in aqueous solutions. To find out if the AC turbulent effect is applicable even in water solvents, the effect of solvent was investigated.

Table 6-3 Pros and cons of aqueous and organic solvent

	Aqueuous	Organic
Pros (+)	Environmental friendly Economical	No water electryolysis
Cons (-)	Water electrolysis	Expensive

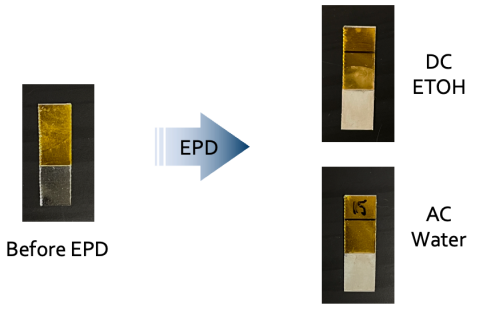

Figure 6-7 DC and AC EPD on SS electrode in ethanol and water

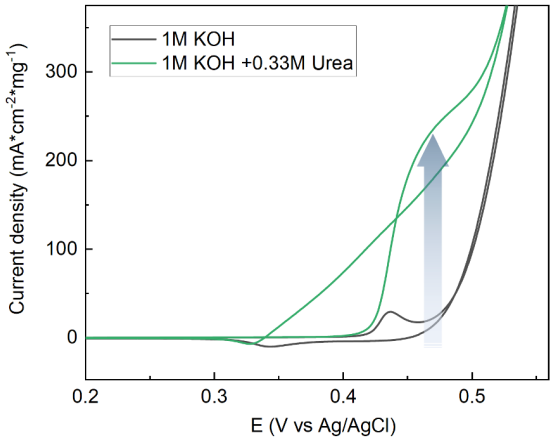

Figure 6-8 CV with presence and absence of urea (1M KOH + 0.33M Urea)

Figure 6-7 shows the result of EPD coating on a stainless steel electrode., which confirms the uniform deposition without deterioration from water electrolysis when using AC field at water

solvent. As with DC-EPD in ethanol solvent, AC in water solvent produces the same coating quality. In Figure 6-8, the CV with and without urea in 1M KOH showed a significant increase in current density at 0.46V, which is a 12 times difference in current response.

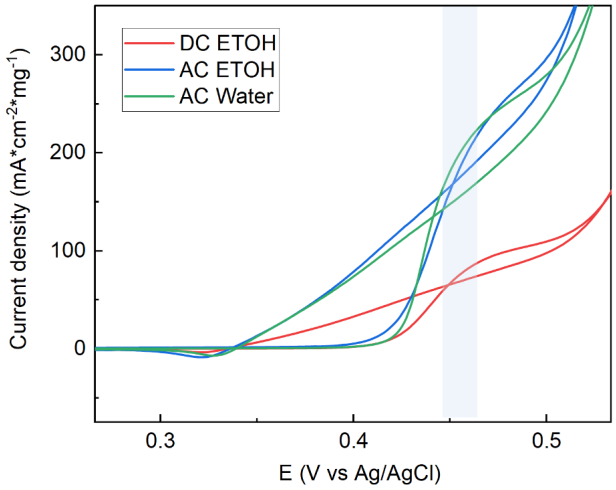

Figure 6-9 Comparison of DC vs AC in EtOH, and AC in EtOH vs AC in water

Figure 6-9 shows the CV obtained using different solvents. In the same organic solvent (ethanol), the AC-EPD electrode shows 2.5 times greater electrochemical response than the DC-EPD electrode. In this case, bubble formation is not an issue, so the only difference is packing behavior under different electric fields. As reported in the previous chapter, the AC electric field contributes to the increase in the current response. In comparing CV from different solvents under the same AC electric field, both show similar current responses, in other words, both are higher than from DC. We can conclude from this result that packing control was achieved even when water solvents were used under AC fields, as well as the suppression of electrolysis.

$$W = f \int \left[\mu \left(\frac{V}{d} \right) AC \right] \, dt \tag{6-3}$$

$$\text{mobility } \mu = \frac{\xi \varepsilon}{\eta} \text{ visocosity} \tag{6-4}$$

Although there is a minute difference between the two, there is 6% difference in the current response. From Hamaker's equation, it can be assumed that the difference is due to mobility. Ethanol's viscosity is 14% higher than water's, and its mobility is inversely proportional to its viscosity, which could explain the slight packing difference.

6.4 DC-EPD of hierarchical NiO paticle and voltage effect

This study investigates the effect of applied voltage during the EPD process as an engineering aspect. A EPD voltage range of 100V to 500V was observed with NiO sphere in ethanol solution. In all samples, a deposition area of 0.25 cm^2 was maintained.

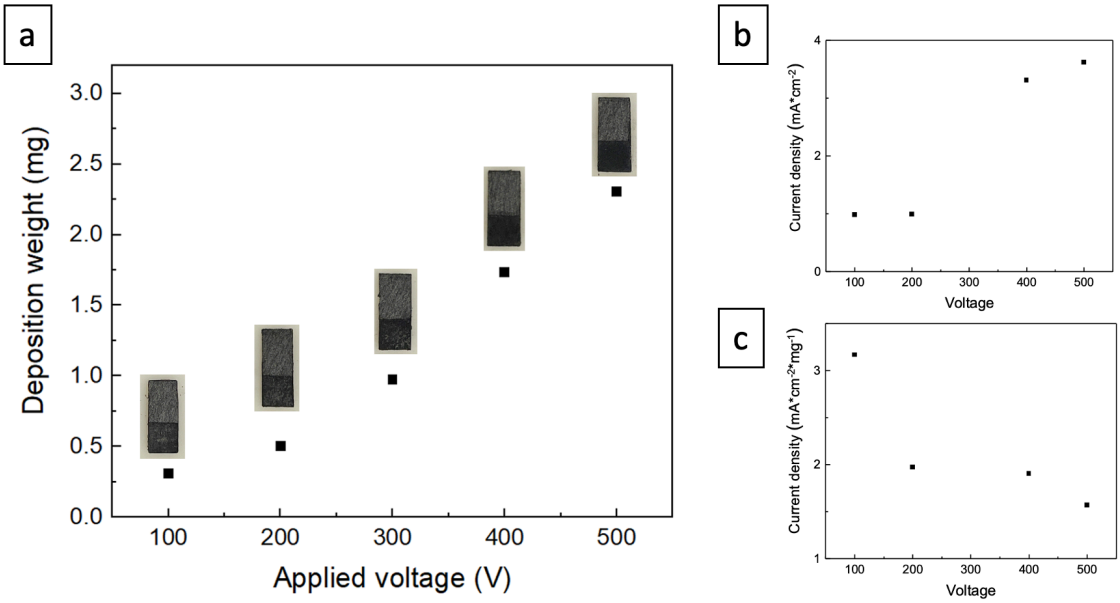

Figure 6-10 EPD of NiO varying applied voltage

An increase in voltage led to an increase in NiO deposition on the substrate (carbon paper). According to Hamaker's formula for EPD below, there is a linear relationship between weight and applied voltage.

$$W = \int_{t1}^{t2} \mu E A C \, dt \tag{6-5}$$

Figure 6-10 shows the peak current density for CV tests conducted in the presence of urea using a variety of EPD voltages. In Figure 6-10, the designated working electrode area (0.25 cm^2) increases as the loading amount of NiO increases. If only the area of the working electrode is considered in Figure 6-10 c to measure the current density, it is expected that the current density will also increase, since more NiO particles are exposed to the analyte with a larger area to cover. Increasing the EPD voltage, however, reduced the peak current density when considering weight instead of area to calculate current density. The picture of the deposited surface in Figure 6-10a by EPD shows that all NiO covers the surface of the electrode when the voltage is raised to 400V or 500V. NiO will continue to deposit on top of deposited particles even after NiO covers all regions. Stacking will block carbon fiber pores, reducing porosity, and preventing more NiO from participating in the UOR. Applied to the EPD part and engineering aspects, it emphasizes the importance of setting up the range of EPD conditions when exploring how catalyst morphology affects the current response.

6.5 Comparison between dip coating method and EPD

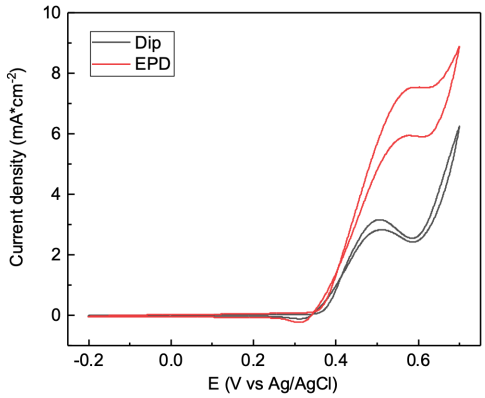

Figure 6-11 CV comparison of dip coating and EPD at 0.33M urea in 1M KOH

A comparison was conducted between two different loading methods: dip coating and EPD. In the dip coating method, the carbon paper substrate was immersed for one minute in a suspension containing NiO particles (ethanol). A complete drying of the carbon paper was conducted prior to the CV test. The CV result in Figure 6-11 demonstrates that the current response prepared by EPD (7.2 $mA*cm^{-2}$) is 2.6 times more than the current response prepared by dip coating (2.8 $mA*cm^{-2}$.) EPD's advantage of enabling deposition even into complex shapes of the substrate is acknowledged by this result. Due to the electric field-induced attraction to the substrate, deposition takes place deep within the pores of the carbon paper substrate, leading to more availability of sites for reactions.

6.6 Summary

In EPD coating process, alternating current was used to control the deposition behavior. In the parametric study of DC-EPD, the deposition yield was mainly influenced by the applied potential and time, and we can predict this from the kinetic equation. As a result of modifying the waveform and frequency of the AC electric field, the packing behavior during EPD was controlled, resulting in a significant increase in the electrochemical response towards urea, when the AC-EPD method was used.

AC-EPD not only prevents water electrolysis, but also modifies the deposition morphology in aqueous suspensions, which could allow AC-EPD to be applied to the area that requires the consideration of the environment.

Chapter 7 Paper-based sensor integration and application to urea detection

7.1 Introduction

Due to the fact that paper is inexpensive, chemically stable, and environmentally friendly, there is a growing interest in using it as point-of-care testing devices. In addition, the paper has a porous fiber matrix that allows liquid samples to infiltrate naturally through capillary action. A catalyst can also be loaded easily with the capillary action like the pump without the power. As an example, it is possible to distribute catalyst solutions inside cellulose fiber structures with the flow of solvent (e.g., DI water). Based on my SEM analysis of the #1 chromatography paper, the fibers have an average diameter of 14 μm and an average pore size of 43 μm (defined as the area of vacant space within the fibers). It means that metal catalysts that have a size of several μm or less are easily able to penetrate inside pores.

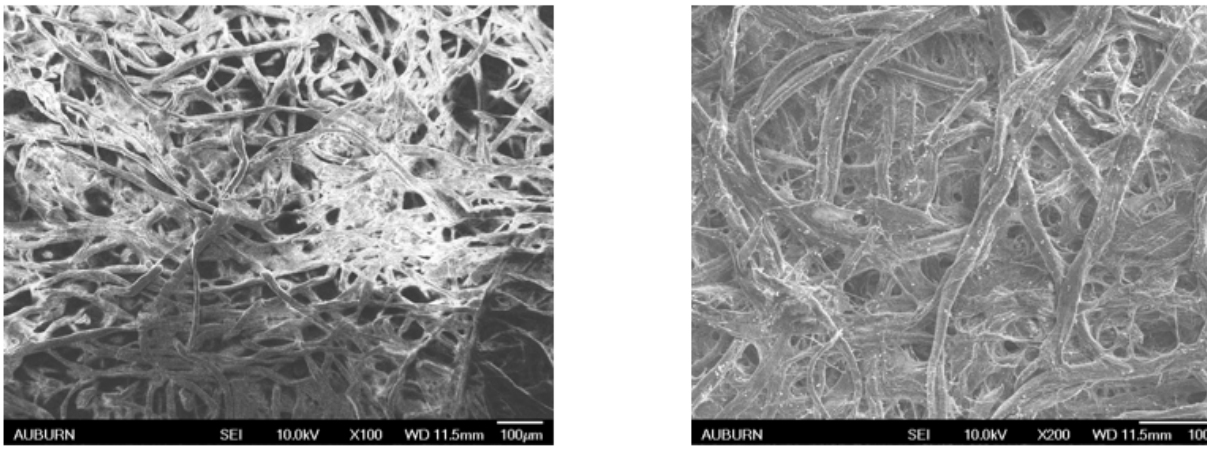

Figure 7-1 a) The pristine #1 chromatography (Whatman, GE), b) #1 chromatography paper with 50 nm NiO particle. Drop casting was used for loading of NiO.

It is technically possible to place 280 NiO particles on the fiber of the shortest part when I place a 50 nm NiO particle linearly on it. A single pore can be filled with almost 900,000 particles. As shown in Figure 7-1 b), the NiO particles are deposited on all sides of the filter paper as a result

of drop casting. In the fibers and pores, some aggregates can easily be observed. When magnified, the small nano-sized particles can be identified through the paper, which indicates that the #1 chromatography paper is a desirable platform for the sensor's working electrode to increase the surface area of the reaction. A uniform distribution can be achieved by capillary force, which does not require an external driving force for solvent to flow within pores. The NiO or CNT move along with the solvent deep into the pore of the paper substrate, and when the substrate is dried, only the NiO or CNT are left on the surface of the cellulose. The process of loading catalyst by using the capillary force of paper can simplify the process and ensure an even distribution of particles throughout the complex structure. As a result, more active spots will be available for the urea reaction, which will increase the current density. We can, however, think about what kind of catalyst combination could be used to utilize the natural scaffold of paper. The types and sizes of catalysts that can be used for urea detection, as well as the distribution behavior of these catalysts, should be studied in order to increase the sensitivity of the paper substrate even further.

The purpose of this work is to investigate the fabrication of a three-electrode system on a paper substrate. Until now, the quantitative measurement of metabolites in human fluids, such as lactate, glucose, and urea, has been performed using enzyme or non-enzymatic based amperometric sensors and conventional potentiostats. An electrochemical cell is controlled by a potentiostat, which possesses two functions: (i) adjusting the current at a counter electrode (CE) so that the potential of the working electrode (WE) remains constant in relation to the reference electrode (RE), and (ii) converting the current at the working electrode to the voltage by a transimpedance amplifier with a high gain. Paper analytical devices are well suited to electrochemical detection because (i) electrodes can easily be miniaturized and fabricated onto paper; (ii) electrodes do not require complex/expensive materials or instrumentation; and (iii)

portable potentiostats are already available for on-site analysis. Therefore, electrochemical detection combined with paper analytical devices offers a good combination for developing inexpensive, portable, and sensitive devices. Thus, both the substrate study and the cellulose paper contribute to the capability of integrating wearable devices.

7.2 Consideration of electrode design and fabrication process

I first introduced the screen printing method as a circuit fabrication method over paper, as it has the advantage of being easy to fabricate, inexpensive, allowing for large-scale production, and ensuring good reproducibility of electrode on paper. Based on the application for point-of-care devices, the design of the electrode was taken into consideration. Solidworks CAD software was used to design a smaller-scale sensor.

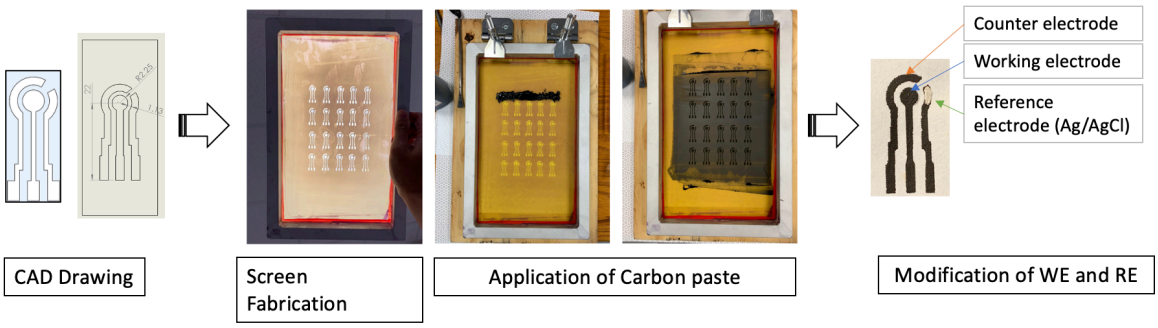

Figure 7-2 Fabrication of three-electrode system by screen printing. Sample (right) is printed on #1 filter paper.

In sensor fabrication, Whatman's No.1 chromatography paper is the most commonly used paper. There is uniformity on both sides, a medium flow rate (130 mm/30 m), and a thickness of 0.18 mm. 98 percent of it is cellulose, without any additives like strengthening or whitening agents, reducing interference from other substances. Counter electrode were designed to provide enough current to both working electrode and reference electrode, hence the larger area. An area of 15

mm^2 was chosen for the working electrode. There should be a gap between electrodes of 1.13 mm to 1.5 mm, so they don't overlap. According to the electrochemical test, the screen-printed electrode could detect 0.33 M urea in 1 M KOH solution via cyclic voltammetry (CV). As a catalyst, Ni was sputtered on the working electrode as one of the loading methods.

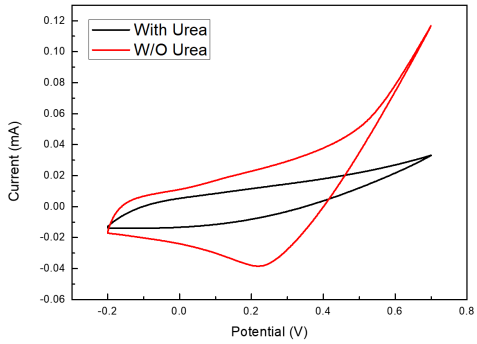

Figure 7-3 preliminary CV data of the paper-based screen printed electrode.

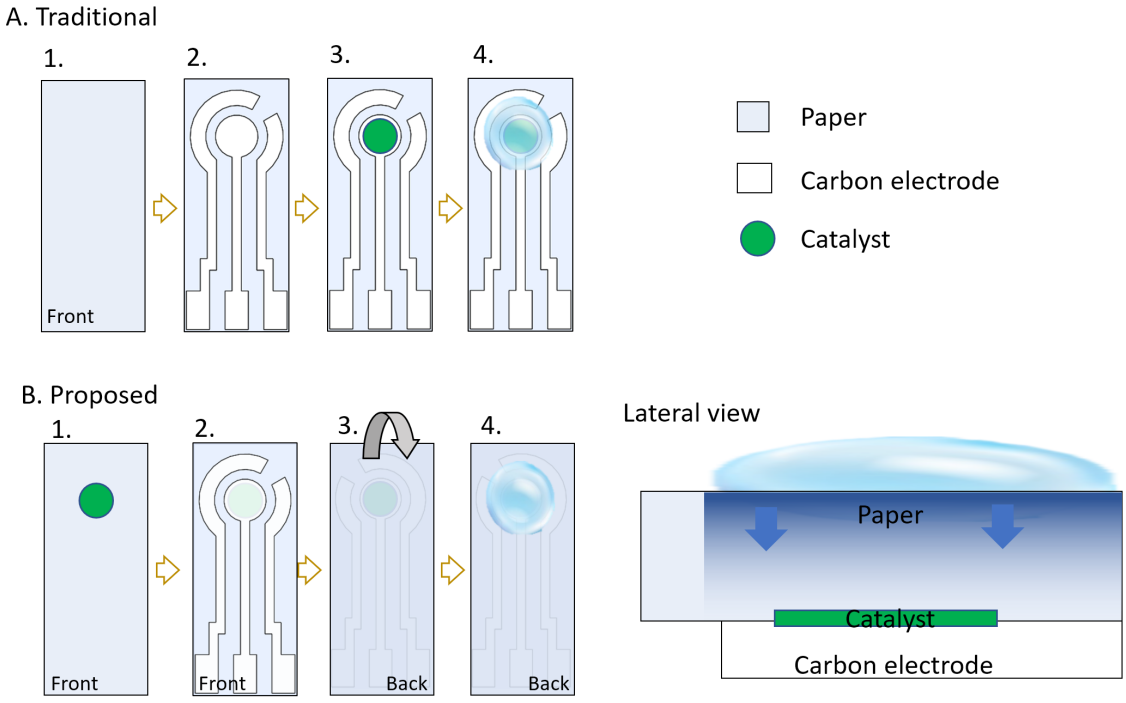

Figure 7-4 Reversed loading of catalyst on backside of printed electrode

Various design considerations were explored. In Figure 7-6, a reversed catalyst loading concept is illustrated. In this design, the paper's absorption property is fully exploited. It is just paper without any treatment on the backside of the electrode; it can soak up the solution containing NiO. As the NiO particles fill inside of the paper, they are all over the cellulose fibers when the paper is dried. Simple loading of catalyst could be achieved efficiently by using the capillary force of paper. The high specific area of cellulose fibers with loaded catalyst maximizes the active spot for the urea reaction during electrochemical analysis, which increases current density directly.

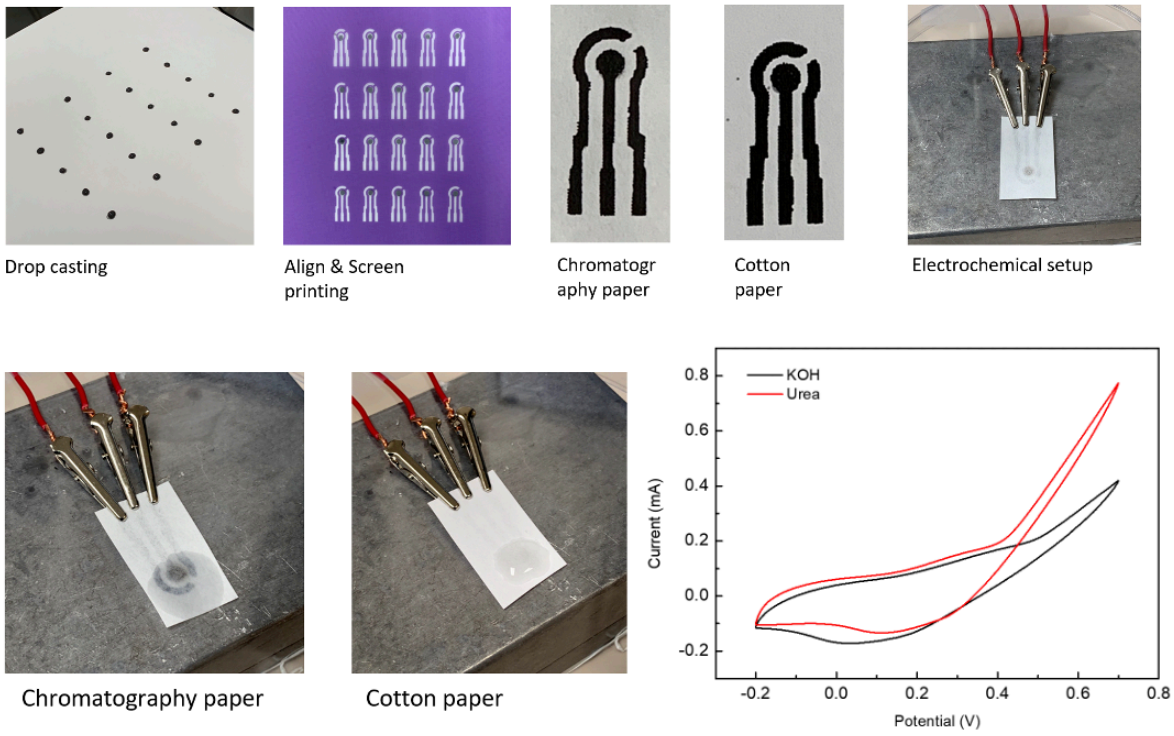

Figure 7-5 Electrochemical result with reversed design.

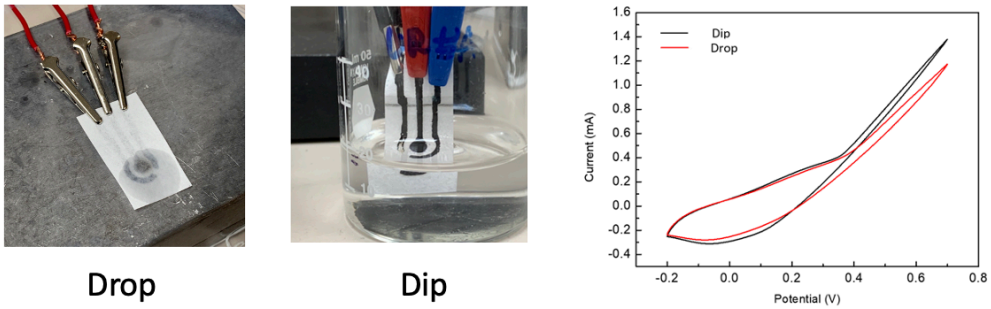

Figure 7-6 Drop of analyte vs. Dip in the analyte solution

Because the paper itself functions as a reservoir of an analyte, it shows certain detection of urea and requires a small amount of analyte solution to do the EC test. Figure 44 illustrates two different ways to conduct the electrochemical test: dipping the electrode in the analyte solution or dropping a small amount of the analyte solution onto the electrode surface. A comparison of electrochemical test results showed nearly the same current density between the two. It implies that the paper itself acts as a reservoir for the analyte solution, and in the long-term test, we would be able to add more papers to create a bigger reservoir for the analyte solution.

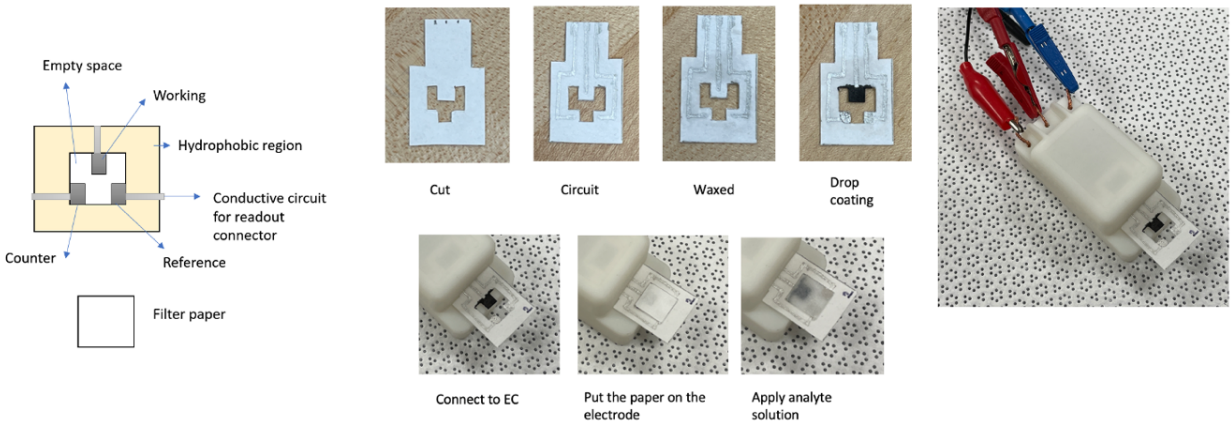

Figure 7-7 the design which considers simple loading of catalyst to the working electrode and separate reservoir for analyte

Figure 7-9 shows another type of design that can be used for easy drop-casting of catalyst for ease of fabrication. A drop of catalyst solution was applied to the designated area for working electrodes. A further soak of catalyst solution occurred unintentionally during drop-casting. It was possible to define only the working electrode area for the loading of catalyst by cutting out unwanted areas. The small piece of paper served as a reservoir and was located above the three electrodes. Due to the writability of the paper, the circuit was drawn with a simple silver conductive pen.

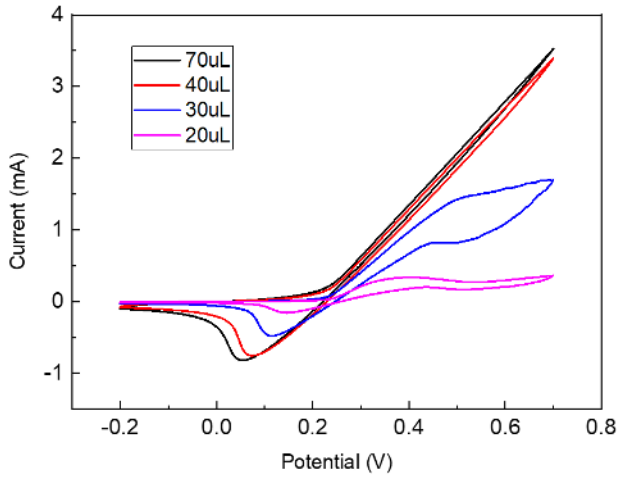

Figure 7-8 different amounts of analyte solution (#1filter paper, carbon paste strip, 0.33M urea in 1MKOH)

The proper amount of analyte for paper electrode was determined by varying the analyte solution amount on the reservoir from 20 µl to 70 µl. Using less than 40 µl of analyte solution lowered the current density, which means we need at least 40 µl (20 µl/cm^2) of analyte sample for our sensor configuration. From the literature, other electrochemical setups used sample amounts from 20 µL to more than 50 µL known area was generally 1cm^2. With our measurement, we are able to get a reading down to 20 µl/cm^2. As the paper effectively functions as a reservoir, the range of analyte amount for reliable detection is comparable to other sensors in the literature.

7.3 Paper strip electrode

In a subsequent result, I changed the configuration of the paper substrate for convenience's sake. The counters and reference electrodes were made from individual paper strips. Carbon black was applied to the conductive strip in the first step, similar to screen printing, and catalyst was loaded in the second step. After that, individual counter electrodes and reference electrode strips were assembled. The EC response varies depending on the loading method, which forms a different morphology of the loaded catalyst. In electrodeposition, the catalyst layer covers the paper where the carbon paste is applied, so that the cellulose structure remains intact without blocking the pores. The stability issue of the paper was discovered during the electrodeposition process. In electrodeposition, a bubble may affect the uniformity of the coating layer. During the ED, the swelling of the cellulose fibers may lead to a loss of conductivity due to the disconnection between the conductive material and the paper. This instability resulted in a low yield of deposited layers.

Table 7-1 Comparison of different catalyst loading methods for the fabrication of paper strip

Method	Advantage	Challenge
Carbon pasted paper + ED	Can deposit complex shape of substrate, thin layer of deposition	need conductive network, multi process is required
Carbon pasted paper + EPD	Can deposit complex shape of substrate	need conductive network, multi process is required, difficult to deposit deep inside of structure
Mixed CNT+NiO dip-coated paper	Easy one step process	Dispersion of CNT and NiO in solution

An alternative deposition method was DC-EPD on conductive paper strips prepared with carbon black. To perform DC-EPD, the paper strip must be submerged in a suspension containing NiO powder. The uniformity of the fiber was difficult to control because of swelling during the process, as in the case of ED.

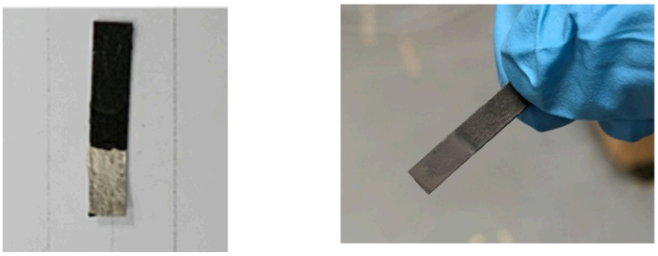

Figure 7-9 paper strip prepared by ED and EPD

NiO dip coating (or drop casting) was introduced for a better material solution. In contrast to two previous approaches, it is prepared by mixing conductive ink and catalyst nanopowder in a solution. Inside of all cellulose network, catalyst and conductive material are presented together. To begin with, carbon black (CB) powder was introduced as a conductive material to mix with NiO. In order to determine the optimal mixing ratio, the effect of the ratio between conductive material (CB) and catalyst (NiO) was investigated. In Figure 7-11, the current increases with the increase of conductive material. (The CB amount is increased into solution while NiO is maintained, then the solution is applied to the paper strip and dried.)

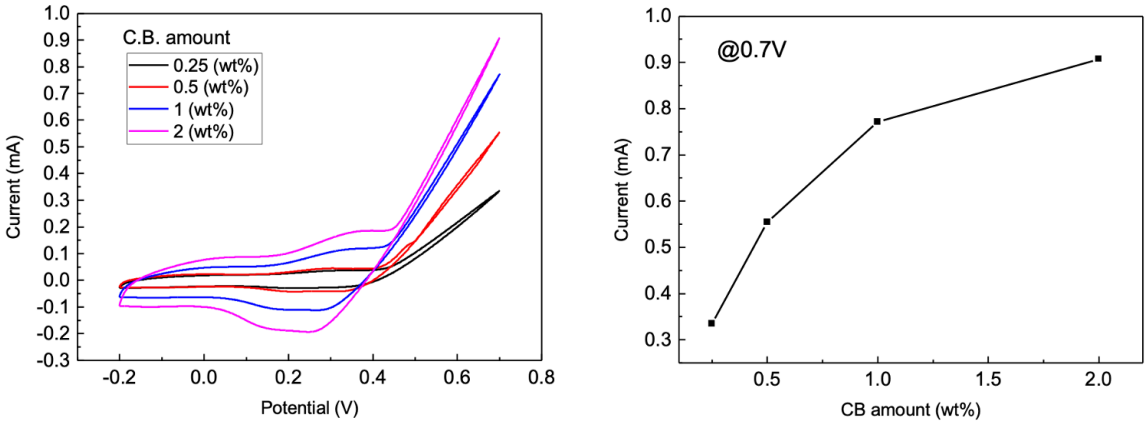

Figure 7-10 increase in conductivity with amount of CB

The reason for this is that there are more pathways for the electron produced from the reaction between NiO and urea during electrochemical tests, thus more chances for the electron to be captured through the circuit as a result. However, the optimal ratio of CB should be considered to prevent blocking cellulose pores. CNT is another conductive material that was selected because of its applicability, small diameter, and the ease with which it can be interwoven with NiO powder on cellulose fiber structures. As shown in Figure 7-13, the strip prepared by dipping in a solution of CNTs and NiO has a higher degree of flexibility, which makes it a better fit for wearable applications.

Figure 7-11 Bending the paper prepared by screen printing and Drop casting(dip)

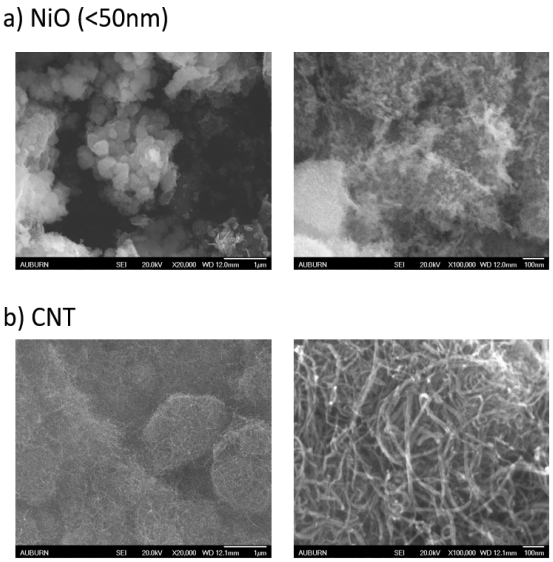

Figure 7-12 pristine NiO powder and CNT

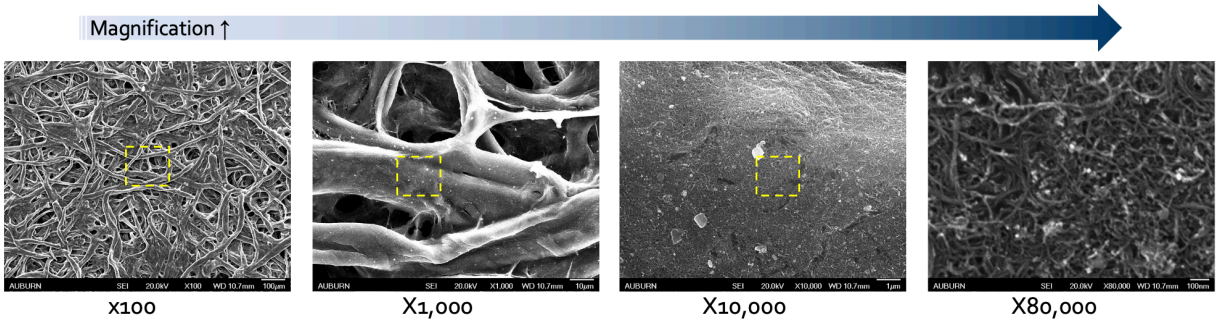

Figure 7-13 CNT+NiO applied on the #1 Whatman paper (100X, 1kX, 10kX, and 80kX respectively.)

The capillary force of paper allows it to penetrate deep inside the pore when it is dipped into a solution containing CNT and NiO. SEM confirmed that the overall complex fibrous cellulose structure was preserved at lower magnifications. On the surface of the cellulose fiber, NiO and CNT were observed to be intertwined with each other at magnifications up to 10 kX.

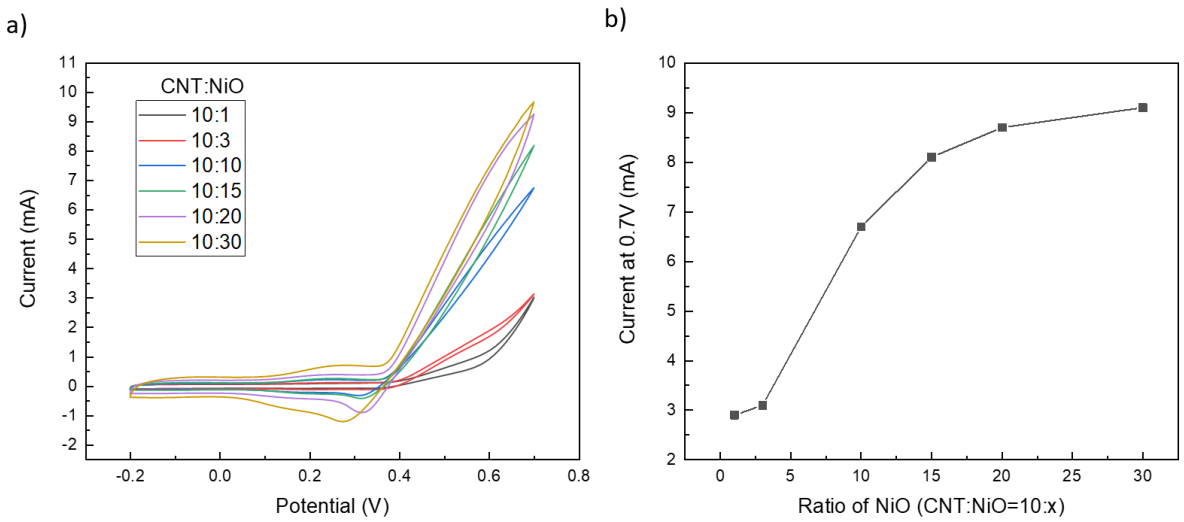

Figure 7-14 a) CV result with different ratio of CNT:NiO (0.33M Urea + 1M KOH) (100mV/s), and b) the peak potential at 0.7V

With the CNT amount maintained, the effect of the ratio between CNT and NiO was investigated. Figure 41b shows that the peak current for the urea reaction increased as NiO concentration increased from 1 to 30 mg/ml. For further experiments, the ratio of CNT:NiO was set to 10:15 since it reached a plateau at 15 mg/ml for efficiency toward the amount of NiO.

Figure 7-17 compares the CV results from two different approaches, DC-EPD and dipping method (CNT+NiO). The mixed ratio between CNT and NiO was set as 10:15. At 0.55V, the current of CNT+NiO dipped sample was 2.7 times higher than EPD sample. Figure 7-17 (top) shows SEM photos of a dipping sample that maintains the porous network of the paper and contains nanoparticles of NiO and CNT. In contrast, the sample prepared by DC-EPD (bottom) does not maintain its porous network.

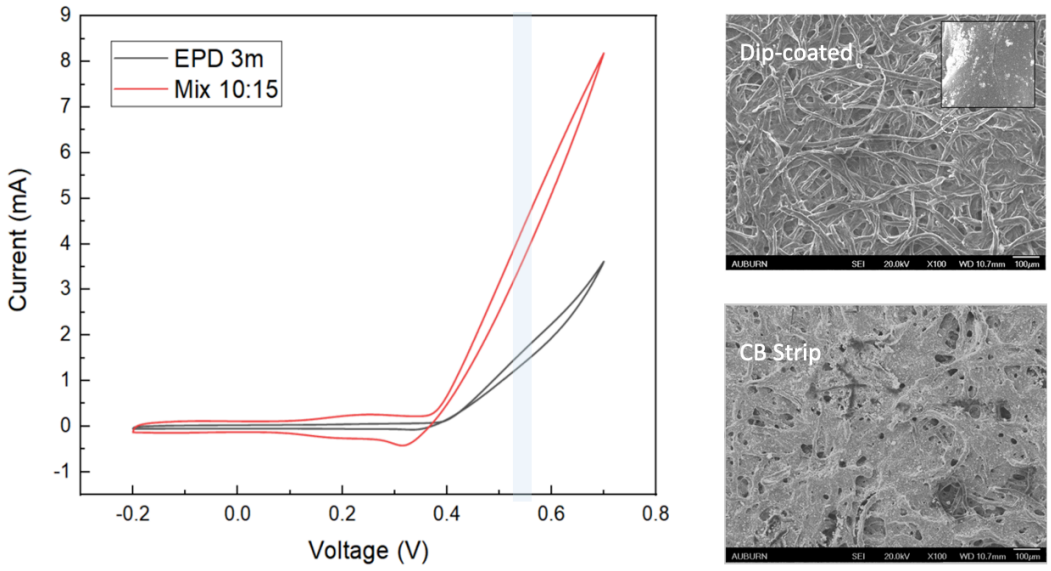

Figure 7-15 Comparison of morphology from different loading process: CNT+NiO dipping(top) and EPD(bottom)

The EPD loading process results in NiO particles moving in one direction, blocking pores near the surface of the paper. The current difference between the two samples is due to this reason. In this way, substrate utilization can vary depending on how the catalyst is loaded. In the experiment, the solution of NiO and CNTs dipped in cellulose paper was quite effective in dispersing the NiO particles with CNTs and maintaining the cellulose network. Additionally, it provided electron pathways from urea oxidation. As a result, the current response to urea in electrochemical tests is higher than that in DC-EPDs.

An analysis of parametric variables was conducted in this part. Furthermore, many approaches will still need to be investigated based on these preliminary results in order to appeal to the engineering perspective of utilizing paper in future urea sensors.

Chapter 8 Conclusions

Three different perspectives were explored in the dissertation for developing a highly sensitive non-enzymatic urea sensor: the hierarchical catalyst synthesis by hydrothermal method, the modified loading method by AC-EPD, and the use of paper as a substrate to utilize cellulose networks.

With the SDBS soft template, the synthesis process became simpler, but the current response of the hierarchical structure became much higher than that of nanoparticles or spheres. It was investigated that the ratio between SDBS and Ni^{2+} in the precursor solution plays a critical role in forming the hierarchical structure. The complex between SDBS and Ni^{2+} influences to forms the giant vesicle structure from hydrothermal synthesis, and further growth within the vesicle leads to the final hierarchical structure in which 2D building block nanosheets comprise 3D hollow structures. The reaction surface area of the hierarchical structure could be increased significantly, leading to a highly sensitive electrochemical urea sensor due to the hierarchical structure's abundance of electrochemical reaction sites.

In EPD coating process, alternating current was explored to control the deposition behavior. From the parametric study of DC-EPD, the deposition yield was mainly influenced by the applied potential and time, which allows us to predict a yield from the kinetic equation. As a result of modifying the waveform and frequency of the AC electric field, the packing behavior during EPD was controlled, resulting in the increase of the electrochemical response towards urea. It was confirmed that AC-EPD not only prevents water electrolysis, but also modifies the deposition morphology in aqueous suspensions, which could also provide the benefitthe environment.

Paper is a very suitable choice for flexible device applications. It is also worth noting that if the complex network of paper is utilized well, then the capability of enhancing the sensitivity, and thus overcoming the limitations of the non-enzymatic sensor, could be achieved. As part of the engineering aspects of this project, parametric studies in paper-based sensor fabrication were carried out in order to enhance sensitivity of the sensors built on paper.

Chapter 9 Future work

The concept of hierarchical structure is applicable to various other applications. In our hierarchical case, since it has a thin nano-sheet building block, it will be beneficial to the gas sensing application, considering the analyte sensitivity for gas sensors using metal oxides is highly dependent on the thickness of the catalyst layer.

The electrochemical test in my research was conducted with basic solution for accelerating conversion from NiO to NiOOH that contributes the electrochemical reaction with urea. The investigation on sensing at a neutral pH range is desirable to apply the developed catalysts for the wearable application, when considering the pH of sweat is close to neutral.

In the reported results, NiO is only taken into account in a model catalyst, however by incorporating other elements into the reaction, the UOR will be further improved by the synergistic effect. It is important to develop the process to maintain the hierarchical structure even after other metallic compounds are introduced into the synthetic system.

During AC-EPD processes, the motion of fluids or packing is difficult to identify due to the complex nature of the process. In order to develop a comprehensive mechanism, it would be beneficial to incorporate the experimental results and the simulation study.

References

[1] B. K. Boggs, R. L. King, and G. G. Botte, "Urea electrolysis: direct hydrogen production from urine," *Chem. Commun.*, no. 32, pp. 4859–4861, Aug. 2009, doi: 10.1039/B905974A.

[2] L. Liu, H. Mo, S. Wei, and D. Raftery, "Quantitative analysis of urea in human urine and serum by 1 H nuclear magnetic resonance," *Analyst*, vol. 137, no. 3, pp. 595–600, 2012, doi: 10.1039/C2AN15780B.

[3] J. Liu, R. Siavash Moakhar, A. Sudalaiyadum Perumal, H. N. Roman, S. Mahshid, and S. Wachsmann-Hogiu, "An AgNP-deposited commercial electrochemistry test strip as a platform for urea detection," *Sci Rep*, vol. 10, no. 1, p. 9527, Jun. 2020, doi: 10.1038/s41598-020-66422-x.

[4] T. H. V. Kumar and A. K. Sundramoorthy, "Non-Enzymatic Electrochemical Detection of Urea on Silver Nanoparticles Anchored Nitrogen-Doped Single-Walled Carbon Nanotube Modified Electrode," *J. Electrochem. Soc.*, vol. 165, no. 8, p. B3006, Feb. 2018, doi: 10.1149/2.0021808jes.

[5] N. S. Nguyen, G. Das, and H. H. Yoon, "Nickel/cobalt oxide-decorated 3D graphene nanocomposite electrode for enhanced electrochemical detection of urea," *Biosensors and Bioelectronics*, vol. 77, pp. 372–377, Mar. 2016, doi: 10.1016/j.bios.2015.09.046.

[6] K. Kim *et al.*, "Fabrication of a Urea Biosensor for Real-Time Dynamic Fluid Measurement," *Sensors*, vol. 18, no. 8, Art. no. 8, Aug. 2018, doi: 10.3390/s18082607.

[7] H. Nie, Z. Yao, X. Zhou, Z. Yang, and S. Huang, "Nonenzymatic electrochemical detection of glucose using well-distributed nickel nanoparticles on straight multi-walled carbon nanotubes," *Biosens Bioelectron*, vol. 30, no. 1, pp. 28–34, Dec. 2011, doi: 10.1016/j.bios.2011.08.022.

[8] M. Vidotti, M. R. Silva, R. P. Salvador, S. I. C. de Torresi, and L. H. Dall'Antonia, "Electrocatalytic oxidation of urea by nanostructured nickel/cobalt hydroxide electrodes," *Electrochimica Acta*, vol. 53, no. 11, pp. 4030–4034, Apr. 2008, doi: 10.1016/j.electacta.2007.11.029.

[9] K. Jukk, J. Kozlova, P. Ritslaid, V. Sammelselg, N. Alexeyeva, and K. Tammeveski, "Sputter-deposited Pt nanoparticle/multi-walled carbon nanotube composite catalyst for oxygen reduction reaction," *Journal of Electroanalytical Chemistry*, vol. 708, pp. 31–38, Nov. 2013, doi: 10.1016/j.jelechem.2013.09.009.

[10] Y.-C. Song *et al.*, "Effect of the oxygen reduction catalyst loading method on the performance of air breathable cathodes for microbial fuel cells," *J Appl Electrochem*, vol. 42, no. 6, pp. 391–398, Jun. 2012, doi: 10.1007/s10800-012-0410-8.

[11] E. Hariprasad and T. P. Radhakrishnan, "A Highly Efficient and Extensively Reusable 'Dip Catalyst' Based on a Silver-Nanoparticle-Embedded Polymer Thin Film," *Chemistry – A European Journal*, vol. 16, no. 48, pp. 14378–14384, 2010, doi: https://doi.org/10.1002/chem.201001679.

[12] M.-S. Wu, R.-Y. Ji, and Y.-R. Zheng, "Nickel hydroxide electrode with a monolayer of nanocup arrays as an effective electrocatalyst for enhanced electrolysis of urea," *Electrochimica Acta*, vol. 144, pp. 194–199, Oct. 2014, doi: 10.1016/j.electacta.2014.08.098.

[13] A. W. Martinez, S. T. Phillips, M. J. Butte, and G. M. Whitesides, “Patterned Paper as a Platform for Inexpensive, Low-Volume, Portable Bioassays,” *Angewandte Chemie*, vol. 119, no. 8, pp. 1340–1342, 2007, doi: https://doi.org/10.1002/ange.200603817.
[14] J.-H. Lee, “Gas sensors using hierarchical and hollow oxide nanostructures: Overview,” *Sensors and Actuators B: Chemical*, vol. 140, no. 1, pp. 319–336, Jun. 2009, doi: 10.1016/j.snb.2009.04.026.
[15] C. Xu, J. Tamaki, N. Miura, and N. Yamazoe, “Grain size effects on gas sensitivity of porous SnO2-based elements,” *Sensors and Actuators B: Chemical*, vol. 3, no. 2, pp. 147–155, Feb. 1991, doi: 10.1016/0925-4005(91)80207-Z.
[16] J. Li *et al.*, “Morphology-controlled electrochemical sensing properties of CuS crystals for tartrazine and sunset yellow,” *Sensors and Actuators B: Chemical*, vol. 288, pp. 552–563, Jun. 2019, doi: 10.1016/j.snb.2019.03.028.
[17] M. Shoyama and N. Hashimoto, “Effect of poly ethylene glycol addition on the microstructure and sensor characteristics of SnO2 thin films prepared by sol–gel method,” *Sensors and Actuators B: Chemical*, vol. 93, no. 1, pp. 585–589, Aug. 2003, doi: 10.1016/S0925-4005(03)00215-6.
[18] G. Korotcenkov, “Gas response control through structural and chemical modification of metal oxide films: state of the art and approaches,” *Sensors and Actuators B: Chemical*, vol. 107, no. 1, pp. 209–232, May 2005, doi: 10.1016/j.snb.2004.10.006.
[19] Y. Fang, D. Luan, S. Gao, and X. W. (David) Lou, “Rational Design and Engineering of One-Dimensional Hollow Nanostructures for Efficient Electrochemical Energy Storage,” *Angewandte Chemie International Edition*, vol. 60, no. 37, pp. 20102–20118, 2021, doi: 10.1002/anie.202104401.
[20] C.-T. Hung *et al.*, “Gradient Hierarchically Porous Structure for Rapid Capillary-Assisted Catalysis,” *J. Am. Chem. Soc.*, vol. 144, no. 13, pp. 6091–6099, Apr. 2022, doi: 10.1021/jacs.2c01444.
[21] Y. Zhu *et al.*, “An electrochemical exploration of hollow NiCo2O4 submicrospheres and its capacitive performances,” *Journal of Power Sources*, vol. 287, pp. 307–315, Aug. 2015, doi: 10.1016/j.jpowsour.2015.04.053.
[22] X. W. Lou, C. Yuan, and L. A. Archer, “Shell-by-Shell Synthesis of Tin Oxide Hollow Colloids with Nanoarchitectured Walls: Cavity Size Tuning and Functionalization,” *Small*, vol. 3, no. 2, pp. 261–265, 2007, doi: https://doi.org/10.1002/smll.200600445.
[23] P. Shao *et al.*, “Programmable synthesis of metal hydroxide/oxide hollow architectures: towards an efficient and robust photocatalyst for water remediation,” *Journal of Materials Chemistry A*, vol. 5, no. 1, pp. 124–132, 2017, doi: 10.1039/C6TA08042A.
[24] M. Sasidharan, N. Gunawardhana, M. Inoue, S. Yusa, M. Yoshio, and K. Nakashima, “La 2 O 3 hollow nanospheres for high performance lithium-ion rechargeable batteries,” *Chemical Communications*, vol. 48, no. 26, pp. 3200–3202, 2012, doi: 10.1039/C2CC16085D.
[25] S. Liu, M. Xie, X. Guo, and W. Ji, “Synthesis of CeO2 hollow nanospheres via redox reaction based self-templating approach,” *Materials Letters*, vol. 105, pp. 192–195, Aug. 2013, doi: 10.1016/j.matlet.2013.03.133.
[26] P. Dai, Y.-Q. Sun, Z.-W. Bao, J. Zhu, and M.-Z. Wu, “Optical and adsorption properties of mesoporous SiO2/Zn2SiO4:Eu3+ hollow nanospheres,” *Micro & Nano Letters*, vol. 12, no. 4, pp. 248–251, 2017, doi: 10.1049/mnl.2016.0474.

[27] J. Wang *et al.*, "Organic–Rare Earth Hybrid Anode with Superior Cyclability for Lithium Ion Battery," *Advanced Materials Interfaces*, vol. 7, no. 9, p. 1902168, 2020, doi: 10.1002/admi.201902168.
[28] M.-S. Wu, G.-W. Lin, and R.-S. Yang, "Hydrothermal growth of vertically-aligned ordered mesoporous nickel oxide nanosheets on three-dimensional nickel framework for electrocatalytic oxidation of urea in alkaline medium," *Journal of Power Sources*, vol. 272, pp. 711–718, Dec. 2014, doi: 10.1016/j.jpowsour.2014.09.009.
[29] Y. Yin, S. Xin, L. Wan, C. Li, and Y. Guo, "SnO2 hollow spheres: Polymer bead-templated hydrothermal synthesis and their electrochemical properties for lithium storage," *Sci. China Chem.*, vol. 55, no. 7, pp. 1314–1318, Jul. 2012, doi: 10.1007/s11426-012-4659-x.
[30] X. Wang *et al.*, "Synthesis of Anatase TiO2 Tubular Structures Microcrystallites with a High Percentage of 001 Facets by a Simple One-Step Hydrothermal Template Process," *Chemistry – A European Journal*, vol. 16, no. 24, pp. 7106–7109, 2010, doi: https://doi.org/10.1002/chem.200903503.
[31] Y. Liang, Q. Liu, A. M. Asiri, and X. Sun, "Enhanced electrooxidation of urea using NiMoO4·xH2O nanosheet arrays on Ni foam as anode," *Electrochimica Acta*, vol. 153, pp. 456–460, Jan. 2015, doi: 10.1016/j.electacta.2014.11.193.
[32] H. Xu and W. Wang, "Template Synthesis of Multishelled Cu2O Hollow Spheres with a Single-Crystalline Shell Wall," *Angewandte Chemie*, vol. 119, no. 9, pp. 1511–1514, 2007, doi: 10.1002/ange.200603895.
[33] L. Guo, Z. Mu, P. Da, Z. Weng, P. Xi, and C.-H. Yan, "Hollow structures with rare earths: Synthesis and electrocatalytic applications," *EnergyChem*, vol. 4, no. 5, p. 100088, Sep. 2022, doi: 10.1016/j.enchem.2022.100088.
[34] N. Yang, F. Pang, and J. Ge, "One-pot and general synthesis of crystalline mesoporous metal oxides nanoparticles by protective etching: potential materials for catalytic applications," *Journal of Materials Chemistry A*, vol. 3, no. 3, pp. 1133–1141, 2015, doi: 10.1039/C4TA05334F.
[35] K. Byrappa, N. Keerthiraj, and S. M. Byrappa, "14 - Hydrothermal Growth of Crystals—Design and Processing," in *Handbook of Crystal Growth (Second Edition)*, P. Rudolph, Ed. Boston: Elsevier, 2015, pp. 535–575. doi: 10.1016/B978-0-444-63303-3.00014-6.
[36] M. M. Sk, C. Y. Yue, K. Ghosh, and R. K. Jena, "Review on advances in porous nanostructured nickel oxides and their composite electrodes for high-performance supercapacitors," *Journal of Power Sources*, vol. 308, pp. 121–140, Mar. 2016, doi: 10.1016/j.jpowsour.2016.01.056.
[37] K. Byrappa and T. Adschiri, "Hydrothermal technology for nanotechnology," *Progress in Crystal Growth and Characterization of Materials*, vol. 53, no. 2, pp. 117–166, Jun. 2007, doi: 10.1016/j.pcrysgrow.2007.04.001.
[38] W. Yan, D. Wang, and G. G. Botte, "Nickel and cobalt bimetallic hydroxide catalysts for urea electro-oxidation," *Electrochimica Acta*, vol. 61, pp. 25–30, Feb. 2012, doi: 10.1016/j.electacta.2011.11.044.
[39] W. Xu, H. Zhang, G. Li, and Z. Wu, "Nickel-cobalt bimetallic anode catalysts for direct urea fuel cell," *Scientific Reports*, vol. 4, no. 1, Art. no. 1, Aug. 2014, doi: 10.1038/srep05863.
[40] W. Yan, D. Wang, and G. G. Botte, "Electrochemical decomposition of urea with Ni-based catalysts," *Applied Catalysis B: Environmental*, vol. 127, pp. 221–226, Oct. 2012, doi: 10.1016/j.apcatb.2012.08.022.

[41] “Facile synthesis of mesoporous spinel NiCo2O4 nanostructures as highly efficient electrocatalysts for urea electro-oxidation - Nanoscale (RSC Publishing).” https://pubs.rsc.org/en/content/articlelanding/nr/2014/c3nr05359h#!divAbstract (accessed Feb. 16, 2021).
[42] S. Periyasamy, P. Subramanian, E. Levi, D. Aurbach, A. Gedanken, and A. Schechter, “Exceptionally Active and Stable Spinel Nickel Manganese Oxide Electrocatalysts for Urea Oxidation Reaction,” *ACS Appl. Mater. Interfaces*, vol. 8, no. 19, pp. 12176–12185, May 2016, doi: 10.1021/acsami.6b02491.
[43] X. Song and L. Gao, “Facile Synthesis and Hierarchical Assembly of Hollow Nickel Oxide Architectures Bearing Enhanced Photocatalytic Properties,” *J. Phys. Chem. C*, vol. 112, no. 39, pp. 15299–15305, Oct. 2008, doi: 10.1021/jp804921g.
[44] W.-C. Geng *et al.*, “Synthesis of hollow spherical nickel oxide and its gas-sensing properties,” *Rare Met.*, vol. 40, no. 6, pp. 1622–1631, Jun. 2021, doi: 10.1007/s12598-020-01639-3.
[45] Y. Wang, Q. Zhu, and H. Zhang, “Fabrication of β-Ni(OH) 2 and NiO hollow spheres by a facile template-free process,” *Chemical Communications*, vol. 0, no. 41, pp. 5231–5233, 2005, doi: 10.1039/B508807K.
[46] W. Li, Z. Song, X. Deng, X.-Z. Fu, and J.-L. Luo, “Decoration of NiO hollow spheres composed of stacked nanosheets with CeO2 nanoparticles: Enhancement effect of CeO2 for electrocatalytic methanol oxidation,” *Electrochimica Acta*, vol. 337, p. 135684, Mar. 2020, doi: 10.1016/j.electacta.2020.135684.
[47] Q. Li, W. Zeng, Q. Zhou, and Z. Wang, “Highly Sensitive Ethanol Sensing Using NiO Hollow Spheres Synthesized via Hydrothermal Method,” *Chemosensors*, vol. 10, no. 8, Art. no. 8, Aug. 2022, doi: 10.3390/chemosensors10080341.
[48] C. Kuang, W. Zeng, H. Ye, and Y. Li, “A novel approach for fabricating NiO hollow spheres for gas sensors,” *Physica E: Low-dimensional Systems and Nanostructures*, vol. 97, pp. 314–316, Mar. 2018, doi: 10.1016/j.physe.2017.12.006.
[49] C. Nie, W. Zeng, X. Jing, and H. Ye, “NiO hollow nanospheres with different surface by a bubble-template approach and its gas sensing,” *J Mater Sci: Mater Electron*, vol. 29, no. 9, pp. 7480–7488, May 2018, doi: 10.1007/s10854-018-8739-3.
[50] H. Hu *et al.*, “Facile template-free synthesis of hierarchically porous NiO hollow architectures with high-efficiency adsorptive removal of Congo red,” *J Porous Mater*, vol. 26, no. 6, pp. 1743–1753, Dec. 2019, doi: 10.1007/s10934-019-00758-2.
[51] Z. Chen, M. Cao, and C. Hu, “Novel Zn2SnO4 Hierarchical Nanostructures and Their Gas Sensing Properties toward Ethanol,” *J. Phys. Chem. C*, vol. 115, no. 13, pp. 5522–5529, Apr. 2011, doi: 10.1021/jp111785t.
[52] D. S. Hall, D. J. Lockwood, C. Bock, and B. R. MacDougall, “Nickel hydroxides and related materials: a review of their structures, synthesis and properties,” *Proc. R. Soc. A.*, vol. 471, no. 2174, p. 20140792, Feb. 2015, doi: 10.1098/rspa.2014.0792.
[53] H. Bode, K. Dehmelt, and J. Witte, “Zur kenntnis der nickelhydroxidelektrode—I.Über das nickel (II)-hydroxidhydrat,” *Electrochimica Acta*, vol. 11, no. 8, pp. 1079–1087, Aug. 1966, doi: 10.1016/0013-4686(66)80045-2.
[54] M. Dixit, G. N. Subbanna, and P. V. Kamath, “Homogeneous precipitation from solution by urea hydrolysis: a novel chemical route to the α-hydroxides of nickel and cobalt,” *J. Mater. Chem.*, vol. 6, no. 8, pp. 1429–1432, Jan. 1996, doi: 10.1039/JM9960601429.

[55] L.-X. Yang, Y.-J. Zhu, H. Tong, Z.-H. Liang, L. Li, and L. Zhang, "Hydrothermal synthesis of nickel hydroxide nanostructures in mixed solvents of water and alcohol," *Journal of Solid State Chemistry*, vol. 180, no. 7, pp. 2095–2101, Jul. 2007, doi: 10.1016/j.jssc.2007.05.009.
[56] L. Dong, Y. Chu, and W. Sun, "Controllable Synthesis of Nickel Hydroxide and Porous Nickel Oxide Nanostructures with Different Morphologies," *Chemistry – A European Journal*, vol. 14, no. 16, pp. 5064–5072, 2008, doi: 10.1002/chem.200701627.
[57] "Surfactants and Interfacial Phenomena - Milton J. Rosen, Joy T. Kunjappu - Google Books." https://books.google.com/books?hl=en&lr=&id=pdTsgREZp5QC&oi=fnd&pg=PR15&ots=-87FWhrOmR&sig=srEgrGia060tY1Vo6NfWqmIZguA#v=onepage&q&f=false (accessed Oct. 28, 2022).
[58] S. Ghosh, A. Ray, and N. Pramanik, "Self-assembly of surfactants: An overview on general aspects of amphiphiles," *Biophysical Chemistry*, vol. 265, p. 106429, Oct. 2020, doi: 10.1016/j.bpc.2020.106429.
[59] "Physico-Chemical Properties of Selected Anionic, Cationic and Nonionic ... - N.M. van Os, J.R. Haak, L.A.M. Rupert - Google Books." https://books.google.com/books?hl=en&lr=&id=Fj0r-IQneaEC&oi=fnd&pg=PP1&ots=UIlAOEO6YH&sig=Eu6-GfBbXwYsHVslg3cFo2y0zUM#v=onepage&q&f=false (accessed Oct. 28, 2022).
[60] R. Nagarajan, "Molecular Packing Parameter and Surfactant Self-Assembly: The Neglected Role of the Surfactant Tail," *Langmuir*, vol. 18, no. 1, pp. 31–38, Jan. 2002, doi: 10.1021/la010831y.
[61] R. Nagarajan, "Molecular Thermodynamics of Giant Micelles," in *Giant Micelles*, CRC Press, 2007.
[62] J. A. Lewis, "Colloidal Processing of Ceramics," *Journal of the American Ceramic Society*, vol. 83, no. 10, pp. 2341–2359, Dec. 2004, doi: 10.1111/j.1151-2916.2000.tb01560.x.
[63] null Rojas, null Claesson, null Muller, and null Neuman, "The Effect of Salt Concentration on Adsorption of Low-Charge-Density Polyelectrolytes and Interactions between Polyelectrolyte-Coated Surfaces," *J Colloid Interface Sci*, vol. 205, no. 1, pp. 77–88, Sep. 1998, doi: 10.1006/jcis.1998.5596.
[64] S. Biggs and T. W. Healy, "Electrosteric stabilisation of colloidal zirconia with low-molecular-weight polyacrylic acid. An atomic force microscopy study," *Journal of the Chemical Society, Faraday Transactions*, vol. 90, no. 22, pp. 3415–3421, 1994, doi: 10.1039/FT9949003415.
[65] O. O. Van der Biest and L. J. Vandeperre, "ELECTROPHORETIC DEPOSITION OF MATERIALS," *Annu. Rev. Mater. Sci.*, vol. 29, no. 1, pp. 327–352, Aug. 1999, doi: 10.1146/annurev.matsci.29.1.327.
[66] H. C. Hamaker, "Formation of a deposit by electrophoresis," *Trans. Faraday Soc.*, vol. 35, no. 0, pp. 279–287, Jan. 1940, doi: 10.1039/TF9403500279.
[67] T. Ishihara, K. Shimose, T. Kudo, H. Nishiguchi, T. Akbay, and Y. Takita, "Preparation of Yttria-Stabilized Zirconia Thin Films on Strontium-Doped LaMnO3 Cathode Substrates via Electrophoretic Deposition for Solid Oxide Fuel Cells," *Journal of the American Ceramic Society*, vol. 83, no. 8, pp. 1921–1927, 2000, doi: https://doi.org/10.1111/j.1151-2916.2000.tb01491.x.
[68] Z. Zhang, Y. Huang, and Z. Jiang, "Electrophoretic Deposition Forming of SiC-TZP Composites in a Nonaqueous Sol Media," *Journal of the American Ceramic Society*, vol. 77, no. 7, pp. 1946–1949, 1994, doi: https://doi.org/10.1111/j.1151-2916.1994.tb07075.x.

[69] L. Besra and M. Liu, “A review on fundamentals and applications of electrophoretic deposition (EPD),” *Progress in Materials Science*, vol. 52, no. 1, pp. 1–61, Jan. 2007, doi: 10.1016/j.pmatsci.2006.07.001.
[70] N. Sato, M. Kawachi, K. Noto, N. Yoshimoto, and M. Yoshizawa, “Effect of particle size reduction on crack formation in electrophoretically deposited YBCO films,” *Physica C: Superconductivity*, vol. 357–360, pp. 1019–1022, Aug. 2001, doi: 10.1016/S0921-4534(01)00510-X.
[71] R. W. Powers, “The Electrophoretic Forming of Beta-Alumina Ceramic,” *J. Electrochem. Soc.*, vol. 122, no. 4, p. 490, Apr. 1975, doi: 10.1149/1.2134246.
[72] Y.-C. Wang, I.-C. Leu, and M.-H. Hon, “Kinetics of Electrophoretic Deposition for Nanocrystalline Zinc Oxide Coatings,” *Journal of the American Ceramic Society*, vol. 87, no. 1, pp. 84–88, 2004, doi: https://doi.org/10.1111/j.1551-2916.2004.00084.x.
[73] I. ZHITOMIRSKY and L. GAL-OR, “Electrophoretic deposition of hydroxyapatite,” *Journal of Materials Science: Materials in Medicine*, vol. 8, no. 4, pp. 213–219, Apr. 1997, doi: 10.1023/A:1018587623231.
[74] L. Vandeperre, O. Van der Biest, and W. J. Clegg, “Silicon Carbide Laminates with Carbon Interlayers by Electrophoretic Deposition,” *Key Engineering Materials*, vol. 127–131, pp. 567–574, 1997, doi: 10.4028/www.scientific.net/KEM.127-131.567.
[75] E. Bakker and E. Pretsch, “Potentiometric sensors for trace-level analysis,” *TrAC Trends in Analytical Chemistry*, vol. 24, no. 3, pp. 199–207, Mar. 2005, doi: 10.1016/j.trac.2005.01.003.
[76] A. E. HERR *et al.*, “Integrated Microfluidic Platform for Oral Diagnostics,” *Ann N Y Acad Sci*, vol. 1098, pp. 362–374, Mar. 2007, doi: 10.1196/annals.1384.004.
[77] S. F. Clarke and J. R. Foster, “A history of blood glucose meters and their role in self-monitoring of diabetes mellitus,” *British Journal of Biomedical Science*, vol. 69, no. 2, pp. 83–93, Jan. 2012, doi: 10.1080/09674845.2012.12002443.
[78] A. W. Martinez, S. T. Phillips, E. Carrilho, S. W. Thomas, H. Sindi, and G. M. Whitesides, “Simple Telemedicine for Developing Regions: Camera Phones and Paper-Based Microfluidic Devices for Real-Time, Off-Site Diagnosis,” *Anal. Chem.*, vol. 80, no. 10, pp. 3699–3707, May 2008, doi: 10.1021/ac800112r.
[79] O. Amor-Gutiérrez, E. Costa-Rama, and M. T. Fernández Abedul, “Chapter 25 - Determination of glucose with an enzymatic paper-based sensor,” in *Laboratory Methods in Dynamic Electroanalysis*, M. T. Fernandez Abedul, Ed. Elsevier, 2020, pp. 257–265. doi: 10.1016/B978-0-12-815932-3.00025-5.
[80] A. W. Martinez, S. T. Phillips, G. M. Whitesides, and E. Carrilho, “Diagnostics for the Developing World: Microfluidic Paper-Based Analytical Devices,” *Anal. Chem.*, vol. 82, no. 1, pp. 3–10, Jan. 2010, doi: 10.1021/ac9013989.
[81] J. Mettakoonpitak *et al.*, “Electrochemistry on Paper-based Analytical Devices: A Review,” *Electroanalysis*, vol. 28, no. 7, pp. 1420–1436, 2016, doi: 10.1002/elan.201501143.
[82] T. Lappalainen, P. Vento, T. Teerinen, T. Erho, and L. Hakalahti, “Cellulose as a novel substrate for lateral flow assay,” *Nordic Pulp & Paper Research Journal*, vol. 25, no. 4, pp. 536–550, Dec. 2010, doi: 10.3183/npprj-2010-25-04-p529-543.
[83] A. Ainla *et al.*, “Open-Source Potentiostat for Wireless Electrochemical Detection with Smartphones,” *Anal. Chem.*, vol. 90, no. 10, pp. 6240–6246, May 2018, doi: 10.1021/acs.analchem.8b00850.

[84] W. Dungchai, O. Chailapakul, and C. S. Henry, “Electrochemical Detection for Paper-Based Microfluidics,” *Anal. Chem.*, vol. 81, no. 14, pp. 5821–5826, Jul. 2009, doi: 10.1021/ac9007573.
[85] F. Arduini and D. Moscone, “Multifarious aspects of electrochemical paper-based (bio)sensors,” in *Comprehensive Analytical Chemistry*, vol. 89, Elsevier, 2020, pp. 139–161. doi: 10.1016/bs.coac.2020.01.001.
[86] M. Gutiérrez-Capitán, A. Baldi, and C. Fernández-Sánchez, “Electrochemical Paper-Based Biosensor Devices for Rapid Detection of Biomarkers,” *Sensors*, vol. 20, no. 4, Art. no. 4, Jan. 2020, doi: 10.3390/s20040967.
[87] J.-W. Han, B. Kim, J. Li, and M. Meyyappan, “Carbon Nanotube Based Humidity Sensor on Cellulose Paper,” *J. Phys. Chem. C*, vol. 116, no. 41, pp. 22094–22097, Oct. 2012, doi: 10.1021/jp3080223.
[88] C. J. Valentine, K. Takagishi, S. Umezu, R. Daly, and M. De Volder, “Paper-Based Electrochemical Sensors Using Paper as a Scaffold to Create Porous Carbon Nanotube Electrodes,” *ACS Applied Materials & Interfaces*, vol. 12, no. 27, pp. 30680–30685, Jul. 2020, doi: 10.1021/acsami.0c04896.
[89] H. Beitollahi, F. Movahedifar, S. Tajik, and S. Jahani, “A Review on the Effects of Introducing CNTs in the Modification Process of Electrochemical Sensors,” *Electroanalysis*, vol. 31, no. 7, pp. 1195–1203, 2019, doi: https://doi.org/10.1002/elan.201800370.
[90] E. Noviana, C. P. McCord, K. M. Clark, I. Jang, and C. S. Henry, “Electrochemical paper-based devices: sensing approaches and progress toward practical applications,” *Lab Chip*, vol. 20, no. 1, pp. 9–34, Dec. 2019, doi: 10.1039/C9LC00903E.
[91] S. K. Meher, P. Justin, and G. Ranga Rao, “Microwave-Mediated Synthesis for Improved Morphology and Pseudocapacitance Performance of Nickel Oxide,” *ACS Appl. Mater. Interfaces*, vol. 3, no. 6, pp. 2063–2073, Jun. 2011, doi: 10.1021/am200294k.
[92] Y. Wang and Y. Xia, “Electrochemical capacitance characterization of NiO with ordered mesoporous structure synthesized by template SBA-15,” *Electrochimica Acta*, vol. 51, no. 16, pp. 3223–3227, Apr. 2006, doi: 10.1016/j.electacta.2005.09.013.
[93] M. Qin, L. Zhang, and H. Wu, “Dual-template hydrothermal synthesis of multi-channel porous NiCo2O4 hollow spheres as high-performance electromagnetic wave absorber,” *Applied Surface Science*, vol. 515, p. 146132, Jun. 2020, doi: 10.1016/j.apsusc.2020.146132.
[94] X. Luo *et al.*, “In situ growth of hollow Cu2O spheres using anionic vesicles as soft templates,” *Journal of Industrial and Engineering Chemistry*, vol. 59, pp. 410–415, Mar. 2018, doi: 10.1016/j.jiec.2017.10.052.
[95] “Preparation of Thick Films by Electrophoretic Deposition Using Surface Modified Silica Particles Derived from Sol-Gel Method | SpringerLink.” https://link.springer.com/article/10.1023/A:1008789025826 (accessed Jun. 14, 2021).
[96] W. Shan *et al.*, “Electrophoretic deposition of nanosized zeolites in non-aqueous medium and its application in fabricating thin zeolite membranes,” *Microporous and Mesoporous Materials*, vol. 69, no. 1, pp. 35–42, Apr. 2004, doi: 10.1016/j.micromeso.2004.01.003.
[97] T. M. Sridhar, U. Kamachi Mudali, and M. Subbaiyan, “Preparation and characterisation of electrophoretically deposited hydroxyapatite coatings on type 316L stainless steel,” *Corrosion Science*, vol. 45, no. 2, pp. 237–252, Feb. 2003, doi: 10.1016/S0010-938X(02)00091-4.

[98] J. Yum, S.-Y. Seo, S. Lee, and Y.-E. Sung, "Y 3Al5 O 12 : Ce0.05 Phosphor Coatings on Gallium Nitride for White Light Emitting Diodes," *J. Electrochem. Soc.*, vol. 150, no. 2, p. H47, Jan. 2003, doi: 10.1149/1.1535207.
[99] "Superconducting coatings of MgB 2 prepared by electrophoretic deposition | SpringerLink." https://link.springer.com/article/10.1007/s00216-004-2668-0 (accessed Jun. 14, 2021).
[100] N. Dougami and T. Takada, "Modification of metal oxide semiconductor gas sensor by electrophoretic deposition," *Sensors and Actuators B: Chemical*, vol. 93, no. 1, pp. 316–320, Aug. 2003, doi: 10.1016/S0925-4005(03)00219-3.
[101] K. Yamashita, E. Yonehara, X. Ding, M. Nagai, T. Umegaki, and M. Matsuda, "Electrophoretic coating of multilayered apatite composite on alumina ceramics," *Journal of Biomedical Materials Research*, vol. 43, no. 1, pp. 46–53, 1998, doi: 10.1002/(SICI)1097-4636(199821)43:1<46::AID-JBM5>3.0.CO;2-M.
[102] Y. Chung, H. Park, S. Cho, Y. S. Yoon, and D.-J. Kim, "Effect of Processing Parameters on Electrophoretically Deposited ZnO Nanoparticles on Conductive Fabrics," *Meet. Abstr.*, vol. MA2014-01, no. 8, p. 514, Apr. 2014, doi: 10.1149/MA2014-01/8/514.
[103] C. Du, D. Heldbrant, and N. Pan, "Preparation and preliminary property study of carbon nanotubes films by electrophoretic deposition," *Materials Letters*, vol. 57, no. 2, pp. 434–438, Dec. 2002, doi: 10.1016/S0167-577X(02)00806-6.
[104] S. Put, J. Vleugels, G. Anné, and O. Van der Biest, "Functionally graded ceramic and ceramic–metal composites shaped by electrophoretic deposition," *Colloids and Surfaces A: Physicochemical and Engineering Aspects*, vol. 222, no. 1, pp. 223–232, Jul. 2003, doi: 10.1016/S0927-7757(03)00227-9.
[105] B. Ferrari, A. J. Sánchez-Herencia, and R. Moreno, "Electrophoretic Forming of Al2O3/Y-TZP Layered Ceramics from Aqueous Suspensions," *Materials Research Bulletin*, vol. 33, no. 3, pp. 487–499, Mar. 1998, doi: 10.1016/S0025-5408(97)00244-4.
[106] H. S. Maiti, S. Datta, and R. N. Basu, "High-Tc Superconductor Coating on Metal Substrates by an Electrophoretic Technique," *Journal of the American Ceramic Society*, vol. 72, no. 9, pp. 1733–1735, 1989, doi: 10.1111/j.1151-2916.1989.tb06314.x.
[107] J. Van Tassel and C. A. Randall, "Electrophoretic deposition and sintering of thin/Thick PZT films," *Journal of the European Ceramic Society*, vol. 19, no. 6, pp. 955–958, Jun. 1999, doi: 10.1016/S0955-2219(98)00352-5.
[108] B. Neirinck, J. Fransaer, O. V. der Biest, and J. Vleugels, "Aqueous electrophoretic deposition in asymmetric AC electric fields (AC–EPD)," *Electrochemistry Communications*, vol. 11, no. 1, pp. 57–60, Jan. 2009, doi: 10.1016/j.elecom.2008.10.028.
[109] A. Chávez-Valdez, M. Herrmann, and A. R. Boccaccini, "Alternating current electrophoretic deposition (EPD) of TiO2 nanoparticles in aqueous suspensions," *Journal of Colloid and Interface Science*, vol. 375, no. 1, pp. 102–105, Jun. 2012, doi: 10.1016/j.jcis.2012.02.054.
[110] V. Ozhukil Kollath *et al.*, "AC vs. DC electrophoretic deposition of hydroxyapatite on titanium," *Journal of the European Ceramic Society*, vol. 33, no. 13, pp. 2715–2721, Nov. 2013, doi: 10.1016/j.jeurceramsoc.2013.04.030.
[111] "AC Electrophoresis; Deposition of Ceramic Nanaoparticles on In-plane Electrodes at Low Frequencies (RESEARCH NOTE)," *IJE*, vol. 27, no. 5 (B), May 2014, doi: 10.5829/idosi.ije.2014.27.05b.12.
[112] E. Calzavarini, "Anisotropic particles in two-dimensional convective turbulence," *Physics of Fluids*, vol. 32, no. 2, p. 023305, Feb. 2020, doi: 10.1063/1.5141798.

[113] R. Paulose, R. Mohan, and V. Parihar, "Nanostructured nickel oxide and its electrochemical behaviour—A brief review," *Nano-Structures & Nano-Objects*, vol. 11, pp. 102–111, Jul. 2017, doi: 10.1016/j.nanoso.2017.07.003.
[114] C. S. Carney, R. E. Chinn, Ö. N. Doğan, and M. C. Gao, "Isothermal decomposition kinetics of nickel (II) hydroxide powder," *Journal of Alloys and Compounds*, vol. 644, pp. 968–974, Sep. 2015, doi: 10.1016/j.jallcom.2015.03.256.
[115] D. Wang, R. Xu, X. Wang, and Y. Li, "NiO nanorings and their unexpected catalytic property for CO oxidation," *Nanotechnology*, vol. 17, no. 4, pp. 979–983, Jan. 2006, doi: 10.1088/0957-4484/17/4/023.
[116] P. Rana and P. Jeevanandam, "Synthesis of NiO Nanoparticles via Calcination of Surfactant Intercalated Layered Nickel Hydroxides and their Application as Adsorbent," *J Clust Sci*, Feb. 2022, doi: 10.1007/s10876-022-02237-2.
[117] M. El-Kemary, N. Nagy, and I. El-Mehasseb, "Nickel oxide nanoparticles: Synthesis and spectral studies of interactions with glucose," *Materials Science in Semiconductor Processing*, vol. 16, no. 6, pp. 1747–1752, Dec. 2013, doi: 10.1016/j.mssp.2013.05.018.
[118] Y. Lin, Y. Qiao, X. Cheng, Y. Yan, Z. Li, and J. Huang, "Hydrotropic salt promotes anionic surfactant self-assembly into vesicles and ultralong fibers," *Journal of Colloid and Interface Science*, vol. 369, no. 1, pp. 238–244, Mar. 2012, doi: 10.1016/j.jcis.2011.11.067.
[119] L. Zhai, X. Lu, W. Chen, C. Hu, and L. Zheng, "Interaction between spontaneously formed SDBS/CTAB vesicles and polymer studied by fluorescence method," *Colloids and Surfaces A: Physicochemical and Engineering Aspects*, vol. 236, no. 1, pp. 1–5, Apr. 2004, doi: 10.1016/j.colsurfa.2003.10.012.
[120] T. Q. N. Tran, G. Das, and H. H. Yoon, "Nickel-metal organic framework/MWCNT composite electrode for non-enzymatic urea detection," *Sensors and Actuators B: Chemical*, vol. 243, pp. 78–83, May 2017, doi: 10.1016/j.snb.2016.11.126.
[121] J. Yoon, E. Lee, D. Lee, T.-S. Oh, Y. S. Yoon, and D.-J. Kim, "Communication—Highly Sensitive Ag/ZnO Nanorods Composite Electrode for Non-Enzymatic Urea Detection," *J. Electrochem. Soc.*, vol. 164, no. 12, p. B558, Aug. 2017, doi: 10.1149/2.1341712jes.
[122] K. J. Babu, N. Senthilkumar, A. R. Kim, and G. G. kumar, "Freestanding and binder free PVdF-HFP/Ni-Co nanofiber membrane as a versatile platform for the electrocatalytic oxidation and non-enzymatic detection of urea," *Sensors and Actuators B: Chemical*, vol. 241, pp. 541–551, Mar. 2017, doi: 10.1016/j.snb.2016.10.069.
[123] "Conductive 2D Metal-organic Framework (Co, NiCo, Ni) Nanosheets for Enhanced Non-enzymatic Detection of Urea - Wang - 2021 - Electroanalysis - Wiley Online Library." https://analyticalsciencejournals.onlinelibrary.wiley.com/doi/full/10.1002/elan.202060586 (accessed Oct. 03, 2022).
[124] M. Arain *et al.*, "Simpler and highly sensitive enzyme-free sensing of urea via NiO nanostructures modified electrode," *RSC Advances*, vol. 6, no. 45, pp. 39001–39006, 2016, doi: 10.1039/C6RA00521G.
[125] R. Ahmad, N. Tripathy, and Y.-B. Hahn, "Highly stable urea sensor based on ZnO nanorods directly grown on Ag/glass electrodes," *Sensors and Actuators B: Chemical*, vol. 194, pp. 290–295, Apr. 2014, doi: 10.1016/j.snb.2013.12.098.
[126] R. Miao, W. Zeng, and Q. Gao, "SDS-assisted hydrothermal synthesis of NiO flake-flower architectures with enhanced gas-sensing properties," *Applied Surface Science*, vol. 384, pp. 304–310, Oct. 2016, doi: 10.1016/j.apsusc.2016.05.070.

[127] J. Yu and L. Qi, “Template-free fabrication of hierarchically flower-like tungsten trioxide assemblies with enhanced visible-light-driven photocatalytic activity,” *Journal of Hazardous Materials*, vol. 169, no. 1, pp. 221–227, Sep. 2009, doi: 10.1016/j.jhazmat.2009.03.082.
[128] M. Qin, L. Zhang, and H. Wu, “Dual-template hydrothermal synthesis of multi-channel porous NiCo2O4 hollow spheres as high-performance electromagnetic wave absorber,” *Applied Surface Science*, vol. 515, p. 146132, Jun. 2020, doi: 10.1016/j.apsusc.2020.146132.
[129] H. Zhang, D. Yang, D. Li, X. Ma, S. Li, and D. Que, “Controllable Growth of ZnO Microcrystals by a Capping-Molecule-Assisted Hydrothermal Process,” *Crystal Growth & Design*, vol. 5, no. 2, pp. 547–550, Mar. 2005, doi: 10.1021/cg049727f.
[130] Y. Zhao, X. Tan, T. Yu, and S. Wang, “SDS-assisted solvothermal synthesis of BiOBr microspheres with highly visible-light photocatalytic activity,” *Materials Letters*, vol. 164, pp. 243–247, Feb. 2016, doi: 10.1016/j.matlet.2015.10.155.
[131] “The first evidence for unilamellar vesicle formation of ionic liquids in aqueous solutions - Chemical Communications (RSC Publishing).” https://pubs.rsc.org/en/content/articlelanding/2013/cc/c3cc41908h/unauth (accessed Nov. 15, 2021).
[132] K.-T. Lau and C. C. Sorrell, “Electrophoretic mobilities of dissolved polyelectrolyte charging agent and suspended non-colloidal titanium during electrophoretic deposition,” *Materials Science and Engineering: B*, vol. 176, no. 5, pp. 369–381, Mar. 2011, doi: 10.1016/j.mseb.2010.10.012.
[133] A. Clifford, D. Luo, and I. Zhitomirsky, “Colloidal strategies for electrophoretic deposition of organic-inorganic composites for biomedical applications,” *Colloids and Surfaces A: Physicochemical and Engineering Aspects*, vol. 516, pp. 219–225, Mar. 2017, doi: 10.1016/j.colsurfa.2016.12.039.
[134] Y. Wang and D. O. Northwood, “An investigation into TiN-coated 316L stainless steel as a bipolar plate material for PEM fuel cells,” *Journal of Power Sources*, vol. 165, no. 1, pp. 293–298, Feb. 2007, doi: 10.1016/j.jpowsour.2006.12.034.
[135] K. Raju, H.-W. Yu, and D.-H. Yoon, “Aqueous electrophoretic deposition of SiC using asymmetric AC electric fields,” *Ceramics International*, vol. 40, no. 8, Part A, pp. 12609–12612, Sep. 2014, doi: 10.1016/j.ceramint.2014.04.098.
[136] Y. Miao *et al.*, “Electrocatalysis and electroanalysis of nickel, its oxides, hydroxides and oxyhydroxides toward small molecules,” *Biosensors and Bioelectronics*, vol. 53, pp. 428–439, Mar. 2014, doi: 10.1016/j.bios.2013.10.008.